NUCLEAR DATA AND ANGULAR BIASING ASPECTS OF MONTE CARLO SHIELDING CALCULATIONS FOR FUSION REACTORS

by

CHARLES TUDOR PARRY

A THESIS SUBMITTED IN PARTIAL FULFILMENT OF
THE REQUIREMENT FOR THE DEGREE OF
DOCTOR OF PHILOSOPHY
IN THE
UNIVERSITY OF LONDON

OCTOBER 1985

NUCLEAR POWER GROUP
IMPERIAL COLLEGE OF SCIENCE AND TECHNOLOGY

A B S T R A C T

Attempts to obtain energy economically from nuclear fusion reactors have centred on the so-called Tokamak reactors, in which a deuterium-tritium (D-T) plasma is magnetically confined in a toroidal chamber. The D-T nuclear reaction yields helium and 14.2 MeV neutrons as products. The reactor components and personnel need to be shielded from these high energy neutrons and the gamma radiation they produce.

Conventional radiation shielding techniques are broadly applicable; however, the complex configurations of Tokamaks often require the use of Monte Carlo codes. The nuclear cross-section data used by these codes have been prepared for fission reactor problems: the feasibility of their use in fusion reactor calculations is studied. A comparison is made between results obtained using multigroup averaged data and continuous energy (point) data. Both types of data are also tested against experimental measurements of the attenuation of 15 MeV neutrons in mild-steel. The sensitivity of the results in the point calculation to errors in the cross-sections is estimated.

A method is described for sampling an adequate number of Monte Carlo particles down the penetrations that breach Tokamak primary shields. The method utilises adjoint angular fluxes to indicate the relative importances of neutrons within the problem. The viability of the method is compared to that of an alternative method in which the directions of neutrons emerging from collisions are biased towards regions of greatest interest.

C O N T E N T S

LIST OF TABLES

LIST OF FIGURES

LIST OF APPENDICES

1. INTRODUCTION

The production of energy is of paramount importance in modern society. The major source of this energy is presently dependent on the dwindling reserves of fossil fuels and the pending exhaustion of these resources presents the prospect of rising energy costs and possible energy shortages.

An alternative to the burning of fossil fuels in the large-scale, centralised generation of electricity is nuclear power. The fission of uranium has been used successfully as a means for the commercial production of electicity for almost thirty years and the advent of the fast-reactor, which uses uranium and plutonium as fuels, looks set to extend this almost indefinitely. But the fission reaction is not the only nuclear process which can result in the production of energy: there is also fusion.

Nuclear fusion is the process in which light nuclei collide and fuse together to form a heavier composite nucleus. The rest-mass of the new nucleus is less than the sum of the rest-masses of the colliding nuclei and the excess amount is released in the form of its equivalent energy. The aim of a fusion reactor is to convert the energy emitted in a large number of these reactions into a form suitable for the continuous production of electricity.

Of the many possible fusion reactions, the one likely to fulfil the criteria necessary for a viable fusion reactor most easily is that between the two hydrogen isotopes deuterium (D) and tritium (T). These combine to give a helium nucleus (He4) and a neutron (n) accompanied by the release of 28.2×10^{-13} Joules (17.6 MeV) of energy. This is the so-called D-T reaction:

$$D + T = He4 + n + 17.6\ MeV$$

Deuterium is found in naturally occurring hydrogenous material in the ratio of 1/6500 relative to protium (H1 - the most abundant hydrogen isotope). Tritium, however, does not occur in significant amounts in Nature (it is a beta-emitter with a half-life of 12.3 years) and must be manufactured. It can be generated in Lithium by the capture of neutrons; the two reactions for this are:

$$Li6 + n \rightarrow T + He4 + 7.7 \times 10^{-13} \text{ Joules}$$
$$Li7 + n \rightarrow T + He4 + n - 4.0 \times 10^{-13} \text{ Joules}$$

It may be possible to generate sufficient quantities of tritium by capturing some of the neutrons from the D-T reactions in a Lithium blanket surrounding the reaction chamber. In which case, the fuels for the reactor become, essentially, deuterium and lithium.

Fusion offers several advantages over fission in the long-term production of electricity:

(1) the products of the D-T reaction are not radioactive;

(2) the amount of fuel in the reaction zone (about 1 g) precludes the possibility of 'excursions';

(3) the only radioactive component of the fuel-cycle (tritium) can be processed on site;

(4) the known reserves of high-grade lithium ore have an energy content comparable to the known reserves of uranium and thorium. 1 g of lithium could possibly produce 10 MW.hours of electricity in a D-T-Li series of reactions (1).

For a D-T reaction to occur at all the deuterium and tritium nuclei must be travelling with sufficient energy to overcome

the repulsive electrostatic potential between them. This can be achieved in two ways.

One way is to heat and compress extremely rapidly small pellets of deuterium and tritium to a density of about 10^{20} m^{-3} (ie, $\sim 10^4$ times as great as that of ordinary liquids). This order of compression can be achieved by irradiating the pellets with laser light, electron beams or ion beams. The central problems encountered in developing this method, known as inertial confinement fusion or ICF, are in producing a uniform, isentropic and hydrodynamically stable compression of the pellets resulting in a temperature high enough for fusion to occur. Although progress is being achieved in this, the research is still very much in its early stages and there is no prospect of even experimental reactors being considered this century.

A more promising way to achieve sufficiently energetic deuterium and tritium for D-T reactions is to heat a mixture of deuterium and tritium gases to a temperature of about 100 million K. At this temperature the atoms in the gases are ionised and a D-T plasma is formed. Since the particles in a plasma are electrically charged it can be contained by the use of magnetic fields: charged particles follow helical paths around magnetic field lines. Several configurations of magnetic fields could be used for the confinement of a plasma but the most stable ones (that is, ones in which particle losses are predominantly by diffusion) are those in which the magnetic field lines form closed loops.

In order to obtain more energy out of a fusion reactor plasma than needs to be put in, the plasma must be confined for an amount of time long enough for sufficient reactions to occur. This confinement time is dependent upon the particle density of the plasma. The quality of confinement is defined as the product of the energy confinement time

(which is generally defined as the total thermal energy of the plasma divided by its total rate of loss of energy) and the particle density of the plasma. For a plasma to be a net-producer of energy the quality of confinement must satisfy the so-called Lawson criterion which stipulates that, for a D-T plasma, the quality of confinement must be at least 10^{20} m^{-3} s (2). The D-T reaction is chosen in present fusion reactor concepts because out of all possible reactions, the Lawson criterion for it is least stringent and it requires the least plasma temperature to achieve it.

During the 1960s the Soviet Union developed a type of device, called a Tokamak from the Russian for toroidal magnetic chamber, the performance of which showed great potential as the basis of an energy producing fusion reactor. As its name implies, a Tokamak uses a magnetic field with field lines that contain the plasma in a toroidal vacuum vessel. This field is the combination of a toroidal field produced by a set of coils surrounding the chamber (called the toroidal field coils) and a poloidal field, produced by the current flowing through the plasma itself. The resultant magnetic field is helical about the minor axis of the torus and, as such, prevents lateral drift of the plasma to the walls of the chamber. The plasma current is induced by the use of transformer action wherein the plasma plays the part of the secondary circuit. The position and shape of the plasma can be further controlled by a poloidal field produced by coils in which eddy currents are induced by the plasma. These coils are placed outside the chamber, concentric with the major axis of the torus and, together with the primary coils of the transformer, are known as the poloidal field coils.

The features mentioned above are common to all Tokamak reactor designs and are illustrated in Figure 1.

At present all the major magnetically confined fusion devices are Tokamaks; none are power producing and none have attained the conditions necessary for fusion reactions to occur.

There are currently four large experimental Tokamaks in the world:

1. The Tokamak Fusion Test Reactor (TFTR) at Princeton, USA. Began operating in December 1982.

2. The Joint European Torus (JET) at Culham, Oxfordshire. A European collaborative project. Began operating in June 1983 (Figure 2).

3. JT-60 in Japan. Due to begin operating at the end of 1984.

4. T-15, USSR. Due to commence operating in 1985.

All these devices have a major radius of about 3 m. And a minor radius of about 1 m, whereas previous experimental Tokamaks have been, at most, half these dimensions. All four are designed to provide information on the physics of plasmas in conditions approaching those required for fusion to occur. From this information it is hoped to define the parameters for a D-T plasma that could be used in any possible future Tokamaks. The experiments will be carried out, for the most part, with hydrogen plasmas but TFTR and JET will, if the temperature and energy confinement times achieved with hydrogen are favourable, operate with D-T mixtures towards the end of their commissions.

Assuming these experiments are successful and their results encouraging, there still remains the problem of the technological feasibility of Tokamaks. At present about 15% of the Tokamak research effort is directed towards

technological and engineering aspects of prospective fusion reactors (3). Already, EURATOM (the European Atomic Energy Community) is considering the definition and design of the "Next European Tokamak" (NET), and the four main parties in world fusion research - Europe, the USA, the USSR and Japan - are performing a detailed study of a large-scale Tokamaks design (INTOR) (4). Both NET and INTOR are intended to bridge the gap between the present experimental Tokamaks and conceivable demonstration reactors. Should the present experiments yield encouraging results, the INTOR reactor may be constructed and used to test possible approaches to solving the many engineering and technological problems envisaged for an electricity producing Tokamak reactor.

The use of a D-T plasma in a Tokamak demands the presence of shielding to prevent excess irradiation of personnel and of components. The radiation is a result of the fast neutrons (14.2 MeV) emitted in the D-T fusion reactions and gamma-rays resulting from the interactions of these neutrons with the Tokamak structure.

The problems encountered in the design of radiation shielding for Tokamaks are quite considerable and are described in Chapter 2.

The methods developed for the design of shielding for fission reactors are broadly applicable and these are outlined in Chapter 3. However, extensions of and adaptations to these techniques are necessary to meet the increased demands imposed by the extra geometrical complexity of fusion reactors. Some of the methods that have been employed in Tokamak shield design are described in Chapter 4.

In addition to the computational methods of shield design for Tokamaks, the nuclear data used in these methods have also been carried over from fission reactor calculations. A

description of these data and an appraisal of their use in fusion reactor calculations are made in Chapter 5.

Two approaches to the problem of void streaming in Monte Carlo calculations are described in Chapter 6. Both methods involve the biasing of particle histories into the voided regions: one by selecting scattering directions from an appropriately biased distribution and one in which an angular-dependent importance function is invoked in 'splitting and rouletting' (SR). The efficacies of the two methods in a simple neutron streaming problem are tested against a current method of using SR with a scalar importance function.

Finally, some conclusions are drawn from the work described and some suggestions are made as to what may prove fruitful areas of further research into the problems addressed in this Thesis.

2. THE SHIELDING PROBLEMS OF TOKAMAKS

2.1 Introduction

In studying a Tokamak reactor design one is immediately struck by the complexity of the system and the interdependence of the reactor components. Altering the specifications of one subsystem can profoundly affect the expected performance of another. Although perhaps not as critical to the design as some other aspects, the radiation shielding impacts very strongly on the overall configuration and performance specifications of the reactor. Consequently, a close look must be taken at the problems envisaged in the shielding of Tokamaks at an early stage in their design and changes to reactor designs must be made with the effects of these on the shielding borne in mind.

It is also worth noting that Gohar (64) estimates the cost of the shielding to be between 8 and 16% of the total reactor cost.

For the D-T reaction to take place in a plasma an ion temperature of $\geq$10 KeV ($\sim 2 \times 10^6$ K) is required. Radiation (bremmstrahlung and synchrotron) and particle (diffusion) losses will probably ensure that, despite some heating by the alpha particles created in the D-T reaction, supplementary heating will be required to maintain such a high temperature in the magnetically confined plasma.

The renewal of fuel in the reactor chamber would also be a problem and so too would be the complementary task of impurity removal.

Two possible modes of operation are currently being considered in Tokamak designs: the steady-state mode and the pulsed mode. In the steady-state operation fuel is introduced into the plasma at regular intervals. The plasma

itself is kept at ignition temperature continually, by means of supplementary heating if alpha heating proves insufficient, and impurities within the plasma are also removed continually. In pulsed operation the plasma is brought to ignition temperature for a relatively short period only; fuel is introduced and impurities, unreacted fuel and reaction products are removed between these burn periods.

Supplementary heating is likely to be achieved most easily by neutral beam injection, radio-frequency heating and adiabatic compression.

Neutral beam injection can, in principle, be used to heat the fuel and plasma simultaneously in either steady-state or pulsed operation reactors. Beams of high energy neutral deuterium and tritium atoms are directed at the plasma, the particles are ionised and their energies are dissipated within the plasma by collisions.

In radio-frequency heating, certain frequency radio-waves are launched into the plasma in which their energies are absorbed causing its temperature to rise.

A rapid adiabatic compression of the plasma, or a region of the plasma, by means of increasing the magnetic field, causes an increase in the plasma temperature.

In both continuous and pulsed concepts ohmic heating occurs (from the current passing through the plasma) which is predominant immediately after start-up but a progressive decrease in plasma resistivity with temperature causes losses to exceed the heating effect at a temperature of about 2×10^7 K (3).

Fuel can be introduced into the reaction chamber by neutral beam injection (if this is being used), by means of injecting pellets of frozen fuel or by introducing gaseous fuel into the plasma.

In continuous, and some pulsed, reactor designs impurities are removed by means of collector plates, on which the impurities are allowed to impinge, and pumping ducts through which these de-ionised impurities are removed.

A 'blanket' containing a lithium compound will probably be placed around the inside of the vacuum chamber in order to produce tritium using the neutron capture reactions mentioned in Chapter 1.

The neutrons escaping from the plasma will deposit most of their energy in the blanket and its supporting structure (the 'hot-shield'). This energy will be removed in the form of heat by a cooling system. The hot-shield is also the vacuum containing structure and, as such, must maintain its integrity throughout its use. More shielding is provided further out from the vacuum chamber by the 'cold-shield' and gamma-shield. These are designed to absorb or attenuate the neutron and gamma radiation emanating from the plasma after it has traversed the blanket, hot-shield and the space occupied by ducts and support structures immediately behind the hot-shield. (For a schematic outline of these components refer to Figure 7).

The problems anticipated in the shielding of a Tokamak reactor are (a) the specification of bulk-shield thicknesses and materials, with particular regard to the inner shield; and (b) the shielding requirements for the various ducts which penetrate the bulk-shield and cause a severe reduction in the overall shielding performance.

2.2 Bulk-Shield Problems

Attenuation requirements for the whole shield system are determined primarily by the radiation effects on the toroidal field coils (TFCs). In almost all reactor designs superconducting coils are envisaged as being necessary to provide the ~10T field required to contain the plasma.

The shielding required will be such that the following effects are minimised in the field coils:

(i) radiation heating - refrigeration power requirements to counter radiation heating of cryogenic regions should account for only a small percentage of the total reactor output. Making an assumption of 20 MeV per fusion, 500 W of electrical power needed for every 1 W of heat to be removed and a plant thermal efficiency of 33% then 1% of the reactor output would be consumed by an average heat loading of 34 $W.m^{-3}$ in the magnets (5).

(ii) irradiation of superconductors - the neutron and gamma-ray irradiation of superconducting materials (Nb_3Sn and NbTi) cause a decrease in the critical current density which then requires an increase in the amount of superconductor needed to keep the operational current the same. This damage by irradiation can be off-set by annealing at room temperature but, since each anneal would require some months of reactor down-time (16), almost all designs envisage using superconductors which can operate throughout the reactor lifetime without the need for annealing. The TFC shielding should thus be designed to accommodate this demand. Gohar and Abdou (6) suggest a fast-neutron (>0.1 MeV) fluence limit of 10^{18} $n.cm^{-2}$ for Nb_3Sn.

(iii) irradiation of copper substrate in the TFCs - excess irradiation of the TFCs causes the electrical resistivity of these stabilisers to increase by unacceptable amounts. The resistivity rise in copper at 10^{18} $n.cm^{-2}$ (7×10^{-8} $\Omega.cm$) will cause the current density to fall to about one half of its initial value (6 and 7) which is almost certainly prohibitive on the grounds of extra capital costs.

(iv) irradiation damage to insulators - inorganic insulators tend to be very brittle under irradiation, therefore, it is presently believed that organic insulators such as epoxy-resin, will be necessary. Radiation damage to these insulators is irreversible so they would be expected to function throughout the reactor lifetime. There is a lack of data on the behaviour of organic insulators under irradiation at TFC temperatures (~4K) but extrapolation of current results to these low temperatures suggests a maximum allowed dose of about 10^{10} Rad after 6 MW-y.m^{-2} (6 and 8).

Aside from the field coils, one more component is critical in terms of the shielding requirements of a Tokamak - the hot-shield. The hot-shield should be designed so as to prevent the stainless steel structure immediately behind it from having to be replaced during the reactor lifetime. This would be necessary if excessive deterioration of its mechanical properties was caused by irradiation. This criterion should be met without too much difficulty by careful design of the blanket/shield assembly surrounding the vacuum chamber.

The radiation effects are most critical in that part of the vertical inner-limb near the mid-plane of the reactor. However, with judicious use of materials, effective shielding could be provided in the limited space available.

The space available for shielding on the outer-side of the vacuum chamber is less restricted than on the inner-side and, consequently, the bulk-shield design criteria are less demanding: the prime constraint is upon the physical size, an enlargement of which would increase the overall shield cost. This increase is compounded by having to move the TFCs further from the plasma, which results in the need to increase the current in the coils to maintain the same magnetic field strength at the plasma.

However, the protection from radiation of components on the outer-side of the reactor is not altogether simple : access to the vacuum chamber is needed for various ducts and these present streaming paths through the bulk-shield (see Section 2.3); and, provision may need to be made for blanket and hot-shield replacement during the reactor life-time.

2.3 Penetration Problems

Various penetrations will need to be made through the bulk shield surrounding the reactor vacuum chamber. The penetrations envisaged in present designs are dealt with separately below.

(i) Neutral Beam Injector (NBI) Ducts

As has been mentioned, neutral beam injection is one method that has been proposed for heating and refuelling Tokamak reactors. This method entails having large (~1m) diameter ducts in the plane of the torus, coming from each NBI box, situated outside the TFCs, penetrating the bulk shield and opening out into the vacuum chamber. The number and size of these ducts is dependent on the power required of them, which, in turn, is dependent on their envisaged use, and on the amount of first wall surface area required for tritium breeding purposes. Each duct must enter the bulk shield between successive poloidal and toroidal field coils which again restricts their size and affects their number. If the reactor is to be run in beam-driven mode the NBI ducts should be as tangential as possible to the plasma minor axis, which imposes further restrictions on the space available.

It is generally anticipated that about four or five NBIs would be required for an operational Tokamak, with each duct interface with the vacuum chamber being rectangular and about 1.2m high by 0.8m wide to

make the best use of the clearance between the TFCs. Some designs also incorporate the possibility of having a shutter at some point in the NBI duct, which would be closed during a plasma burn. Clearly, a beam-driven, continuous reactor would not use such a device and, in any case, its mechanics may prove prohibitively complex.

Assuming that shielding can be provided around the NBI duct to prevent excess damage to the nearby reactor components, this still leaves the problem of there being a direct line of sight between the plasma and the components (ion sources, cryopanels, bending magnets, calorimeters, etc ..) of the NBI boxes. This problem is very severe with NBIs employing positive-ion sources as then the sources must be fairly close to the axis of the drift-tube. However, recent developments have resulted in the design of negative-ion based systems in which the D-ions used can be bent through 90° and thus enable the ion sources and other components to be placed at a distance from the drift-tube axis (9).

(ii) Radio-Frequency (RF) Heating Ducts

RF heating has great advantages, from a shielding point of view, over neutral beam injection, as a method to supplement atomic heating of the plasma. RF heating may also be needed as a burn temperature control and for current-profile control, during start-up and shut-down, to avoid plasma disruption.

The openings into the vacuum chamber of RF heating devices are usually quite small and, because wave-guides can be bent with little loss in efficiency, RF heating presents, in general, a straightforward shielding problem.

(iii) Divertor and Limiter Ducts

Provision must be made in the design of reactors for the removal of reaction products, unreacted fuel and impurities from the reaction chamber. This can be achieved by allowing them to strike regions near the outer edge of the plasma, which causes them to be neutralised, and by pumping away the gases produced (mostly helium) through some form of duct. The two schemes most often proposed to achieve this are the poloidal divertor method and the limiter method.

The poloidal divertor involves shaping the magnetic field at the outer edge of the plasma so as to cause ionised particles near this edge to strike a plate or plates, usually below the plasma.

The limiter method is an even simpler exhaust system from an engineering standpoint: it consists of a plate pushed into a region in the outer edge of the plasma without the use of impurity diverting magnetic fields. This plate, called a limiter, would require the use of a pumping duct similar to that needed for the divertor; hence, from a shielding point of view, the two systems pose virtually identical problems.

The pumping ducts themselves, unlike NBI drift-tubes, need not be straight so the amount of duct having a direct line of sight with the plasma can be made quite small and the radiation streaming effects can be partially off-set by placing dog-legs within the duct.

The shielding of these ducts, then, does not provide as much cause for concern as that for the NBI ducts. Nevertheless, there would be a large number of these ducts and care should be taken to ensure adequate protection of surrounding structures.

(iv) Fuelling Ducts

Although it is feasible that fuelling could be achieved using the NBIs, uncertainty in plasma profiles during burn-time has resulted in some designs considering the possibility of alternative means of fuelling. The deuterium and tritium fuel could conceivably be injected either in gaseous form or in the form of frozen pellets. In either case, the diameter of the injector ports into the chamber need only be very small (~ a few mm) and their shielding requirements would be correspondingly small (41).

(v) Evacuation Ducts

The vacuum chamber would need to have ducts present for its evacuation. In designs using poloidal diverters or pumped limiters the ducts provided for these devices could also be used as evacuation ducts. In other designs separate ducts would be required. These ducts would be large in number and size. However, they could tolerate bends and could, perhaps, be closed for the duration of the plasma burn. Consequently, their shielding problems would not be as severe as the NBI ducts.

(vi) Diagnostic Ducts

Access will need to be gained to the vacuum chamber for various instrumentation used in data acquisition for diagnostic and control purposes. The penetrations, although large in number, will be small in size and, in general, will not need to be straight; thus, their shielding requirements will not be too problematic (10).

(vii) Coolant Pipes

The blanket, the hot-shield and the divertor/limiter plates will all need to be cooled, thus cooling pipes will be needed close to the reactor chamber. Although not penetrating through to the vacuum chamber region itself, these pipes will provide routes by which radiation could escape relatively unhindered through the bulk-shield. However, they are likely to be of small bore and contain many bends so their effect on the overall shield performance will be very much smaller than the larger penetrations present.

The coolant itself could be either gaseous (helium, for instance) or liquid (water): a liquid coolant being the preferred choice form a shielding point of view because of its greater radiation attenuating properties.

(viii) Maintenance Ports

Any ports required for reactor maintenance could be closed during reactor operation and, hence, not prove too troublesome as regards their shielding.

It should be noted also that some reactor operating schemes require "hands-on" maintenance within a short time after shut-down. This criterion strongly affects the shielding requirements of the reactor: the materials need to be chosen very carefully to keep activation of reactor components below an accepted maximum and the flux penetrating to the outer regions of the reactor must be kept lower than it would without the requirement of personnel access. The extra shielding would result in added complications, not only for the reactor manufacture but also for the scheduled replacements of blanket and first wall segments.

3. CALCULATIONAL METHODS IN SHIELD DESIGN FOR TOKAMAKS

3.1 Introduction

The methods used for the computation of accurate solutions to radiation transport problems fall into two broad categories: deterministic and stochastic. Both calculations rely on the fact that, in practical problems, the number of particles is such that statistical fluctuations in particle densities are small enough to allow the description of particle behaviour in terms of probable particle densities.

In deterministic calculations, equations describing particle densities can be derived (eg, the neutron transport equation, see Appendix A) but their exact solution is impossible, other than in very simple cases, and, for realistic problems, approximations to them are solved. Nevertheless, solutions to these approximate representations generally yield results which can be regarded as very accurate for most practical purposes.

The stochastic (or, more commonly, Monte Carlo) approach is to simulate the passage of a large number of particles throughout the problem space by randomly sampling from the probability distributions that govern individual particle interactions and recording the effects of these particles in chosen regions of the problem space. Needless to say, very large numbers of these particles must be tracked to ensure low statistical variances on the results.

Both deterministic and Monte Carlo methods have been successfully applied to fusion reactor radiation transport problems. The theory behind each of them is briefly described in this Chapter, followed by an appraisal of their relative merits in fusion reactor calculations and a description of their previous use in such calculations.

3.2 Deterministic Methods

3.2.1 Introduction

To date, the most widely employed deterministic method in radiation shielding calculations is the discrete-ordinates or Sn method (11) which is to be outlined here. Descriptions of other numerical methods for solving the neutron transport equation (or approximations to it) are to be found, for example, in References 11, 12 and 13. Recently, finite-element methods have been used to solve the neutron transport equation (14) and diffusion approximations (15) but their direct use in fusion shielding calculations has yet to be reported.

3.2.2 The Discrete-Ordinates Method

The discrete-ordinates method derives its name from the manner in which it treats angular dependence: it considers solutions in a few discrete directions only, which distinguishes it from a large number of other deterministic methods wherein the angular variable is treated by expansion in spherical harmonics. Gaussian type integration of angular integrals are performed, using the approximation:

$$\int_{4\pi} f(\hat{\underline{\Omega}})\, d\hat{\underline{\Omega}} \simeq \sum_{i=1}^{n} w_i\, f(\hat{\underline{\Omega}}_i)$$

where w_i is a weight associated with direction $\hat{\underline{\Omega}}_i$. The $\hat{\underline{\Omega}}_i$ and w_i are known as the 'quadrature set' for the problem. The quadrature set used in the

problem can affect the accuracy of the solution and the efficiency of the calculation and should be chosen with care (11).

The spatial variables of the transport equation are treated by finite-difference methods and the energy variable in terms of energy groups (the multigroup method, see Appendix A).

Treating each of the variables of the transport equation in this fashion results in the equation being replaced by a set of coupled differential equations; the number of which being dependent on the order of angular quadrature, and on the number of groups chosen to represent the range over which solutions are required. The equations are coupled via scattering terms, which are dealt with in the multigroup formation by the use of group cross-sections (see Appendix A), and terms resulting from the treatment of the angular variable. The resulting set of equations can be solved (after applying suitable boundary conditions) by an iterative procedure.

The discrete-ordinates method has been used in the radiation transport codes ANISN (18) and DOT (19). These codes are for one-dimensional and two-dimensional problems respectively.

In finite-element methods a similar procedure to the finite-difference method is applied but the cells over which the equation is solved need not form a regular rectangular mesh. Thus, complex geometries can be modelled using a mesh consisting of irregular triangular elements.

3.3 Monte Carlo Methods

3.3.1 Principles

The passage of a particle through a material can be simulated on a computer by the progressive random sampling of the distributions defining the likely outcome of events encountered in its path; this is the basis of the Monte Carlo method (20). A series of such events from its source ("birth") to its absorption or escape ("death") constitutes the "history" of the particle. The "score" of a particle in a particular region of the problem space can be computed from the parameters the particle has when passing through that region and from a cross-section relating these parameters to the quantity being scored. The score could, for example, represent an estimate of the scalar flux or of a flux-related response.

Since the history of a particle is determined by random sampling, the score recorded by a single particle is a random variable and the average score of a large number of particles, each with different histories, will approximate to the mean of the distribution of this random variable. Thus, in theory, the flux, or other response, due to a given source representation, could be estimated throughout the problem space by recording the responses due to a large number of particle histories emanating from this source. However, such analogue calculations are of little use in practical shielding problems since the score would have a large variance in all but those regions close to the source.

This can be illustrated (21) by noting that the score in such a calculation will have a variance with two main components: σ_a^2 and σ_b^2, where σ_a^2 is due to the statistical uncertainty of a source particle reaching the scoring region and σ_b^2 is due to the method of scoring the flux from the parameters of those particles that do reach the scoring region. The distribution of which σ_a^2 is the variance is binomial and:

$$\sigma_a^2 = np(1-p)$$

where p is the probability of a source particle reaching the scoring region and n is the number of source particles started. In a typical deep-penetration shielding calculation $p \sim 10^{-10}$ and a coefficient of variation of less than about 20% (ie, $\sigma < 0.2$ np) is desired. Therefore, the number of particles that needs to be tracked from the source in an analogue Monte Carlo calculation in order for the variance on the score, due to the statistical uncertainty of a particle reaching the scoring region, to be acceptable is about 2.5×10^{11}. Assuming that each history takes at least 1000 multiplications and each multiplication takes about 10^{-8} seconds then it would take over 500 hours of computing time to track this number of particles - a totally impractical undertaking.

Clearly, analogue Monte Carlo calculations are of no use in predicting particle penetration through realistically sized shields and, for this reason, several techniques have been employed to allow the Monte Carlo method to be applied to practical shielding problems.

3.3.2 Variance Reduction

Many methods are available for "accelerating" Monte Carlo calculations (ie, biasing the histories of particles in order to achieve acceptable statistical variances on results in a reasonable amount of computer time).

Generally known as variance reduction techniques, these methods rely invariably on the use of weighted-particle tracking: each particle being tracked is assigned a weight which is altered at various points in the tracking according to its likely contribution to the score. The weights of the particles are then taken into account when scoring. Thus, in an analogue case, the score, $\hat{S}$, is simply given by:

$$\hat{S} = \sum_t C_t P_t$$

where C_t is the contribution of a track t and P_t is the probability of this track with the summation over all tracks t. In a weighted particle case, the score is given by:

$$\hat{S} = \frac{\sum_t C_t P_t W_t}{W_o}$$

where W_t is the weight of the contributing track t and W_o is the sum of the starting weights of the source particles.

The weight of a particle can be compared to some expected value of its weight at convenient points in its tracking. If its weight is larger than expected it can be split into a number of particles with a more reasonable weight, the number being such that the total weight is conserved. This process is known as splitting and it has a complementary process called Russian Roulette or, more simply, roulette. In roulette a particle that has a weight smaller than that expected is either killed or given a more reasonable weight with a probability such that, on average, the total weight is conserved. The processes of splitting and rouletting are usually used in tandem and the combined process is frequently termed SR.

Using SR one can ensure that there is proliferation of those particles which appear most likely to contribute to the score, albeit with reduced weights, and that particles unlikely to contribute to the score can have their histories terminated.

A simple way to estimate the flux in a scoring region is track length estimation which uses the interpretation of the flux in a region as the total track length travelled by particles in the region divided by the volume of the region (12). Using this estimator the flux score is given by:

$$\phi v_s = \frac{\sum_i \Delta l_i W_i}{W_o V_s}$$

where $\emptyset v_s$ is the estimate of the scalar flux in the scoring volume V_s, Δl_i is the track length in V_s of the particle i, W_i is the weight of the particle i in V_s, W_o is the total weight of source particles used to generate all the i and the summation is over all particles i entering V_s.

The variance on $\emptyset v_s$ measured in this way is given approximately by:

$$\sigma_b^2 \approx \frac{1}{(W_o V_s)^2} \sum_i \{(\Delta l_i)^2 \sigma_{w_i}^2 + w_i^2 \sigma_{\Delta l_i}\}$$

where $\sigma_{w_i}^2$ is the variance on the weights w_i and $\sigma_{\Delta l_i}^2$ is the variance on the track lengths Δl_i (22). Thus, it can be seen that having a large variance on the entrant particle weights in a region increases the variance on the estimate of the flux in that region and so indiscriminate use of SR can actually be detrimental to the calculation one is trying to accelerate.

The variance on the flux estimated by track length estimation is minimised when $\sigma_{w_i}^2$ and $\sigma_{\Delta l_i}^2$ are zero.

In order for $\sigma_{w_i}^2$ to be zero one must ensure that all particles entering the scoring region have the same weight. This is equivalent to demanding that all particles at any point in space have the same weight, since, if two particles arrive at a point in space by different tracks and have different weights and then proceed along the same track to the scoring region, they will arrive there too with different weights. This can be achieved by assigning to all regions of the problem phase-space a value which varies inversely as the expected weight of particles within the region. This value is known as the importance of the region and is utilised in SR as follows.

At convenient points in the calculation, a value, R, is computed which is the ratio of the importance of the region it is presently in to the importance of the region it was in when SR was last performed. If R is greater than one then splitting occurs; if R is less than one then roulette occurs; otherwise no SR is performed. It is easy to see that by defining an importance accurately for each point in the problem phase-space, this method will result in all particles at a particular point in that phase-space having, to a close approximation, the same weight.

It is virtually impossible to have a zero variance on the track lengths of particles entering a scoring region; however, it can be minimised by careful selection of the importance values used throughout the problem.

The importance of a region of phase-space as described above is a measure of the likely contribution to the score of a particle within that region. The importances given to all regions of the phase-space, or the importance map, for the

problem are usually calculated and input prior to the start of the Monte Carlo calculation but, in some codes, they are computed concurrently with the calculation. It is often extremely difficult to define an efficient importance map: too much splitting results in computer time being wasted in tracking large numbers of low-weight particles; too much roulette allows very few particles to reach the scoring region; and, the importances can change quite substantially from group to group in some problems. Hence, deciding on an importance map can be the most labour-consuming part of performing a Monte Carlo calculation.

Fortunately, the definition of the importance of a region of phase-space as being the likely contribution to the score of a particle in that region of phase-space affords the possibility of using the adjoint response for the problem as the importance map (23).

The adjoint response, F*, is the solution to an adjoint transport equation with a source dependent only on the response being scored. The response, F, is related to the adjoint response by:

$$F = \int Q(\underline{r},\underline{\Omega},E)F^*(\underline{r},\underline{\Omega},E)\, d\underline{r}\, dE\, d\underline{\Omega}$$

where Q is the source intensity in particles.$cm^{-3}.s^{-1}$ and integration is over all of the problem phase-space.

Unfortunately, to obtain a value of the adjoint phase-space is as difficult as solving the Monte Carlo problem itself and, indeed, if achieved would negate the need for the Monte Carlo calculation in the first place.

However, significant improvements in variance reduction can be achieved by using approximations to the true adjoint such as that obtained from solving the adjoint form of the diffusion transport equation (24). Hence, the use of SR in Monte Carlo calculations with an adequately defined importance map, is a powerful variance reduction technique. Three other such techniques, described in more detail elsewhere (eg, Reference 12) are outlined here.

(a) Path-Length Stretching

The distance, L, through which a particle must travel before its next collision is given by:

$$L = \{\Sigma_t (E)\}^{-1}.\ln r$$

where $\Sigma_t (E)$ is the total cross-section for the particle of energy E and r is a random variable uniformly distributed between 0 and 1 (12). This distribution can be biased to give longer path-lengths to particles travelling in directions which appear to give them a greater probability of contributing to the score and shorter path-lengths in directions which are not considered likely to do so. In order to do this a preferential direction must be chosen somehow and some distribution indicating the relative importance of other directions must be defined. Once a direction has been selected from the biased distribution it must have its weight adjusted accordingly (62).

(b) Non-Absorption Weighting

When a particle has travelled the distance L, selected from the distribution described in (a) above, it undergoes some form of interaction. It may well be that in this interaction the particle has a finite chance of being absorbed. Any particles so absorbed are obviously removed from the calculation and so the effort that had gone into their tracking has no bearing on the result being considered. However, the distribution from which the outcome of the interaction is selected can be biased so that there is no probability of absorption and the particle, with its weight appropriately reduced, can continue to be tracked.

(c) Directional Biasing

The particles emerging from a collision in a Monte Carlo calculation are selected from the distributions given by the nuclear data being used (see Section 5.1). It is clear that some directions are more important than others. For example, in Figure 3 a particle emerging from a collision at P in the Direction A is more likely to contribute to the score than one emerging in the direction B.

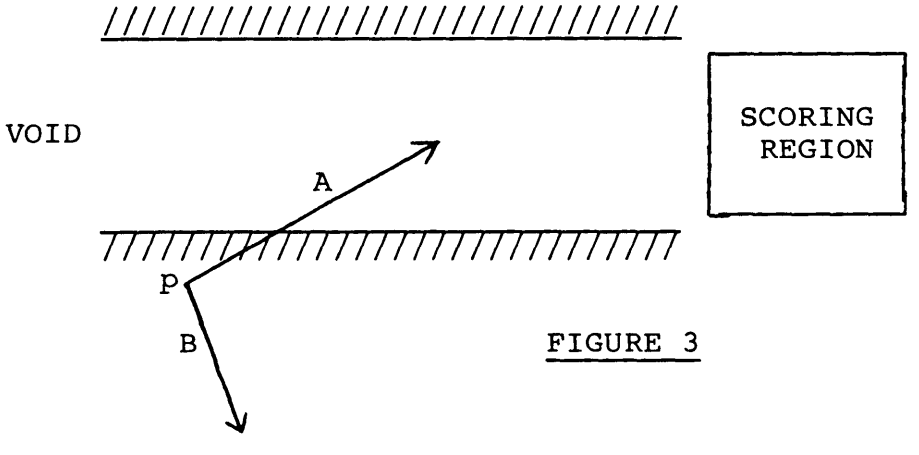

FIGURE 3

The use of SR can be extended to include particle directions if a sufficiently accurate direction-dependent importance function, such as the adjoint angular flux for the problem, is available. Alternatively, the emergent particle directions can be selected from a distribution biased to give a greater probability of particles emerging in a prefered direction. The emergent particles must then have their weights adjusted accordingly. Directional biasing is to be discussed more fully in Chapter 6.

Although two of these techniques can be used separately their use is often enhanced by the concurrent use of SR which can prevent particles from having extreme weights. (The use of non-absorption weighting, which strives to preserve the particle identity by altering the weight, in tandem with SR, which tries to preserve particle weight, is mostly counter-productive.) However, the SR importance map must be chosen with great care in order for it to be compatible with the weights assigned by the additional techniques. Also the biased distributions must be carefully defined, in all cases, to prevent the calculation becoming inefficient (as in the case of a poorly defined importance map for SR).

3.4 Advantages and Disadvantages of Sn and Monte Carlo Calculations in Radiation Shielding

The two main methods used in the computation of solutions to radiation streaming problems - the deterministic Sn method and the stochastic Monte Carlo method - have been described in the preceding sections of this Chapter. A comparison of these two methods in terms of their respective

merits and demerits is now made. The Sn method is considered first, followed by the Monte Carlo method.

The advantages of the Sn method are:

1. Sn is a well established method and has been used with success in a great many types of problems.

2. Provided it can be represented in one or two dimensions, it is usually easy to assimilate the problem geometry into the calculation by means of the finite-difference mesh.

3. The method is deterministic and, as such, errors in fluxes are systematic rather than random.

4. The fluxes can be calculated for all points in the problem.

5. As well as neutrons, secondary gamma-rays can be tracked by the same method, either simultaneously or separately.

6. The method is faster than Monte Carlo for one-dimensional problems and also for the majority of two-dimensional problems.

7. Sn can be used to calculate angular fluxes.

The disadvantages evident in the Sn method are:

1. The iteration convergence is not always well-behaved and the accuracy of a solution is usually dependent on a maximum deviation between successive iterations (this maximum is often expressed as a percentage of the most recent iterate).

2. The discrete nature of the angular dependence can give rise to 'ray effects' which manifest themselves in anomalous, cyclic variations in the calculated fluxes. These effects can be partially offset by increasing the number of angles in the quadrature but this is costly in terms of computer time. Deep-penetration shielding problems are particularly susceptible to ray effects and the quadrature sets are consequently of high order. For example, Jones (25) uses S_8 quadrature in a DOT3.5 calculation on the penetration of 15 MeV neutrons in mild-steel whereas an S_4 quadrature set is recommended for reactor criticality calculations (11).

3. It is usually very difficult to define a quadrature set, spatial mesh, multigroup scheme and polynomial expansion* that are optimal for the efficiency of the problem and, often, several test runs are required before convergence criteria are met.

4. The method treats energy variation by the multigroup method (see Sub-Section 5.1.2) and is prone, therefore, to the errors associated with this approximation (for a more detailed discussion of which see Sub-Section 5.1.4 concerning multigroup data in Monte Carlo calculations).

5. Streaming along voids (ie the introduction of highly anisotropic fluxes) is exceptionally troublesome in the Sn method, partly due to the ray effects already mentioned. However, Clark (26) has recently devised a means of removing most of the problems associated with voids in the Sn method (see Chapter 4).

* ie Legendre Polynomial expansion of scattering angle

The merits of the Monte Carlo method are:

1. The method has been widely used and refined over several years and its use in deep-penetration shielding problems is well-established.

2. Monte Carlo codes can use combinatorial geometry (27) representations to model complex geometries very accurately.

3. The method is faster than Sn for solving three-dimensional problems and some two- dimensional ones (such as time-dependent and deep-penetration problems in which results are required with accuracy in a particular region only).

4. It need not use multigroup data with its attendant disadvantages.

5. Scattering directions in Monte Carlo need not be chosen from a set of discrete directions.

(For further discussion of items 4 and 5 see Sub-Section 5.1.3 concerning point-data for Monte Carlo calculations.)

The disadvantages of the Monte Carlo method are:

1. It is too costly to use, in comparison to S_n, for one-dimensional and most two-dimensional problems.

2. The results are stochastic and thus subject to statistical error.

3. To be cost-effective all realistic problems require a reasonably accurate importance map to bias the problem effectively. Such maps are often difficult to derive and require substantial additional effort.

4. Variances on the results are only good, in general, in a few selected regions of space.

5. In void streaming problems it is very difficult to determine and implement adequate importance maps.

6. It is impractical to use the Monte Carlo method for scoring angular fluxes.

These points can be summarised by saying that Sn is more effective in two-dimensional problems, without ducts or streaming paths, in which the flux is to be known accurately throughout the problem space and that Monte Carlo is better for complex geometry calculations, without streaming, in which the flux is required accurately at a particular region of the problem space only.

In terms of fusion reactor shielding studies, then, Sn can be used to determine the flux within geometrically simple regions of the bulk shield (such as the inboard shield) whereas the complex configuration and numerous voided regions throughout the remainder of the reactor dictate the use of Monte Carlo.

4. PREVIOUS WORK

Discrete-ordinates methods have been frequently employed in radiation transport calculations for Tokamak reactor designs. The method is applicable provided the problem geometry can be adequately expressed in one or two dimensions and no streaming paths are present. The method has proved very successful in the treatment of the Tokamak inboard shield problem (6, 8, 41) but its poor handling of voids has generally precluded its straightforward use in the treatment of problems with radiation streaming down penetrations. Seed (28) found that 90% of the time used in an Sn analysis of a neutral beam duct shield was used in reducing the ray effects caused by streaming. Also, Clark (26) has developed, for the discrete-ordinates codes TWOTRAN, a treatment of voided regions which provides a more accurate solution to such problems than does Sn alone. This hybrid method uses an integral transport theory representation in the void whilst maintaining the usual Sn approach for the surrounding materials. The two methods are fully integrated because the integral transport method used in the void does not interfere unduly with the spatial sweeping of the discete-ordinates method. Clark and others (29) report, however, that although showing improvement on conventional Sn in test duct problems it lacked the accuracy of Monte Carlo.

Several authors have reported the detrimental effect of neutral beam injector duct penetrations on the shielding performance of the bulk shield. Abdou and Jung (8) note that an unshielded NBI duct causes the neutron flux at the TFCs to increase from 1.5×10^{9} $cm^{-2}.s^{-1}$, when shielded, to 1.3×10^{13} $cm^{-2}.s^{-1}$; a figure that is supported by Morrison (5). This increase shows how critical the shielding of these ducts is. Most workers, following the reasoning of Abdou and Jung, have considered the shielding of NBI ducts by local penetration shielding.

Lillie et al (30) overcome the problem of void streaming by using a first-flight treatment of the voids to augment the Sn calculation performed in the surrounding material. Also, several approaches to the NBI duct problem have been made in which the Sn method is used for bulk-material calculations whilst Monte Carlo is employed for the void regions (31, 32, 33).

Urban et al (31), for example, in their treatment of streaming in the ETF use 'trapping surfaces' in a Monte Carlo calculation: when a particle crosses such a surface the space, direction, energy and time coordinates and the particle weight are written to a file; the information on this file can then be used to construct a secondary source for subsequent calculations. Such a trapping surface was used to define a secondary source at the NBI duct mouth for a Monte Carlo calculation on the radiation streaming down the void. This second calculation provided surface sources along the duct for an RZ geometry discrete-ordinates calculation in the bulk shield. The procedure was repeated for a pumping duct entering the NBI duct at right-angles. A reasonable agreement with a complete Monte Carlo analysis of the problem was achieved.

There are several arguments against using interfaced Sn and Monte Carlo calculations:

1. It is often difficult to define surfaces, common to both the Sn and Monte Carlo geometries, which can be used as interfaces.

2. The statistical errors associated with Monte Carlo are usually difficult to transmit to subsequent calculations and so correct estimates of the errors on final results are not generally obtainable.

3. The Monte Carlo method cannot ordinarily produce a full group, angular flux over all points on an interface with an S_n calculation.

4. Considerably effort needs to be expended in transferring computed surface distributions from one calculation to surface source distributions in another. Computer codes written for this purpose are usually very problem-dependent.

Perhaps a more appealing approach to the void streaming problem is straightforward Monte Carlo encompassing both the bulk shield and the duct regions, since this technique is very capable of treating complex geometries with voided regions. However, the design of shielding for the TFCs is a deep-penetration problem and as such demands the use of variance reduction techniques if Monte Carlo is to be used efficiently. Determination of an adequate importance map to use with these variance reduction techniques is a problem that is made more complicated by the presence of the streaming paths and is one that has been addressed by many authors.

Morrison (34) sought a solution to the problem of importance specification by the use of adjoint Monte Carlo calculations. He produced a version of the Monte Carlo code MCBEND (21) which was operable in the adjoint mode (35). Working on a three-dimensional model of the CCTR Mk II (36), he first performed a forward neutron calculation using a first-flight source to an interface at the duct mouth, this caused all the source particles, appropriately weighted, to enter the duct. The interface was then used as a source for a Monte Carlo calculation of neutron transport down the duct with all parts of the problem geometry, apart from the void, duct wall and external duct shield, input as black absorbers. The resulting flux recorded at the TFC was then

used as a source spectrum for an adjoint Monte Carlo calculation over the entire problem geometry with the source at the TFC and all materials properly specified. Finally, Morrison used the adjoint fluxes scored throughout the geometry as an importance function for a forward calculation, of the flux at the TFC, without a first-flight option and with the full material composition specified.

The technique provided reasonable results (with a coefficient of variation of 22%) but involved considerable effort in obtaining the importance function. The requirement of a global importance function is not something easily met by an adjoint Monte Carlo calculation since, by its very nature, the results are accurate only for a specified region of the problem. Consequently, importances of regions in which a poor estimate of the adjoint is achieved need to be 'fixed up' by means, for example, of interpolation between adjacent regions. A further complication is that, in order for the importance function to be sampled efficiently, the adjoint flux must be scored in many small-sized scoring regions: a requirement that results in an increase variance on the fluxes and a commensurate increase in the computing time required for adequate results.

Goldstein and Greenspan (37) have approached the void problem by means of a recursive Monte Carlo method. One of the features of this method is its reliability in low-importance regions that would prove troublesome in the method of Morrison. In the recursive method the problem is divided into a number of regions defined by surfaces placed about one mean-free-path apart, called reference surfaces. An adjoint source distribtion at the detector region for the forward problem is mapped onto the nearest reference surface, thus defining an importance function for this surface. The importance functions for successive regions can then be found by forward Monte Carlo calculations from the importance distributions on the preceding surface, until every region

from the physical source to the detector has had its importance function defined. Goldstein (38) has applied the technique to the study of a duct penetration problem in a Tokamak with some success. However, the method appears to have several disadvantages.

1. The choice of reference surfaces is largely intuitive.

2. The importance estimates are prone to statistical error.

3. The optimum distance of one mfp between reference surfaces is unattainable for all materials and at all particle energies and so must be liable to compromise.

4. Any errors in an estimate of a region importance are progagated to regions closer to the physical source.

5. The number of surface source particles to be used in estimating the importances is problem-dependent.

6. The overall method is complicated and time-consuming.

Hence, the only apparent advantages over the iterative adjoint-forward Monte Carlo technique of Morrison are that an importance is given to all regions of problem space and the importance function distribution due to many different detectors can be found from, essentially, one run.

An alternative approach, made by some workers, to Monte Carlo streaming problems is that of biasing the particle histories in a manner that takes into account the particles' directions, as described in Sub-Section 3.3.2.

Carter (39) has developed a technique of angular biasing for the Monte Carlo code MCNP that utilises the DXTRAN option of the code. Two concentric spheres are placed at points within the problem towards which the particles are to be

biased. The inner-sphere radius is specified by the user, the outer-sphere radius is determined for each collision site from the condition that the direction of flight be within the solid angle subtended by the inner-sphere one quarter of the time on average. At a collision a pseudo-particle is sent in the direction of the spheres, according to a somewhat arbitrarily defined density function, and given an appropriately altered weight. This pseudo-particle is tracked as a normal particle from the point at which its chosen direction of flight intersects the outer-sphere boundary. A normal scattering is also sampled at the collision point if the chosen direction of flight for this particle lies within the solid angle subtended by the outer sphere its history is terminated, otherwise it continues as usual.

This angle biasing scheme was applied to a problem consisting of a 10.2 cm diameter pipe with two 90° bends defining three 152.4 cm legs. A 14 MeV cosine distributed neutron source was placed at one entrance to the pipe and the current emerging from the other was recorded. Three sets of spheres were placed in the problem: one at each of the two bends and one at the scoring end of the duct.

No comparison with a second method of calculation was performed so a measure of the technique's efficiency can not be made. Also, the selection of the region importances and the weighting of the pseudo-particles is ad hoc, with no guarantee of them being efficient.

Tang, Hoffmann and Stevens (40) have developed an angle biasing technique for multigroup Monte Carlo calculations using the MORSE code. The quadrature used for selecting the angle of scatter (see Sub-Section 5.1.2) is adjusted using the adjoint angular flux for the problem which is found using the discrete-ordinates code DOT-III. This adjustment results in a preferential scatter towards regions of high importance.

The particle weights are altered accordingly. The technique was applied to a 150 cm diameter cylinder with a cylindrical void of radius 7.62 cm along its axial length and a 14 MeV neutron source uniformly distributed over its bottom surface. Scalar fluxes were compared to a similar calculation without angular biasing. The use of angular biasing reduced the fractional standard deviation recorded in each of the four positions by about one-half (to values below 0.2 in all cases).

The technique is presently only available for multigroup calculations and, as such, suffers from the disadvantages of the multigroup method (see Sub-Section 5.1.4). It also uses an adjoint angular flux averaged over regions of the problem space with consequent loss of detail and its dependence on DOT restricts its application to geometries repesentable in two dimensions, precluding its use, for example, on L-shaped ducts. Nevertheless, bearing in mind a two-fold reduction in standard deviation requires (using the same technique) a four-fold increase in the computing time (see Sub-Section 3.3.1), the improvements reported are quite substantial.

5. DATA CONSIDERATIONS

5.1 Introduction

5.1.1 Nuclear Cross-Section Libraries

A prerequisite of any radiation transport calculation is a knowledge of the reaction cross-sections, over a pertinent range of energies, for the materials present in the problem.

The cross-sections for a particular reaction should contain information on the number of secondary particles, if any, produced by an incident particle of a particular energy and on the angular and energy distributions of these secondaries.

Over the past few decades a tremendous amount of effort has been expended world-wide in measuring the cross-sections of a vast number of reactions of value in nuclear reactor (fission and fusion) calculations. Most of this information, augmented with theoretical data where necessary, has been collated, evaluated for accuracy and stored as microscopic cross-sections in nuclear data libraries.

Examples of such libraries are the ENDF/B libraries (42), the UKNDL (43) and KEDAK (44).

The data is held in the form of point pairs (E, σ) where E is the energy of the incident neutron and σ is the appropriate cross-section. The cross-sections at energies intermediate to those specified in the pairs can be derived by logarithmic or linear interpolation. The number

of point pairs varies from nuclide to nuclide and from cross-section to cross-section.

The cross-section information held in nuclear data libraries are not used directly by the computational code performing a calculation: to be of use the information needs to be processed into a format comprehensible to the code. The two formats used in practically all reactor shielding calculations are 'multigroup' and, for Monte Carlo, 'point'.

5.1.2 Multigroup Averaged Data

Any mathematical equation attempting to describe the transport of radiation in its most general terms needs to consider seven independent variables for the particle: three referring to its position in space; three describing its direction of motion; a time variable; and a variable indicating its speed or energy. In solving such equations the energy term is most often treated by the 'multigroup approximation'. This involves dividing the range of interest into a series of abutting intervals called energy groups. The equation being solved is then integrated over each of these groups and solved as a series of 'one-speed equations' coupled to one another by group-to-group scattering terms (11, 45). This procedure is illustrated with reference to the time-dependent neutron transport equation in Appendix A.

Multigroup data can be derived from the nuclear data libraries by processing codes. For example, the code AMPX (46) can process multigroup data from the ENDF/B (42) library, whilst the code GALAXY

(47) can derive multigroup formatted data from the UKNDL. An example of a multigroup data file is EURLIB (48) which was prepared by IKE at Karlsruhe and ESIS at Ispra, mainly from ENDF/B-IV data.

In solving a particular problem with multigroup data a set of such data needs to be defined for each isotope (or isotopic mixture) in the problem. Aside from knowing the isotope for which it is preparing the data, the processing code also needs to know:

1. the range of energies for which the data is to be used;

2. the number and widths of the groups covering this range;

3. the order of approximation to be used in the Legendre expansion;

4. the flux-weighting-spectrum to be used;

5. which of the available reactions on the nuclear data library for the isotope it is to process; and

6. if the processing code can compute Doppler broadening for the cross-sections in the nuclear data library, the temperature of the isotope.

Of these requirements, only the first three, in general, need to be the same for all isotopes in the problem.

Although the multigroup method was conceived as a means of treating the energy variable when solving transport equations by deterministic methods, the multigroup data it gives rise to has some distinct advantages when used in Monte Carlo calculations. These advantages are discussed here.

A Monte Carlo calculation using multigroup data assigns each particle to a group according to its energy. All particles within a group are treated without regard to their individual energies. Most notably, the scattering laws relate to scattering probabilities from group to group using the group constants defined in Appendix A. The energy group of a particle emerging from a scatter event is implicitly contained within the transfer cross-section for a collision and is selected with a probability given by the ratio:

$$\sigma_{s_0,g'\to g} : \sum_{g} \sigma_{s_0,g'\to g}$$

where $\sigma_{s_0,g'\to g}$ is the group constant for scatter from group g' to group g for the first Legendre moment.

The angular distributions are represented in multigroup data as Legendre expansions of the cosine of the scattering angle and angles of scatter can be selected from these distributions. However, to do so is computationally time consuming and it is more usual to select from a discrete set of angles, with

probabilities derived from the Legendre expansions by means of a generalised Gaussian quadrature (49). In the Coveyou technique (53) the number of these discrete directions can not exceed $\frac{1}{2}(N+1)$ where N is the order of the Legendre expansion approximation.

5.1.3 Point Data

The requirement that nuclear cross-sections should be supplied in multigroup form arose only out of the desire to make the mathematical equations describing the transport of radiation more amenable to solution by deterministic methods. In the Monte Carlo technique, since the calculation is in the nature of a simulation of the behaviour of the radiation and not an attempt to solve a transport equation, it should be possible to make use of the data in nuclear data libraries without losing some of its detail by averaging.

To this end, codes have been written to prepare data from nuclear data libraries in a form which enables Monte Carlo codes to gain full benefit from their cross-section information. Monte Carlo codes employing this format of data are known as continuous energy or 'point' codes because they allow the particles they track to retain their individual point energies; the data sets themselves are called 'point' or 'point averaged'. (Throughout the remainder of this chapter reference will be made to DICE-VI (50) which is a suite of program subroutines, suitable for use in Monte Carlo codes, that employs data from the UKNDL in point form).

Since in calculations using point data each particle tracked has a specific energy the cross-sections used are such that they are effectively continuous functions of energy. This is achieved, in general, by dividing the energy range of interest into groups in a manner similar to the multigroup method. However, the number of groups in a point averaged data set is far greater than that in a multigroup set: DICE-VI, for example, uses data with over 8000 groups for neutrons covering the range 15 MeV to 0.1 eV, whereas in multigroup one would expect, perhaps, about 100 groups.

The cross-sections are assumed to be constant over each of the energy groups and are derived by averaging the cross-sections from the nuclear data libraries over the group widths. The averaging process, unlike multigroup, is straightforward: it involves no variables other than the cross-sections themselves; in particular, there is no need to weight with a flux spectrum as there is in the preparation of multigroup data. DICE-VI, as an example, uses an harmonic average over the group width as the group cross-section.

In continuous energy Monte Carlo calculations the angle of scatter for secondary particles can be sampled directly from the angular distribution for a particular reaction which is represented as a set of discrete-angles and associated probabilities. If the number of the discrete angles in this representation is sufficiently large then linear interpolation can be used to yield the probability of scatter through angles intermediate to those specified. For example, DICE-VI uses 32 equiprobable angular intervals. It is convenient

for the discrete angles to be chosen such that they define equiprobable angular intervals, as this allows for a rapid selection of scatter angle in the following manner.

Suppose that the number of discrete angles, μ_i, and hence, the number of intervals (μ_i, μ_{i+1}) chosen is N and that ρ is a number selected at random in the interval (0,1), then the angle of scatter μ can be found from:

$$\mu = \mu_j - (j - N\rho)(\mu_j - \mu_{j-1})$$

where μ refers to the cosine of the polar angle of scatter and j is that i immediately greater than $N\rho$; the azimuthal angle ϕ is selected from a uniform distribution in the range $0 \leq \phi \leq 2\pi$.

5.1.4 The Relative Merits of Multigroup and Point Data For Fusion Reactor Monte Carlo Shielding Calculations

It is generally maintained that the use of multigroup data in radiation shielding calculations provides results to a degree of accuracy that is greater than that justified by the uncertainties in the nuclear data. To a large extent this is true, as is witnessed by its continuing and extensive use in modern shielding codes. However, it is apparent that in Monte Carlo codes point data affords a more accurate representation of the physical process being simulated and should, therefore, provide more reliable results. In

particular, with point data there is no loss of cross-section detail caused by averaging as there is in multigroup; the direction of scatter is not restricted to one of a number of discrete directions; and the laws governing energy loss in a collision can be used explicitly rather than in terms of transfer cross-sections.

A severe test of calculations employing multigroup data is in the handling of the anisotropic scatter of neutrons. At energies above about 0.1 MeV the angular distributions of scattered neutrons in the centre-of-mass frame of reference become, in general, forward-peaked. This anisotropy increases with increasing energy. Moreover, scattering that is isotropic in the centre-of-mass system becomes forward-peaked in the laboratory frame of reference, regardless of energy. However, this effect is significant only for light nuclei. Thus, in the laboratory frame of reference, anisotropy is most evident in scattering from light nuclei and in the scattering of fast neutrons from all nuclei. Treatment of this anisotropy greatly influences the effectiveness of neutron transport methods in predicting neutron behaviour, particularly deep within shields. The satisfactory representation of highly anisotropic scatters in multigroup methods involves a prohibitively high number of terms in the Legendre approximation of the angular distribution being used (63). For example, see Figures 4 and 5 (taken from Reference 51) for Legendre representations of the Li_7 group-to-group scatter cross-section from a group with energies in (14.55 - 14.92 MeV) to a group with energies in (9.512 - 10 MeV).

Using discrete angles of scatter in Monte Carlo can give rise to ray effects (notably in problems involving streaming) similar to those that can occur when using the S_n method (see Section 3.4). There is also an additional anisotropy introduced by using the multigroup method: the restrictions it imposes on the energies of the neutrons correspondingly restrict the angles through which these neutrons can scatter.

Clearly, none of the above problems occur when point data is used. However, with the point data presently available no facilities exist for the combined tracking of neutrons and gamma-photons.* This is a great disadvantage, in particular, in fusion reactor calculations where gamma induced insulation damage and gamma heating of the toroidal field coils are major constraints on the overall shield design.

Furthermore, the treatment of interactions by codes using point data is more complex than when multigroup data is employed and, hence, demands more computer time.

5.2 A Comparison of Results from Tokamak Monte Carlo Calculations with Various Nuclear Data

5.2.1 Point Data and Multigroup Data Comparison

In order to assess the difference in results obtained using multigroup averaged and point data in Monte Carlo shielding calculations for fusion

---

* The Los Alamos Code MCNP now has the ability to perform coupled, point-energy neutron-photon calculations (65).

reactors, both methods were used to predict neutron fluxes in a simplified model of a reactor.

The point data available for use (DICE-VI) employs data from the UKNDL; thus, to prevent differences in microscopic data from masking the effects of multigroup averaging, the multigroup data to be compared were derived from the same UKNDL files. The processing code GALAXY (47) was used to prepare P_5 multigroup data for the materials in Table 1.

The neutron energy groups chosen were the same as the first 80 groups in the EURLIB (48) multigroup set and are shown in Table 2. All the data were prepared using the same flux-weighting-spectrum which was identical to that used in the preparation of the EURLIB data (Table 3).

The model for which the calculations were made was based on the Culham Conceptual Reactor Mk II (36). To ease the modelling, circular cross-sections were assumed for the main reactor components and no ducts were included. The toroidal curvature was simulated using cylinders truncated with reflecting planes at 9° to each other. The toroidal field coils (TFCs) were represented by including a half in each sector defined by the reflecting planes; thus allowing 20 TFCs in the problem (Figure 6). The dimensions of the configuration are indicated in Figure 7. Combinatorial geometry (27) techniques were used to assimilate the model into the code MCBEND.

The finite-element diffusion code FENDER was used to provide the importance map for the problem. An adjoint source with a value of unity in all groups

was placed at the outer limb of the TFC which was represented as continuous in the RZ geometry of FENDER. The mesh used is shown in Figure 8. Reflecting planes were included in both the FENDER and the MCBEND geometries to exploit the symmetry about the horizontal axis. The voided regions were represented in the FENDER calculation by low density (10^{-6} atoms/barn.cm^{-3}) aluminium.

The source neutrons in MCBEND were started at points randomly distributed within the plasma which was assigned a diameter 80% that of the vacuum chamber diameter to the first wall. The selection of the source neutrons' directions was biased so as to be isotropic in the positive z half-space. In the multigroup data calculation all source neutrons were in the first energy group; in the point data run the source was assumed mono-energetic with an energy of 14.2 MeV.

The calculations were performed on an ICL 2976 computer. The multigroup run took 5820 seconds* of CPU time to track the histories of 10000 particles sampled from the source whereas the point run took 7056 CPU seconds* to track the same number of samples. The coefficients of variation on the group fluxes scored in the TFC due to Monte Carlo statistics ranged from 8.4% to 48.9% in the point data case and from 10.0% to 58.4% in the multigroup case. The total copper damage rate in the TFC was also computed in each case to within a coefficient of variation of 5%.

---

* 1.0 ICL CPU second in this type of problem is approximately equal to 0.15 CPU seconds on an IBM 3033.

The Cu damage cross-sections were taken from Doran and Graves (52).

A graph comparing the two sets of group fluxes obtained in the TFC is shown in Figure 9 and the Cu damage rates over the groups are shown in Figure 10.

The Cu damage rate recorded in the point data run was 19% higher than that in the multigroup case (Table 4).

Whilst this discrepancy is tolerable in preliminary designs of shield layouts for fusion reactors, it would become very important in any final design.

There are three possible causes for the discrepancy:

1. the angular distribution representation in the multigroup method;

2. the energy-loss laws used in the multigroup method;

3. the flux-weighting-spectrum used in preparing the multigroup data.

It would be possible to test the contribution of the first cause to the observed discrepancy, by increasing the order of the Legendre approximation to one greater than P_5. However, a P_5 expansion is generally considered to provide accurate enough results for most shielding calculations, making higher order expansions unnecessarily expensive. The second possible cause is inherent in the Monte-Carlo method's treatment of multigroup data and is not readily examined. A test of the third possibility was performed and is described below.

5.2.2 The Effect of Using Multigroup Data with a Fusion Spectrum Weighting

The flux-weighting-spectrum used in the preparation of the P_5 multigroup data employed in the comparison described above was compared to the flux-per-energy interval in the various scoring regions as computed in the point data run of the same comparison. The greatest difference between the two occurred in the hot-shield of the reactor model and over the first ten energy groups (ie, 15 MeV →6.5 MeV) of the multigroup scheme (Figure 11).

To see what affect changing the flux-weighting-spectrum to one more representative of a fusion reactor spectrum would have on the results the following investigation was performed.

Firstly, the flux in the hot-shield over the first 15 energy groups was calculated more precisely by running a second point-data MCBEND which used importances provided by a FENDER calculation with the adjoint source placed in the hot-shield region. The flux-per-energy-interval resulting from this calculation was then used as a flux- weighting-spectrum in the preparation of P_5 multi- group data from the UKNDL. The fusion spectrum covered the first 10 groups whilst the remaining 5 groups were 1/E weighted.

A MCBEND calculation using the newly prepared multi-group data was used to compute the flux in the hot-shield for the 15 groups. A comparison of the flux recorded in the hot-shield with that in the previous MCBEND calculation using multigroup data is shown in Figure 12.

The difference in the values of the group fluxes is seen to be small and there is no diminishing of

the discrepancy between the fluxes obtained in this multigroup data run and the previous point data run.

It can be concluded, then, that using a flux spectrum that is more typical of that expected in a fusion reactor, as a weighting function in the preparation of multigroup data, is not likely to improve the results of Monte Carlo calculations over those obtained from using multigroup data that have been prepared with a 'fission' flux-weighting-spectrum.

5.2.3 EURLIB and UKNDL Multigroup Comparison

In addition to the Monte Carlo calculations using point data and P_5 multigroup averaged data derived from the UKNDL, the same problem was computed using the P_3 EURLIB multigroup averaged data. A comparison of the fluxes obtained in the toroidal field coils using this data to those obtained using the UKNDL data is shown in Figure 13. The integrated copper damage responses are shown in Table 4. The discrepancy between the EURLIB results and the point-data results is even greater than that between the UKNDL multigroup results and the point data. The discrepancy is too large to be considered insignificant even in provisional calculations for a Tokamak shield design and deserves further investigation.

5.3 A Benchmark Test of EURLIB and DICE Format Data

5.3.1 Introduction

The discrepancies recorded in the work described in the previous section, between the results obtained using multigroup data and those obtained using point data are large enough to merit investigation.

The standard method of testing the integrity of cross-section data is to use the data to predict the results of an experiment specially designed for this purpose. Such tests are commonly known as benchmarks.

It was decided to use the EURLIB multigroup data and the UKNDL point data in otherwise identical Monte Carlo calculations to predict the results recorded in a suitable benchmark experiment and to compare the accuracies of their predictions.

A search of the readily available literature showed that very few benchmarks concerned with fusion reactor shielding had been performed. Some which had are described briefly here. Of these, most were deemed unsuitable, for various reasons, for the purposes of the present study.

Marshall and Knight (54) performed measurements of the attenuation of fast neutrons through water, concrete, steel, polythene and combinations of steel and polythene, and also of scattered neutrons, from a 14 MeV source, along a concrete maze. As the experiments were not intended for comparison with computed results their geometries did not lend themselves easily to modelling. Also, there were no details of shield composition given; the measurement position was fixed and measurements (of the neutron dose-equivalent) were made for the various shield thicknesses thus requiring any comparative calculations to comprise of separate calculations, one for each shield thickness.

Hashikura et al (55) have performed benchmark tests on 14 MeV neutrons streaming down various ducts and slits in concrete shields. The neutrons were

produced in a tritiated target by bombardment with deuteron from a 160 KeV Cockroft and Walton generator. The neutron energy spectra were measured at one point at the end of each of the ducts, which would again entail performing more than one calculation in any computational comparison. Another reason for not using this as a benchmark experiment was that the results are quoted as integral fluxes and sketch graphs of the neutron spectra, whereas, ideally, a more detailed set of results would have been preferred for comparison especially if results were to have been computed for only one point in each calculation.

Benchmark experiments to test the EURLIB-3 multigroup data have been performed by Schriewer et al (56). Included in these benchmarks was a test of the ability of the data to predict, in discrete-ordinates calculations, the neutron leakage spectrum from an iron cylinder placed axially adjacent to a generator target producing 14 MeV neutrons. The reference consulted had, however, very brief experimental details and the results were presented only in the form of graphs. Moreover, it was clear that measurements of neutron attenuation had not been made.

Santoro et al at the Oak Ridge National Laboratory, USA, have performed a series of experiments (57 and 58) in which they measured the spectra of neutrons and gamma-rays emerging from the reactions of ~14 MeV neutrons in fusion reactor shield materials and from the shielding of these neutrons through a cylindrical duct. The materials used included stainless-steel, iron, borated polythylene and Hevimet (a tungsten alloy). The experimental configurations were such that they could be modelled

easily and the details given were sufficient to model the cases with very good accuracy. Again, however, the results were presented only in graph form. The spectra were measured at fixed points away from the shield and no measurements were made of the neutron attenuation within the shield. Several benchmarks with fusion reactor blanket materials have also been performed but these were considered to be of secondary importance to the radiation shielding studies, for which measurements of neutron spectra at several points within the shield were preferable so as to measure the neutron attenuation.

The benchmark experiment chosen was originally performed by the National Radiological Protection Board (NRPB) to assess the reliability of EURLIB data in DOT3.5 (a two-dimensional discrete-ordinates code) calculations of the attenuation by iron of 15 MeV neutrons (25). This experiment was chosen because it appeared easy to model, it had measurements at four points within the shield and the dominant shield material was iron which is used extensively in fusion reactor shield designs; moreover, the experiments were reasonably well documented in a report which was easily obtainable. The experimental details are available in Reference 25 but will be outlined here for completeness.

5.3.2 Description of the NRPB Benchmark Experiment on the Attenuation of 15 MeV Neutrons by Iron

The arrangement through which the attenuation of the 15 MeV neutrons was to be measured consisted of 27 vertical mild-steel plates each measuring 183 cm x 183 cm x 5 cm and placed in parallel so that the overall shape of the shield was approximately cubic.

The shield was surrounded by concrete blocks for most but not all of its length.

The neutrons were generated at a point on the horizontal axis of the shield 4.2 cm in front of the first plate. A tritiated target placed at this point was bombarded by a beam of 300 KeV deuterons from a SAMES particle accelerator to produce an intense source of 15 MeV neutrons (of up to 10^{12} neutrons.s^{-1}).

Since the calculated and measured results were to be normalised to one source neutron, the neutron output monitors were calibrated by fission foils mounted behind the target at 155° to the direction of the deuteron beam.

Measurements of the saturated activity of a number of threshold activation and fission foils were made at four positions within the shield. During each irradiation the eleven foils were mounted in a circle, the centre of each foil being about 4 cm from the horizontal axis of the shield. The circle of foils was placed within the air gaps following plates 3, 6, 9 and 12. A measurement was made in only one position on each run and at least three separate measurements were made at each position.

5.3.3 Calculation of the Detector Responses in the NRPB Benchmark by Monte Carlo

The EURLIB multigroup data was used in a MCBEND calculation to predict one of the detector responses recorded in the NRPB benchmark experiment.

In order to reduce the variance on the Monte Carlo results splitting and Russian Roulette were performed with the adjoint scalar fluxes from the

code FENDER used as importance values. Since FENDER is a two-dimensional code the problem geometry was approximated with a cylinder of mild-steel surrounded for most of its length by a cylindrical shell of concrete. The density of the mild-steel used in the FENDER calculation was reduced to take account of the air gaps between the steel plates in the actual problem and the cross-sectional area of the cylinder was chosen to be the same as that of the steel plates. The densities of the mild-steel and concrete used in the FENDER problem are shown in Table 5.

To allow the code to treat the void regions with the diffusion approximation, very low density aluminium (10^{-6} atoms/barn.cm^{-3}) was used to fill the air gap between the plates and the concrete surround.

Reflecting planes were placed along both the horizontal and vertical axes of symmetry.

A point, isotropic source emitting neutrons in the first energy group of the EURLIB scheme (13.5 → 14.9 MeV) was placed on the horizontal axis of the shield 4.2 cm in front of the first steel plate (Figure 14). It was decided to calculate the saturated activities of a sulphur foil placed at each of the four measurement positions in the experiment, that is, in the air gaps following plates 3, 6, 9 and 12. The group fluxes and integrated sulphur responses were calculated over volumes measuring 8 cm x 8 cm x 1 cm centred on the horizontal axis and placed within the air gaps behind the relevant steel plates.

The S32(n,p)P32 reaction was chosen for study since the range of neutron energies for which the response is significant (it has a threshold at about 3 MeV) corresponds to that over which the nuclear data for fusion reactor calculations needs to be tested and also because the experimental errors quoted for this reaction were relatively small. The group cross-sections used in the calculation for this reaction were condensed from the International Reactor Dosimetry File (59).

The calculation was performed on an ICL 2976 computer until the coefficient of variation due to Monte Carlo statistics on the response recorded in the fourth (ie, furthest from the source) scoring region was below 10%.

The calculated saturated activities for the sulphur foil (normalised to one neutron) are shown with the measured values in Table 6.

The EURLIB data overpredicts the response in the two scoring regions nearest the source and underpredicts it in the two furthest from the source. The percentage differences in the calculated and measured responses (with respect to the measured) are +62%, +9%, -15% and -24% for the scoring regions.

These results can be compared to those obtained by D G Jones in his analysis of the NRPB benchmark experiment with DOT3.5 and EURLIB (25). Jones obtained results which indicated a 70% underestimate of the flux in the range 0.3-3 MeV at the fourth scoring region. Also, the results of Schriewer et al (56) showed that using EURLIB data in DOT calculations to predict the neutron leakage

spectrum from an iron cylinder, due to a 14 MeV neutron source, produced an underestimate of the flux between about 1.3 and 11.5 MeV. This was attributed to the energy degradation from inelastic scattering being too strong.

There are several possible causes of error in a benchmark; these can be separated into experimental errors and calculational errors and can be categorised as follows:

I Experimental Errors

(a) systematic errors in the experiment, eg in calibrating the energy and intensity of the source or in the calibration of the activation foils;

(b) random errors in the measurements.

II Calculational Errors

(a) errors in the representation of the experimental arrangement in the calculation and, in particular, the source;

(b) approximations inherent in the calculational technique;

(c) errors in the conversion factors used to give the response from the calculated group fluxes;

(d) errors in the nuclear data - specifically in the microscopic cross-sections but also covering the

preparation into a form suitable for the calculation.

The combinatorial geometry modelling routines of MCEBND are versatile enough to represent most complex sources and material configurations with great accuracy. In the NRPB benchmark the experimental arrangement was kept simple deliberately and can be modelled almost exactly so that this contribution to the error II (a) is negligible. However, the source is simplified in the calculation to an isotropic one which may introduce some error.

The Monte Carlo method itself is a tried and trusted technique for radiation transport calculations and the code MCBEND has been used extensively for many years; thus, the error II (b) can be considered negligible.

The error II (c) is not known exactly in this case; however, it would certainty be less than II (d) and so its relative contribution to the discrepancy is small but, perhaps, not entirely insignificant.

Systematic experimental errors, I (a), would manifest themselves as consistent errors throughout the measured results; the only such error recorded is a possible one of 20% on the calibration of the source.

Random errors can not be eliminated but can be limited by careful experimental procedure. The random errors in the NRPB benchmark are assumed to be negligible.

Possibly then, the largest contribution to the overall calculational error is that from uncertainties in the nuclear data. The measured group-flux for the first energy group in the first measuring position falls by a factor of about 5000 to that in the last (25). The inverse square law accounts for a factor of about 12.

The sensitivity of the flux to the cross-section uncertainties can be estimated from the measured fluxes by assuming an exponential decrease in the flux given by:

$$\phi(x) = \phi(o)e^{-\Sigma_t x}$$

where Σ_t is the total macroscopic cross-section. From which:

$$d\phi = -\phi(o)xe^{-\Sigma_t x}\, d\Sigma_t$$

$$\therefore \quad \frac{d\phi}{\phi} = -x d\Sigma_t$$

$$= \ln \left(\frac{\phi(x)}{\phi(o)}\right) \frac{d\Sigma_t}{\Sigma_t}$$

$$\simeq 6 \frac{d\Sigma_t}{\Sigma_t}$$

This rough calculation shows that a fractional error in the total nuclear cross-section for neutrons in the first energy group would result in a fractional error in the calculated flux about 6 times as great. Clearly then, a 10% error in the cross-sections may account for the observed discrepancy between the measured sulphur responses in the NRPB benchmark and those computed using EURLIB data in a MCBEND calculation.

5.3.4 Calculation of the Nuclear Data Sensitivities in the NRPB Benchmark Calculation

The sensitivities for a MCBEND calculation using point data can be estimated, using a perturbation method, by the DUCKPOND facility (60). A MCBEND calculation was performed with DUCKPOND to estimate the sensitivities of the responses in the NRPB benchmark to uncertainties in the nuclear cross-sections of the UKNDL.

The MCBEND calculation using point data (DICE-VI) was identical to that using EURLIB data except that:

1. the source was given a point energy of 14.2 MeV which is the median energy of the first group in the EURLIB multigroup scheme (the error associated with this is acceptably small since the total cross-section for iron at 15 MeV is very little different from that at 14.2 MeV)

2. DUCKPOND was used to estimate the sensitivities of the sulphur response to uncertainties in the elastic and non-elastic cross-sections, over the same group scheme as that used in the EURLIB calculation for scoring the group fluxes.

The responses calculated for the S32(n,p)P32 reaction were overpredicted in all four measurement positions. The percentage differences between calculation and measurement from the scoring position nearest the source to the furthest are 76%, 50.1%, 34.7% and 13.9% respectively.

The sensitivities estimated by DUCKPOND in this second MCBEND calculation were used to calculate approximate variances on the calculated responses due to the uncertainties in the cross-section data from (61). The theory behind this is described in Appendix B.

The calculated responses in the four scoring regions with their variances, inclusive of the contributions from uncertainties in the nuclear cross-sections and from the statistical variances due to the Monte Carlo method, are shown in

Table 7. A diagram comparing the calculated results and the measured results are shown in Figure 15.

The cross-sections to which the responses proved most sensitive were the non-elastic cross-sections of iron for neutrons with energies above 11 MeV and in the range 4.5 MeV to 2.5 MeV.

The addition to the calculated results of a variance due to cross-section uncertainties brings the measured results to within one standard deviation of the calculated in all the scoring regions bar the first.

The reasons for the discrepancy in the first scoring region are not obvious but it must be due to some error caused by the approximations used in modelling the experiment. Such an error would probably also have affected the results calculated in the other three regions. Furthermore, the gradient of the graph in Figure 15 is indicative of an error in the source representation.

However, it is clear that in all four scoring regions a major contribution to the variance is from uncertainties in the cross-sections. If accurate Monte Carlo calculations are to be made for fusion reactor shielding design studies the accuracies of the cross-section data used need to be improved.

An improvement could be obtained by adjusting the cross-sections so as to make them produce results which agree with some set of experimental measurements. This technique has proved useful in the past when the adjusted cross-sections have been

used in calculations on configurations which resemble those on which experiments were made. If the geometry or material composition is significantly different then the adjusted cross-sections become less reliable and the accuracies of the calculated results are brought into doubt.

A more satisfactory improvement would be to remeasure those cross-sections to which calculated responses important to fusion reactor shielding are most sensitive. For example, it has been shown in this chapter that the calculation of neutron attenuation in iron by Monte Carlo is very sensitive to the iron non-elastic cross-section in the range 4.5 MeV to 2.5 MeV and above 11 MeV. Further calculations of the sensitivities to pertinent cross-sections of responses important to fusion reactor shielding should be performed. From these calculations the cross-sections contributing greatly to the variance on the calculated values of important responses can be assessed. These cross-sections should then be remeasured. Until this is done the accuracy of Monte Carlo calculations is going to be greatly limited by the uncertainties in these cross-sections.

6. ANGULAR BIASING OF A MONTE CARLO RADIATION TRANSPORT CODE

6.1 Introduction

As suggested in Chapter 4, there are two distinct approaches to the problem of streaming in Monte Carlo calculations. One is to employ a method other than Monte Carlo (such as line-of-sight or an albedo method) for the treatment of radiation transport within the streaming paths and interfacing the results of this calculation with the Monte Carlo calculation used for the main body of the problem (66). Another is to use Monte Carlo for the whole problem but to employ special techniques to overcome the problems presented by radiation streaming.

The former approach is inherently complicated. It can be broken down into two calculations, one for the bulk material and one for the streaming region, the source for one being augmented by the results of the other. These two calculations are not separate: they are coupled in that fluxes computed in the streaming calculation will provide secondary sources for the calculations in the surrounding material and vice versa. Thus, the application of this approach entails repetitive bulk material/streaming calculations: a process which can prove expensive, if accurate solutions are sought, and demands the interfacing of results from one calculation for use in the other, which often entails the writing of supplementary codes and can lose detail in the variances on the Monte Carlo results. The albedo data often used in such calculations can be difficult to obtain, are not always accurate and can be invalid for the particular case (eg, when plane surface albedo data are applied to curved surfaces). Also, some techniques for dealing with streaming are limited in their handling of complex ducts. Nevertheless, such techniques have proved adequate for design work in the past (66).

Incorporating techniques into the Monte Carlo code itself which deal intrinsically with the streaming problem is more satisfying than the first approach in that it eliminates the repetitive solution of two coupled calculations and the concomitant need for interfacing their results. It also allows accurate representation of the variances on the results and there is no need, in general, for albedo data. Such an approach should prove more efficient in terms of manual effort, as there would be very little extra manipulation to be performed, and in computing time, as the calculation need not be repeated until an acceptable convergence is obtained.

There has been a growing awareness in the shielding community recently that, with computing time becoming cheaper relative to man-hours, it is less feasible to spend time in indirect computations than it is to have an automated method, requiring the minimum of manual preparation, run directly with, perhaps, an extra amount of computing time (67). For this reason, the approach of incorporating special techniques to deal with streaming into the body of the code is pursued in this thesis.

In this Chapter two methods of accelerating Monte Carlo calcuations with dominant streaming paths are described: directional importance biasing and collision angle biasing. Both entail encouraging particles to use the streaming paths by means of an angular importance function. Directional importance biasing employs this angular importance function in much the same way as splitting and Russian Roulette employ a scalar importance function. In collision angle biasing the direction of a particle emerging from a collision is sampled from the angular importance distribution for a particle of that energy at the point of collision; the particle is then weighted according to the probability of it being scattered in that direction

had the direction been sampled from the distribution given by the nuclear data.

6.2 Directional Importance Biasing in Monte Carlo

6.2.1 Previous Possibilities in MCBEND

Directional importance biasing is an extension of splitting and rouletting (SR) to include a particle's direction as well as its energy and position. It requires the use of some form of importance function that includes the particles' directions.

An option for angular biasing particle histories had been made available in MCBEND in early 1983. The method used consisted of defining, largely by intuition, a direction of greatest importance for each material region, constructing around this direction a set of angular intervals and giving an importance value, again by intuition, to each of these intervals. The weight of a particle emitted from a collision was adjusted, in the same manner as SR, according to the importance of the angular interval of the appropriate distribution it emerged into. (See Sub-section 3.3.2.)

An obvious disadvantage of this method is that 'the direction of greatest importance' is fixed for each material region and so, abrupt changes in this direction - such as would occur around the bend of a duct - call for the specification of different material regions in these localities. However, a more important disadvantage is the ad hoc nature of specifying the importance distribution for each material region: the

direction seen as being of greatest importance by the user need not necessarily be so in reality (this is especially true in complex problems with voids or highly absorbing regions) and the angular intervals and importances will not accurately reflect the true angular importance distribution at all points for which they are defined. Nevertheless, the basic idea of the method is reasonably sound and the importances need only be approximate to give a noticable improvement on the variance of results over cases without any variance reduction.

The method was tested on a closed, three-legged duct of circular cross-section sheathed in stainless-steel and embedded within concrete. A diagram of the problem geometry, indicating the regions used in defining the angular distributions, is shown in Figure 16. A point source of 14.2 MeV neutrons was placed on the axis of the open-ended leg of the duct 18 cm from its opening.

Firstly, MCBEND was run without variance reduction of any kind, then the angular biasing option was run to bias the particles towards the closed end of the duct. Both runs used the first 80 groups of the EURLIB multigroup data (Table 2) and both scored the flux in 10 regions throughout the problem. The direction of greatest importance for each region was defined by four target points one at the open end of the duct, one at the closed end and one at each of the two duct bends. The distributions for the angular biasing were as shown in Figure 17.

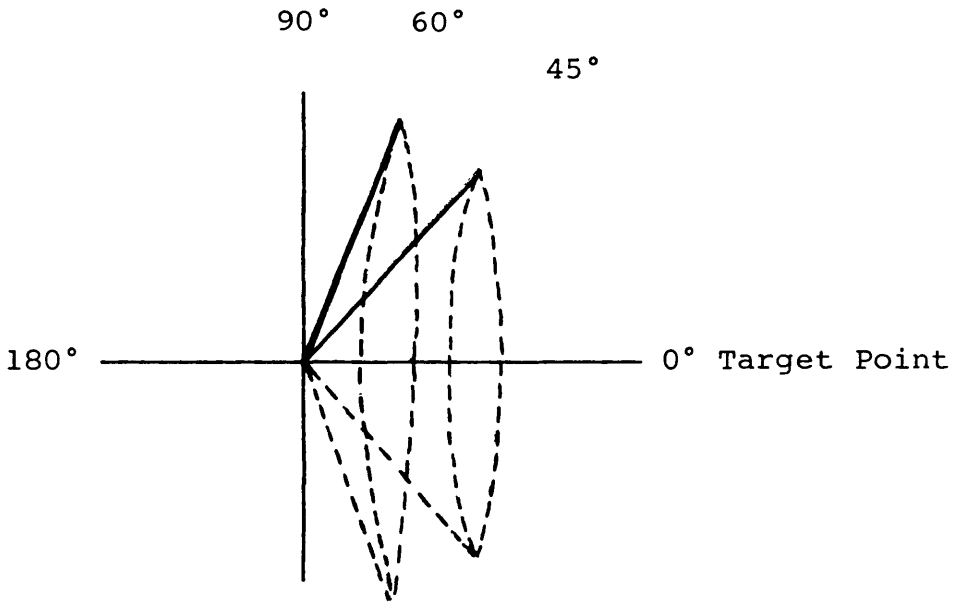

Angular Interval	Importance
0° - 45°	1.0
45° - 60°	0.75
60° - 90°	0.5
90° - 180°	0.1

FIGURE 17: Quadrature for Test of Old Angular Biasing Method in MCBEND

In the case where no angular biasing was used only 9 groups scored in the scoring region at the closed end of the duct, of these only 3 (groups 39, 40 and 41) had a coefficient of variation on the flux of less than 100% (the least being one of 69% for group 41). With angular biasing, scores were obtained in 18 groups but only 3 (groups 36, 42 and 45) had a coefficient of variation of less than 100% (the least being 74.3% for group 42).

An importance function was defined for an xyz-mesh overlaid on the problem geometry. The importances were chosen from the attenuation expected in each of the three coordinate directions. Using this importance function in the problem, without angular biasing, resulted in the flux being scored in 45 groups with 26 having a coefficient of variation of less than 100% (the lowest being one of 60%). Using this importance function in conjunction with the angular biasing scheme of Figure 17, resulted in 43 groups being scored in with 11 having a coefficient of variation of less than 100% (the lowest being one of 65.5%).

Although the results from these simple calculations are very crude, they illustrate that the use of this angular biasing method in MCBEND is not likely to prove beneficial in solving a problem unless the biasing parameters are carefully defined, a requirement that may entail the use of several test runs in much the same manner as when guessing spatial or energy dependent importances.

In spite of the discouraging results, it was thought that the method could be refined by allowing the angular importance distributions to be defined over a finer mesh than the material regions and by using as importances for the intervals values closer to the actual importances of particles travelling in those intervals. The first improvement would have been straightforward: the second would have been more difficult.

An idea of assessing the importance of each of the angular intervals, by recording the contributions

made to the final score by particles travelling in each of them, was dismissed as impractical since large numbers of particles would need to be sampled before estimated importances converged upon suitably accurate values and, assuming a large number of these distributions and bearing in mind the group dependence of such importances, a prohibitive amount of computer storage would be required.

If this method of angular biasing was to be utilised with any success it was clear that a better understanding of the importance of particle directions throughout the problem geometry was required.

6.2.2 Definition of An Angular Importance Function

As was mentioned in Sub-section 3.3.2 the importance in a Monte Carlo calculation of a particle with a particular energy and at a particular point in the problem geometry, can be equated with the adjoint scalar flux of particles with that energy and at that point in space. Likewise, the importance of a particle with a particular energy, at a particular point in the problem geometry and with a particular direction can be equated to the adjoint angular flux of particles with that energy, position and direction. If it could be obtained easily and cheaply, the adjoint angular flux could be used as an importance function for accelerating a Monte Carlo problem in which the angular biasing of particle histories is to be employed.

The finite-element code FENDER (15) can be used to calculate a diffusion approximation to the adjoint scalar group fluxes of neutrons over a two-dimensional mesh; the Monte Carlo code MCBEND can use these adjoint fluxes as importances for accelerating the problem using splitting and rouletting.

Unfortunately, as it stands, FENDER is incapable of computing angular fluxes so what was required, in order to define an angular importance function, was a means of finding the adjoint angular flux over the problem space, avoiding (like FENDER) the necessity of manually transfering these to MCBEND. A simple way to do this was for MCBEND to derive the adjoint angular flux from the adjoint scalar fluxes provided by FENDER. This was achieved to a degree of approximation consistent with the diffusion theory used to derive the scalar flux itself, in the manner described in Appendix C.

The result is that, in two dimensions,

$$\psi_g^*(r,\underline{\omega}) = \frac{1}{4\pi}\left[\phi_g^*(\underline{r}) + 3D_g\left|\underline{\nabla}\phi_g^*(\underline{r})\right|\cdot\mu\right]$$

where $\psi_g^*(r,\underline{\omega})$ is the adjoint group angular flux at $\underline{r}$ in direction $\underline{\omega}$;

$\phi_g^*(\underline{r})$ is the adjoint group scalar flux;

D_g is the group diffusion coefficient of the material containing $\underline{r}$;

$\underline{\omega}$ is the direction of the flux gradient;

and

$$\mu = \frac{\underline{\nabla}\phi^*_g(\underline{r}).\omega}{|\underline{\nabla}\phi^*_g(\underline{r})|}$$

ie, the cosine of the angle between the gradient of the scalar flux and the direction of the particle.

This expression is a diffusion approximation to the adjoint angular flux and, as such, it assumes a shallow flux gradient and a low absorption cross-section. In conditions other than these it is possible for the expression to give an angular flux that is negative. Since importances can not be negative (a particle can not make a negative contribution to the result) the equation must be altered in some way to prevent it giving a negative value for the adjoint angular flux.

Several schemes to prevent the expression becoming negative were tried. Included in these were: the introduction of a minimum value, expressed as a fraction of the adjoint scalar flux, below which the importance was assumed to be constant; using a function that went linearly to zero at $\mu = -1$ for negative μ; and using the reciprocal of the importance for μ for $-\mu$.

The scheme that gave satisfactory results most consistently, however, was one which used a 'flux-limited' diffusion constant for negative μ. (The schemes need only be applied to importances for negative μ since the expression above can not give

negative angular fluxes for positive μ.)
Flux-limited diffusion theory is an attempt to reconcile classical diffusion theory, as characterised by Fick's Law, with the physical requirement that the magnitude of the current at all points should be less than the scalar flux at those points (68). This can be achieved by defining a D'_g, somewhat arbitrarily, as

$$D'_g = \frac{1}{1/D_g + 3\left|\underline{\nabla}\phi^*(\underline{r})\right| \; / \; \phi^*_g(\underline{r})}$$

with D'_g replacing D_g in the expression for the adjoint form of Fick's Law for a group g, ie:

$$\underline{J}^*_g(\underline{r}) = D'_g \left|\underline{\nabla}\phi^*_g(\underline{r})\right|$$

it can be seen that:

(a) $\left|\underline{J}_g(\underline{r})\right| \to \frac{\phi^*_g(\underline{r})}{3}$ as $\left|\underline{\nabla}\phi^*_g(\underline{r})\right| \to \infty$,

(b) $\left|\underline{J}_g(\underline{r})\right| < \frac{\phi^*_g(\underline{r})}{3}$ always,

and

(c) $\underline{J}^*_g(\underline{r}) \to D_g \, \underline{\nabla}\phi^*_g(\underline{r})$ as $\underline{\nabla}\phi^*_g(\underline{r}) \to 0$.

Of the conditions above, (b) ensures that the expression for $\psi^*(\underline{r},\underline{\omega})$ is always positive. Hence, this expressin can now be altered to give a flux-limited diffusion theory approximation to the adjoint angular flux as:

$$\psi_g^*(\underline{r},\underline{\omega}) \approx \frac{1}{4\pi}\left[\phi_g^*(\underline{r}) + 3D_g'\left|\underline{\nabla}\phi_g^*(\underline{r})\right|\cdot\mu\right]$$

for $-1 \leq \mu < 0$

$$\approx \frac{1}{4\pi}\left[\phi_g^*(\underline{r}) + 3D_g\left|\underline{\nabla}\phi_g^*(\underline{r})\right|\cdot\mu\right]$$

for $0 \leq \mu \leq 1$

Since this expression is to be used as an importance function, in which it is only the ratio of the importances that has any bearing on the outcome of the biasing process, the $1/4\pi$ term can be dropped and the angular importance written as:

$$I_g(\underline{r},\underline{\omega}) = \phi_g^*(\underline{r}) + 3D_g'\left|\underline{\nabla}\phi_g^*(\underline{r})\right|\cdot\mu$$

for $-1 \leq \mu < 0$

$$= \phi_g^*(\underline{r}) + 3D_g\left|\underline{\nabla}\phi_g^*(\underline{r})\right|\cdot\mu$$

for $0 \leq \mu \leq 1$

Thus, it has been shown that, provided the gradients of the adjoint scalar fluxes and the diffusion constants can be found, for all points in the problem-space, from the information provided to MCBEND by FENDER, it is possible to define an approximation to the adjoint angular flux. This can then be used by MCBEND as an importance function to bias strongly direction-dependent problems. The extra programming required to include the diffusion constants with the other information provided by FENDER is minimal; the gradient of the adjoint scalar flux can be found from this information, by MCBEND, using the method described in the following section.

The importances given by this expression for $I_g(\underline{r},\underline{\omega})$ to particles travelling in directions defined for a range of μ values and for a range of values of the ratio $D_g\left|\underline{\nabla}\phi^*_g\right|:\phi^*_g$ are shown in Table 9.

6.2.3 Derivation of the Gradient of the Adjoint Scalar Flux over the FENDER Finite-Element Mesh

The finite-element code FENDER writes the information it produces for MCBEND onto a computer file. This file is in the form of a large array that contains all the data required to specify the dimensions of the mesh for which the adjoint scalar fluxes were computed and the values of these fluxes at each of the nodes within the mesh.

The adjoint group scalar flux can be found for any point within the mesh, which can contain both triangular and rectangular elements, and for any group g, by interpolation. This can be illustrated with reference to a triangular element of mesh as follows:

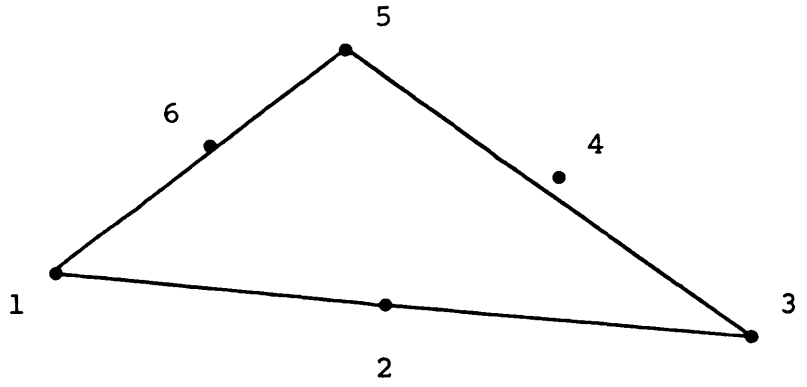

FIGURE 18: Numbering of Nodes on a Triangular Element

All triangular elements have six nodes (one node at each corner and one at each of the side mid-points) and are numbered as in the arbitrary element depicted in Figure 18. At any point, P say, within a triangular element the adjoint scalar flux for a group g, ϕ^*_g, is given by:

$$\phi^*_g = \sum_{i=1} \phi^*_{g,i} \cdot S_i$$

where $\phi^*_{g,i}$ is the adjoint scalar flux for group g at the node i and S_i is the shape function at i.

The shape functions at the nodes of a triangular element are given in Table 10.

To derive the gradient of this flux for use in the expression for the angular importance function the following approach was adopted:

$$\phi^*_g = \sum_{i=1}^{6} \phi^*_{g,i} \cdot S_i$$

$$\therefore \quad \frac{\partial \phi^*_g}{\partial L_k} = \sum_{i=1}^{6} \phi^*_{g,i} \cdot \frac{\partial S_i}{\partial L_k}, \quad \text{for } k = 1, 2 \text{ and } 3,$$

where the L_k are the 'natural coordinates' for P and are defined as:

$$L_k = A_k X + B_k Y + C_k,$$

where the A_k, B_k and C_k are constants of the element and X and Y are the x- and y-coordinates (ie, the 'global coordinates') of the point P.

The gradient of the adjoint group scalar flux in two dimensions is:

$$\underline{\nabla} \phi^*_g = \underline{i} \frac{\partial \phi^*_g}{\partial x} + \underline{j} \frac{\partial \phi^*_g}{\partial y}$$

where $\underline{i}$ and $\underline{j}$ are unit vectors in the x and y directions respectively.

Using the chain rule,

$$\frac{\partial \phi_g^*}{\partial x} = \frac{\partial \phi_g^*}{\partial L_1} \cdot \frac{\partial L_1}{\partial x} + \frac{\partial \phi_g^*}{\partial L_2} \cdot \frac{\partial L_2}{\partial x} + \frac{\partial \phi_g^*}{\partial L_3} \cdot \frac{\partial L_3}{\partial x}$$

$$= A_1 \frac{\partial \phi_g^*}{\partial L_1} + A_2 \frac{\partial \phi_g^*}{\partial L_2} + A_3 \frac{\partial \phi_g^*}{\partial L_3}$$

$$= \sum_{k=1}^{3} A_k \frac{\partial \phi_g^*}{\partial L_k}$$

$$= \sum_{k=1}^{3} A_k \left(\sum_{i=1}^{6} \phi_{g,i}^* \cdot \frac{\partial S_i}{\partial L_k} \right).$$

Similarly,

$$\frac{\partial \phi_g^*}{\partial y} = \sum_{k=1}^{3} B_k \left(\sum_{i=1}^{6} \phi_{g,i}^* \cdot \frac{\partial S_i}{\partial L_k} \right).$$

For a rectangular element the derivation of the gradient is similar and the procedure is described here.

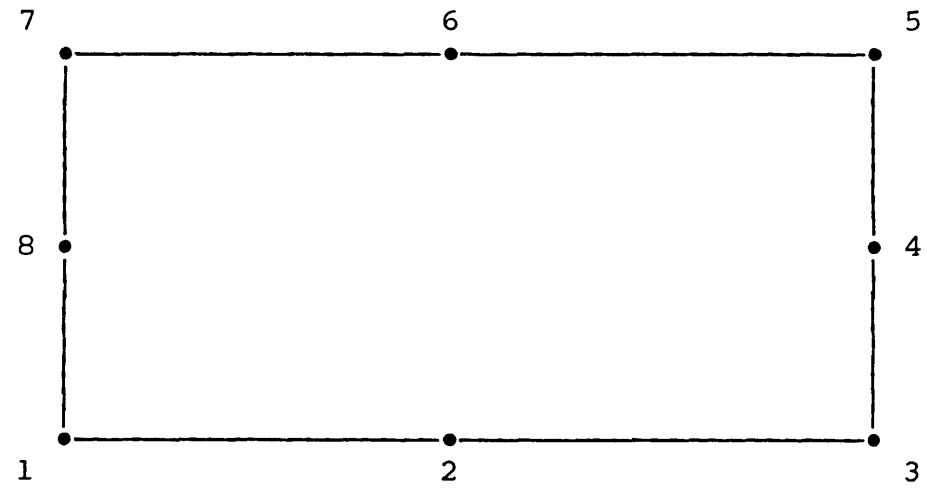

FIGURE 19: Numbering of Nodes on a Rectangular Element

At any point P within an arbitrary rectangular element, numbered locally as in Figure 19, the adjoint scalar flux for a group g, ϕ^*_g, is given by:

$$\phi^*_g = \sum_{i=1}^{8} \phi^*_{g,i} \cdot S_i,$$

where $\phi^*_{g,i}$ is the adjoint scalar flux for group g at node i and S_i is the shape function at i.

The shape functions at the nodes of a rectangular element are given in Table 11.

Then,

$$\frac{\partial \phi^*_g}{\partial U} = \sum_{i=1}^{8} \phi^*_{g,i} \cdot \frac{\partial S_i}{\partial U}$$

and

$$\frac{\partial \phi^*_g}{\partial V} = \sum_{i=1}^{8} \phi^*_{g,i} \cdot \frac{\partial S_i}{\partial V}$$

where U and V are the natural coordinates of P and are defined as:

$$U = A_u X + B_u Y + C_u$$

and $V = A_v X + B_v Y + C_v$

where X and Y are the x- and y-coordinates (global coordinates) of P and the A_u, A_v, B_u, B_v, C_u and C_v are constants of the element.

From which,

$$\frac{\partial \phi^*_g}{\partial x} = \frac{\partial \phi^*_g}{\partial U} \cdot \frac{\partial U}{\partial x} + \frac{\partial \phi^*_g}{\partial V} \cdot \frac{\partial V}{\partial x}$$

$$= A_u \frac{\partial \phi^*_g}{\partial U} + A_v \frac{\partial \phi^*_g}{\partial V}$$

$$= A_u \frac{\partial \phi^*_g}{\partial U} + A_v \frac{\partial \phi^*_g}{\partial V}$$

$$= A_u \sum_{i=1}^{8} \phi^*_{g,i} \cdot \frac{\partial S_i}{\partial U} + A_v \sum_{i=1}^{8} \phi^*_{g,i} \cdot \frac{\partial S_i}{\partial V}$$

Similarly,

$$\frac{\partial \phi_g^*}{\partial y} = B_u \sum_{i=1}^{8} \phi_{g,i}^* \cdot \frac{\partial S_i}{\partial U} + B_v \sum_{i=1}^{8} \phi_{g,i}^* \cdot \frac{\partial S_i}{\partial V}$$

The gradients of the shape functions with respect to the natural coordinates for both the triangular and rectangular elements are known (Tables 12 and 13) and so the gradient, $\underline{\nabla}\phi_g^*$, of the adjoint group scalar flux can be found for all points within the problem space.

6.2.4 Implementation of the Angular Importance Function in MCBEND

Knowing the adjoint group scalar flux and its gradient at all points within the problem, the expression for $I_g(\underline{r},\underline{\omega})$ given in Sub-section 6.2.2 can be used to define an angular importance function for all $\underline{r}$ within the problem. Thus, each time splitting and rouletting (SR) is to be performed, such as after a collision, on a particle of energy E at position $\underline{r}$, MCBEND can retrieve the values of the adjoint scalar flux and diffusion constant for the group containing E, compute the gradient of this flux, in the manner described in Sub-section 6.2.3 and, using these values can assign an importance $I_g(\underline{r},\underline{\omega})$ to the particle. This importance can be compared to the importance the particle had at the previous consideration of SR and splitting or rouletting performed accordingly.

However, the elements in a FENDER mesh should have dimensions of about one mean-free-path (69). Consequently, the magnitude and direction of the gradient of the adjoint scalar flux should not change inordinately within each element. With regard to this fact, the routines incorporated into MCBEND to allow the use of directional importance biasing were provided with the option of computing, for each element and for each group, the gradient of the adjoint scalar flux averaged over the element when a particle of the group first undergoes SR within the element; this average gradient is then used for all subsequent considerations of SR in that element for particles of that group.

The procedure for averaging the gradient over a triangular element is described below and the results are quoted afterwards for a rectangular one.

The gradient of the adjoint scalar flux for a group g averaged over an element can be written as:

$$\left\langle \underline{\nabla}\phi_g^*(\underline{r}) \right\rangle = \underline{i}\left\langle \frac{\partial \phi_g^*(\underline{r})}{\partial x} \right\rangle + \underline{j}\left\langle \frac{\partial \phi_g^*(\underline{r})}{\partial y} \right\rangle$$

where $\langle\ \rangle$ denotes averaging over the element. For triangular elements,

$$\left\langle \frac{\partial \phi_g^*(\underline{r})}{\partial x} \right\rangle = \sum_{k=1}^{3} A_k \left\langle \frac{\partial \phi_g^*(\underline{r})}{\partial L_k} \right\rangle$$

and

$$\left\langle \frac{\partial \phi_g^*(\underline{r})}{\partial y} \right\rangle = \sum_{k=1}^{3} B_k \left\langle \frac{\partial \phi_g^*(\underline{r})}{\partial L_k} \right\rangle$$

where the A_k, B_k and L_k are as described in Sub-section 6.2.3.

But,

$$\left\langle \frac{\partial \phi_g^*(\underline{r})}{\partial L_k} \right\rangle = \sum_{i=1}^{6} \phi_{g,i}^* \left\langle \frac{\partial S_i}{\partial L_k} \right\rangle$$

where $\phi_{g,i}^*$ is the adjoint scalar flux for a group g at node i.

Therefore,

$$\left\langle \frac{\partial \phi_g^*(\underline{r})}{\partial x} \right\rangle = \sum_{k=1}^{3} A_k \sum_{i=1}^{6} \phi_{g,i}^* \left\langle \frac{\partial S_i}{\partial L_k} \right\rangle$$

and

$$\left\langle \frac{\partial \phi_g^*(\underline{r})}{\partial y} \right\rangle = \sum_{k=1}^{3} B_k \sum_{i=1}^{6} \phi_{g,i}^* \left\langle \frac{\partial S_i}{\partial L_k} \right\rangle$$

The $\left\langle \frac{\partial S_i}{\partial L_k} \right\rangle$ can be computed knowing that $\left\langle L_k \right\rangle = \frac{1}{3}$ (70) and are shown in Table 14.

For rectangular elements

$$\left\langle \frac{\partial \phi_g^*(\underline{r})}{\partial x} \right\rangle = A_u \sum_{i=1}^{8} \phi_{g,i}^* \left\langle \frac{\partial S_i}{\partial U} \right\rangle + A_v \sum_{i=1}^{8} \phi_{g,i}^* \left\langle \frac{\partial S_i}{\partial V} \right\rangle$$

and

$$\left\langle \frac{\partial \phi_g^*(\underline{r})}{\partial y} \right\rangle = B_u \sum_{i=1}^{8} \phi_{g,i}^* \left\langle \frac{\partial S_i}{\partial U} \right\rangle + B_u \sum_{i=1}^{8} \phi_{g,i}^* \left\langle \frac{\partial S_i}{\partial V} \right\rangle$$

The $\left\langle \frac{\partial S_i}{\partial U} \right\rangle$ and $\left\langle \frac{\partial S_i}{\partial V} \right\rangle$ can be computed, knowing that (70)

$$\left\langle U^n V^m \right\rangle = \frac{1}{(m+1)(n+1)}, \quad \text{for n and m, both even}$$

$$= 0, \quad \text{otherwise,}$$

and are shown in Table 15.

It is this average value of the gradient of the adjoint group scalar flux over the element that is used to define an importance distribution at all points within the element. Thus:

$$I_g(\underline{r},\underline{\omega}) = \phi^*_g(\underline{r}) + 3D' \left| \underline{\nabla}\phi^*_g(\underline{r}) \right| . \mu$$

$$\text{for } -1 \leq \mu \quad 0$$

$$= \phi^*_g(\underline{r}) + 3D \left| \underline{\nabla}\phi^*_g(\underline{r}) \right| . \mu$$

$$\text{for } 0 \leq \mu \leq 1$$

where values are as defined in Sub-section 6.2.2. Note that the value used for the adjoint group scalar flux in this expression is its actual value at $\underline{r}$ (as found by either quadratic or linear interpolation between the values at the nodes) and not its average value over the element.

The only change that needs to be made to the FENDER code in order for MCBEND to compute the adjoint angular fluxes in the manner described in this section, is that the diffusion constants for all the elements be added to the file that is produced by FENDER and used by MCBEND.

6.2.5 Comparison of the Directional Importance Technique to the Scalar Imporance Technique

The directional importance biasing technique described in the preceding Sub-sections has been incorporated into the Monte Carlo code MCBEND and can be used in any situation in which FENDER

produced importances are applicable. That is, whenever the importance function for the problem can be reasonably approximated on a two-dimensional finite-element mesh by solving a diffusion approximation to the transport equation.

In order to assess the efficiency of the new method it was applied to a problem that had previously been solved using the adjoint scalar flux from a FENDER calculation as an importance function. This same flux was used by MCBEND to derive a directional importance function in the manner described in the preceding Sub-sections.

Prior to this comparison an option was introduced into MCBEND which computed the mean weight (with its standard error) of particles contributing to the score. The weights were scored for all scoring energy groups and all scoring regions requested by the user. The variance on the weights of scoring particles is, in effect, the $\sigma^2_{w_i}$ of Sub-section 3.3.2 and is a measure of the degree to which the variance reduction technique employed has contributed to the total variance of the score. A knowledge of this variance is helpful in examining the relative efficiencies of variance reduction techniques.

The problem chosen to be solved by the two methods was kept deliberately simple and has no particular significance to fusion reactor shielding other than the 14.2 MeV neutron source energy. The problem geometry was as shown in Figure 20 with iron as the bulk-material indicated. All the iron

block boundaries were treated as being total absorbers.

FENDER was used to find the adjoint scalar fluxes over a mesh consisting entirely of triangular elements in the xy-plane of Figure 20. The 450 elements were of equal dimensions in a 15 x 15 rectangular array. The adjoint source was placed in the two elements enclosed by the x=70 cm line, the y=5 cm line and the outer boundaries of the xy-plane. Both elements were given a source strength of 0.5. The problem was solved for the first eight groups of the NADCON (71) group scheme which are shown in Table 16. The adjoint scalar fluxes were found in 130 CPU seconds on an ICL 2976 computer.

MCBEND was used, firstly, to find the flux in the scoring region due to the source, as indicated in Figure 20, with the adjoint scalar flux as an importance function: the scalar fluxes for the same group scheme as used in the FENDER calculation, were computed, as well as the total scalar flux for the energy range covered by these eight groups. The calculation took 7000.0 CPU seconds, in which time 14488 source neutrons were sampled and the total scalar flux for the range 4.72 MeV to 14.2 MeV, recorded in the scoring region, normalised to one source neutron per second, was 1.506×10^{-11} $cm^{-2}.s^{-1}$. The group fluxes recorded in the calculation are given, with their coefficients of variation, the coefficients of variation on the weights of particles contributing to each score and the number of particles contributing to each score, in Table 17.

After this calculation a second calculation was performed with MCBEND, identical to the first

except in that an angular importance function was used instead of the scalar importance function. Seven thousand, two-hundred and thirty-six source neutrons were sampled in 7000.0 CPU seconds, resulting in a total scalar flux of 1.560×10^{-11} $cm^{-2}.s^{-1}$. The group results for this calculation are shown in Table 18.

The coefficients of variation recorded for the respective total fluxes were 7.6% for the scalar importance run and 7.7% for the directional importance run. Although there was little disagreement between the values of the group fluxes calculated and the variances on these fluxes it is interesting to note:

(a) a higher proportion of particles, in relation to the number of samples, contributed to the scores in the directional importance case than in the scalar importance case;

(b) the variances on the weights of particles in the scoring region contributing to each of the group scores are very much higher for the directional importance run.

It had been hoped that using an angular importance function would prove beneficial to the calculation in that, by assessing the importance of a particle direction before allowing it to be moved to its next event, it would allow a greater number of particle histories to be sampled and thus result in a greater number of particles contributing to the score. It would seem that, in this calculation, this supposed benefit was offset by an increase in the amount of splitting (indicated by the increased proportion of samples

contributing to the scores). Another factor explaining the lack of success of the angular importance method in this case is that the ratio of the adjoint flux gradient to the adjoint flux, away from the boundaries, was only about 0.1: a value that gives (see Table 19, D ≈ 3.0 cm) a particle travelling in the direction of the gradient an importance about 3.6 times greater than a particle travelling in the opposite direction. A greater ratio could be expected around the boundaries of a void and in this situation one would expect an increase in the efficiency of the directional importance method over the scalar importance method.

A second comparison between the scalar importance method of biasing and the directional importance method was made in which a void was included. A similar problem to the previous comparison was employed except that a voided slot of dimensions 5 cm x 5 cm x 55 cm was incorporated in the centre of the iron block with its greatest dimension being in the y-direction of Figure 20.

The importances were found by FENDER in the same manner as for the previous comparison except that the void was treated by the albedo-kernel treatment of Chucas (72). The calculation took 130 CPU seconds.

Both the scalar importance and directional importance MCBEND runs were for 5000.0 CPU seconds each; the former sampled 14488 source samples, the latter sampled 8899. The total scalar fluxes computed were 3.679×10^{-11} $cm^{-2}.s^{-1}$, with a coefficient of variation of 7.0%, and

3.640×10^{-11} $cm^{-2}.s^{-1}$, with a coefficient of variation of 6.7%, respectively. (Both results being normalised to one source neutron.) The group results for the problems are given in Tables 19 and 20 respectively.

Although the variances of the results were better in the directional importance case, the improvement was not substantial. As in the comparison of the two methods when no void was present, less samples were taken in the directional biased case than in the scalar biased case and a greater number of particles scored, thus indicating that more splitting had occurred. Also, the variances on the weights of scoring particles were, again, greater in the directional importance case.

The disappointing performance of the directional biasing method in the comparison including the void prompted a closer analysis of the behaviour of the neutrons in the problem.

A map of the gradients of the adjoint scalar flux for several of the elements in the mesh over which the adjoint fluxes were defined revealed that, for elements close to and adjoining the void, the gradients were almost exactly perpendicular to the long edge of the slot (ie, in the x-direction) and pointed into the void. This occurred as a direct consequence of the manner in which the void is treated in FENDER by the albedo-kernel method of Chucas. The basis of this method is that it computes group albedos for the material surrounding the void during the FENDER calculation, thus avoiding the need for any albedo

data to be input. Unfortunately, in this method no angular dependence of the current emerging into the void is calculated since the calculation is by a diffusion method and only the current in the direction perpendicular to the void boundary is computed. Thus, the attenuation down the slot is primarily geometric, from a line-of-sight treatment, and is totally swamped by the large gradients computed across the slot. The resulting gradients from this method cause a MCBEND calculation using directional importance biasing to encourage particles to travel across the slot rather than along it. This is not so detrimental to the method as to render it unworkable (since the same is true for the scalar importance biasing method, as is borne out by the results of the comparison) but the method can not be used to its full effect and, hence, can not have its potential fully assessed until an angular dependent treatment of voided regions in FENDER is available.

6.3 Collision Angle Biasing

6.3.1 Introduction

Like directional importance biasing, collision angle biasing is a means of encouraging particles to travel in directions more favourable to them contributing to the score, ie important directions. This is achieved by selecting the direction of a particle emerging from a collision from a biased distribution. The bias is such that, on average, the particles emerge into the more important directions. The introduction of this bias is offset by the attachment of a weight

to the particle which is taken into account when the contribution of the particle to the score is being computed.

The attached weight, $W(\underline{r}, \underline{\Omega}', E')$ is, necessarily, in inverse proportion to the amount of bias it has received and is, as such, given by:

$$W(\underline{r},\underline{\Omega}_i,E') = \frac{\mathcal{P}_1(\underline{r},\underline{\Omega}_i\rightarrow\underline{\Omega}',E_i\rightarrow E')}{\mathcal{P}_2(\underline{r},\underline{\Omega}_i\rightarrow\underline{\Omega}',E_i\rightarrow E')} \cdot W(\underline{r},\underline{\Omega}_i,E_i)$$

where $W(\underline{r},\underline{\Omega}_i,E_i)$ is the weight of the particle prior to a collision at $\underline{r}$, when it has a direction $\underline{\Omega}_i$ and an energy E_i;

$\mathcal{P}_1(\underline{r},\underline{\Omega}_i\rightarrow\underline{\Omega}',E_i\rightarrow E')$ is the probability of a particle emerging from a collision at $\underline{r}$ into the direction $\underline{\Omega}'$ with an energy E', as given by the nuclear data;

$\mathcal{P}_2(\underline{r},\underline{\Omega}_i\rightarrow\underline{\Omega}',E_i\rightarrow E')$ is the probability at $\underline{r}$, given by the distribution from which $\underline{\Omega}'$ and E' are sampled, of the particle emerging into the direction $\underline{\Omega}'$ with an energy E'.

Thus, in order for the method to be applicable both $\mathcal{P}_1$ and $\mathcal{P}_2$ must be known.

$\mathcal{P}_1$ is given by the nuclear data being used for the problem. However, ordinarily, these data are used to provide the Monte Carlo code with the energies and directions of the particles emerging from collisions and are not, in general, structured to

provide the probability $\mathfrak{P}_1$ when given the direction $\underline{\Omega}'$ and the energy E'. Nevertheless, the use of point-estimators in some codes has resulted in them being given the ability to ascertain this probability from the nuclear data. For other codes and nuclear data the task of finding $\mathfrak{P}_1$ will require substantial programming alterations and additions, especially if the method is to be considered for use with point data, as would be preferable on the grounds of accuracy (see Sub-section 5.1.4).

The probability $\mathfrak{P}_2$ is found from the distribution from which the $\underline{\Omega}'$ and E' are selected. Obviously, this distribution should be chosen with care as a badly chosen one could easily result in a reduction in efficiency. The distribution should be defined for all points in the problem space, it should be defined for all energies and it should reflect, reasonably accurately, that distribution which would result in a minimum variance on the final result. In short, the distribution chosen should fulfil those criteria that must be fulfilled by a good importance function. In fact, the group adjoint angular flux at a point is an almost ideal function to use as such a distribution (73).

Hence, a code with the capability of computing, from its nuclear data, the probability $\mathfrak{P}_1$ and which has a knowledge of the adjoint angular flux, could be used to solve a problem by means of the collision angle biasing technique.

6.3.2 A Simple Problem to Test the Collision Angle Biasing Technique

Of the two requirements mentioned in the preceding paragraph the provision of one - an approximation to the adjoint angular flux - in the Monte Carlo code MCBEND has been fully discussed in Section 6.2.

MCBEND has a point-estimator facility that can find, approximately, the probability, $\mathcal{P}_1$, of the scatter of a particle of a given energy into a given angle. This facility is, at present, ony available when multigroup data is being used: there is no such option available when point data is to be used. Potentially, the accuracy with which $\mathcal{P}_1$ can be found from DICE-VI (the point data that is used by MCBEND) is greater than that afforded by mutligroup data; for that reason, the MCBEND routines that deal with the DICE data are being altered so as to permit the computation of $\mathcal{P}_1$.

Because of the current limitations of the DICE-IV data in this respect, the potential of the collision angle biasing method in MCBEND was examined by constructing a problem in which only isotropic, monoenergetic scattering, with only one secondary neutron, was allowed. With such constraints the problem of finding $\mathcal{P}_1$ is removed since scatter into all possible solid angles is equally likely and $\mathcal{P}_1$ then equals $\frac{1}{4\pi}$. Thus, for isotropic, monoenergetic scattering the problem of implementing collision angle biasing reduces to selecting the angle of scatter from the adjoint angular flux and finding the probability $\mathcal{P}_2$ so that the scattered particle can be weighted

appropriately. These were performed as described in the following paragraphs.

Since the adjoint angular flux is only defined in the xy-plane the selection of the angle of scatter, $\underline{\Omega}'$, was separated into two parts: the selection of the azimuthal angle, $\underline{\omega}'$, and the selection of the polar angle, θ'.

(a) Selection of the Azimuthal Angle

The azimuthal angle, η, is selected from a distribution defined by the angular importance function in the xy-plane. As seen in Sub-section 6.2.4 an angular importance function can be defined, for one group, in terms of the adjoint scalar flux and its gradient, by the expression:

$$I(\underline{r},\underline{\omega}) = \emptyset^*(\underline{r}) + 3D' \left| \left\langle \underline{\nabla}\emptyset^*(\underline{r}) \right\rangle \right| . \mu \qquad -1 \leq \mu < 0$$

$$= \emptyset^*(\underline{r}) + 3D \left| \left\langle \underline{\nabla}\emptyset^*(\underline{r}) \right\rangle \right| . \mu \qquad 0 \leq \mu \leq 1$$

where $I(\underline{r},\underline{\omega})d\underline{r}\ d\underline{\omega}$ is the importance of a particle within $d\underline{r}$ of $\underline{r}$ and with a direction within $d\underline{\omega}$ of $\underline{\omega}$,

$\emptyset^*(\underline{r})$ is the adjoint scalar flux at $\underline{r}$ of particles in the group,

D is the diffusion coefficient at $\underline{r}$ for particles in the group,

$$D' = \frac{1}{1/D + 3\left|\left\langle \underline{\nabla}\emptyset^*(\underline{r})\right\rangle\right|/\emptyset^*(\underline{r})},$$

and

$$\mu = \frac{\underline{\nabla}\emptyset^*(\underline{r}).\underline{\omega}}{\left|\left\langle \underline{\nabla}\emptyset^*(r)\right\rangle\right|} = \cos\,\eta.$$

This expression was normalised to give a probability distribution as follows:

Put $\mathfrak{P}(\underline{r},\eta) = N_1\, I(\underline{r},\underline{\omega})$,

where $\mathfrak{P}(\underline{r},\eta)$ is the probability distribution for the azimuthal angle of particles at $\underline{r}$ and N_1 is a normalising constant to be found.

Since, $\int_0^{\pi/2} \mathfrak{P}(\underline{r},\eta)\, d\eta = 1$

then $N_1 \int_0^{\pi/2} (\emptyset^*(\underline{r}) + 3D\left|\left\langle \underline{\nabla}\emptyset^*(\underline{r})\right\rangle\right|.\cos\,\eta) = 1$

$$= \quad N_1 = \frac{1}{\emptyset^*(\underline{r}).\pi + 3\,(D - D')\left|\left\langle \underline{\nabla}\emptyset^*(\underline{r})\right\rangle\right|}$$

An η can be selected randomly from the distribution $(\underline{r},\eta)$; this was performed by the use of the rejection technique (eg (62)). Having chosen η, the direction $\underline{\omega}'$ was defined as one of the two vectors in the xy-plane making an angle η with the gradient vector $\left\langle \underline{\nabla}\emptyset^*(\underline{r})\right\rangle$: each was given a 50% chance of selection.

(b) Selection of the Polar Angle

The polar angle was selected uniformly between 0 and π radians. The x- and y-direction cosines were then normalised so as to make the sum of all three direction cosines of $\underline{\Omega}'$ equal to unity.

The probability, $\mathcal{P}(\underline{r},\underline{\Omega})d\underline{\Omega}$ of selecting, at $\underline{r}$, an angle of trajection within $d\underline{\Omega}$ of $\underline{\Omega}$, by this process, can be found as follows. From Figure 21 it is seen that:

$$\mathcal{P}(\underline{r},\underline{\Omega})d\underline{\Omega} = R\,\mathcal{P}(\underline{r},\theta)\mathcal{P}(\underline{r},\eta)\,\sin\theta\,d\theta d\eta$$

where $\mathcal{P}(\underline{r},\theta)$ is the probability distribution for selecting the polar angle,

and R is the normalisation constant which, from integrating $\mathcal{P}(\underline{r},\underline{\Omega})$ over 4π-space, is equation to $\pi/4$.

Thus,

$$\mathcal{P}(\underline{r},\underline{\Omega})\,d\underline{\Omega} = \frac{1}{4}\,(\underline{r},\eta)\,d\underline{\Omega},$$

since $\mathcal{P}(\underline{r},\theta) = \frac{1}{\pi}$, and the weight given to a particle emerging in direction $\underline{\Omega}'$ is

$$W(\underline{r},\underline{\Omega}') = \frac{\phi^*(\underline{r}).\pi + 3(D-D').|\underline{\nabla}\phi^*(\underline{r})|}{\pi.I(\underline{r},\underline{\omega}')}.W(\underline{r},\underline{\Omega}_i)$$

where $W(\underline{r},\underline{\Omega}_i)$ is the weight of the particle before the collision at $\underline{r}$.

Using the approach described in the preceding paragraphs, a comparison of the method of collision angle biasing with the directional importance and scalar importance biasing methods was made, in which the test problem geometry was that of Figure 20 where the 'bulk material' was a homogeneous block of material in which all scattering of neutrons was isotropic and monoenergetic.

In the first comparison to be made the bulk material was given a mean-free-path (MFP) of 5 cm and an equal probability of either scattering or absorbing (with no secondary neutron production). A MFP of 5 cm, corresponding to a total interaction cross-section (Σ_t) of 0.2 cm^{-1}; thus, a scattering cross-section (Σ_s) of 0.1 cm^{-1} and an absorption cross-section (Σ_a) of 0.1 cm^{-1} was given to the bulk material.

The CONSTANTS option in FENDER was used to define the material properties (a Σ_t of 0.2 cm^{-1} corresponds to a diffusion constant, D, of 1.667 cm). The bulk material was covered by a triangular element mesh in an equally-spaced 15 x 15 rectangular array. The adjoint scalar flux importances for this two-group problem (the code requires a second "dummy" group in order to

provide fluxes for just one group) were produced in 66.2 CPU seconds.

These FENDER produced adjoint fluxes were used initially to provide the customary FEMCAT scalar importance function for the MCBEND problem. The source and scoring region were as indicated in Figure 20. The problem was run for a CPU time of 5000.0 seconds, in which time 322829 source neutrons were sampled, resulting in a flux of 3.094×10^{-13} cm^{-2} per source neutron with a coefficient of variation on this result of 7.0%. One thousand and eighty-six particles contributed to the score and the coefficient of variation on the weights of these contributing particles was 37.3%.

The scalar adjoint fluxes from FENDER were then used by MCBEND to produce an angular importance function to be used in directional importance biasing for the same problem. The problem was also run for 5000.0 CPU seconds, in which time 332649 samples were taken, resulting in a flux of 3.904×10^{-13} cm^{-2} per source neutron with a coefficient of variation of 6.0%. The coefficient of variation on the weights of particles contributing to the score was 56.2% and the number of these particles was 1176.

Finally, the scalar adjoint fluxes from FENDER were used to solve the problem by the use of the collision biasing technique described in this Chapter. However, even after 5000.0 CPU seconds, no flux was recorded in the scoring region using this method. (Some particles did enter the scoring region but these were evidently progeny of the same source neutron sample and since, for

statistical reasons, MCBEND only records the scores after a contribution from two samples, no flux resulted.)

In an effort to gain some appreciation of the potential of the collision angle biasing method the three calculations above were repeated but, this time, for a bulk material with a zero absorption probability. The MFP was maintained at 5 cm so that the same FENDER mesh could be employed. Thus, $\Sigma_s = \Sigma_t = 0.2$ cm^{-1} and $\Sigma_a = 0.0$. The FENDER calculation was run for 64.2 CPU seconds.

All three MCBEND runs were again for 5000.0 CPU seconds each. The scalar importance run sampled 40751 source neutrons and recorded a flux of 4.998×10^{-7} cm^{-2} per source neutron with a coefficient of variation of 9.2%. The coefficient of variation on the weights of particles contributing to the score was 0.9% and the number of these particles was 346. In the directional importance run a flux of 4.645×10^{-7} cm^{-2} per source neutron was computed with a coefficient of variation of 12.4%. From the 45994 source samples taken, 308 particles contributed to the score with a coefficient of variation on their weights of 50.9%. With collision angle biasing 270735 source samples were taken resulting in a flux of 3.483×10^{-7} cm^{-2} per source neutron with a coefficient of variation of 23.9%. One thousand, six-hundred and ninety-seven particles contributed to the score with a coefficient of variation on their weights of 240.1%.

These calculations showed that, in the form presented, the collision angle bising method is not a viable alternative to either the scalar importance biasing or the directional importance biasing methods. Its failure to produce a result in the first set of calculations suggests, most definitely, that it would be of no use in a deep-penetration problem. It is also easy to see that its use in a great many problems would results in extremely small weights for some particles: a circumstance that could easily produce floating point underflow errors in the computation, especially when summing the squares of these weights for calculation of the variance on the scores.

However, in the collision angle biasing case the primary contribution to the total variance on the score is from the large variance on the weights of the scoring particles. If it was possible to control the variance on these weights the method could prove far more effective. One means of doing this would be to employ splitting and rouletting (SR) with either a scalar or a directional importance function - an approach adopted, with some success, by Booth (74) when using the angular biasing technique of Carter (39) described in Chapter 4. The method of collision angle biasing described in this Chapter is particularly suited for use in tandem with SR since the degree to which the weight of the particle is altered after a collision is determined from the same importance function as that used in SR: this avoids the possibility of the alterations made to the particle weight by the collision angle biasing method adversely affecting one of the properties that makes the adjoint

scalar flux an ideal importance function, namely, that it assigns to each region of the problem phase-space an importance that varies inversely as the expected weight of particles within that region (see Sub-section 3.3.2).

Using SR would almost certainly reduce the variance on the weights of scoring particles but whether the consequent reduction of the total variance on the score would offset the extra time required for performing SR - to the extent that using the two biasing methods in conjunction is more efficient than using just SR - is still open to question.

Although no firm conclusions can be drawn from the work so far carried out, the use of collision angle biasing has been shown to be viable in principle. A complete assessment of the potential of the method must wait, however, until its combined use with SR has been shown to be at least as effective as other available variance reduction techniques in the type of problems addressed in this Sub-section (that is, bulk shielding problems with no streaming paths). And, as with the directional importance biasing method, its efficacy in streaming problems could be enhanced by the use of a void treatment in FENDER that more accurately predicts the flux gradients around the void.

7. CONCLUSIONS AND SUGGESTIONS FOR FURTHER WORK

The problems presented to the radiation shielding engineer by the complexities of Tokamak fusion reactor designs have been outlined in Chapter 2. In general, the computational methods employed in fission reactor shielding calculations are applicable to these problems but there are some aspects which require specific investigation. Two of these aspects have been addressed in this thesis, they are: the suitability of presently available nuclear data for fusion reactor calculations and the treatment of radiation streaming in these calculations. Both are important.

The EURLIB data used in multigroup Monte Carlo calculations has been prepared with a fission-spectrum based weighting spectrum. Two calculations were performed on the radial shield of a Tokamak without a duct: one calculation used UKNDL data prepared in multigroup form with the same weighting spectrum as that used in EURLIB; the other used UKNDL data prepared in multigroup form with a weighting spectrum given by a similar calculation but with point data. There were no significant differences between the calculated fluxes of the two cases. Thus, the use of a flux-weighting spectrum that is more representative of a fusion reactor flux spectrum does not improve the accuracy of multigroup Monte Carlo calculations for fusion reactors.

The discrepancies in the results recorded in Monte Carlo calculations of the copper damage rates in the toroidal field coils of a Tokamak without a duct prompted a benchmark calculation on the attenuation of 15 MeV neutrons in a mild-steel shield. A calculation of the S32(n,p)P32 saturated activity using EURLIB data over-predicted the response in regions near the source and under-predicted it away from the source. A similar calculation using DICE-VI

point data over-predicted the response in all scoring regions.

A sensitivity study performed on this second calculation with the DUCKPOND facility in MCBEND showed that the response was most dependent on the non-elastic cross-sections of iron for neutrons with energies above 11 MeV and between about 2.5 MeV and 4.5 MeV.

It is clear from these results that if the nuclear data to be used in fusion reactor shielding calculations are to be considered reliable then improvements must be made to certain cross-sections. Cross-sections shown to be inadequate from further benchmark studies should be remeasured and incorporated into the data libraries.

With the advent of D-T plasmas in the JET and TFTR the opportunity should be taken to make extensive shielding measurements on these reactors, as a benchmark based on these measurements would be the ultimate test of not only the calculational procedures but also the nuclear data. Until improvements to the nuclear data have been made the uncertainties in the cross-sections will be the prime limitation on the accuracy of shielding calculations and the benefits from potential advances in computational techniques will not be fully realised.

A means of deriving an approximation to the adjoint angular flux for a problem has been made available to the Monte Carlo shielding code MCBEND. The derivation is consistent with the diffusion approximation used by the finite-element code FENDER to compute the adjoint scalar flux from which the angular flux is obtained. The adjoint angular flux is defined for all points in a two-dimensional finite-element mesh and can be used as a direction dependent importance

function for a MCBEND calculation provided such a function can be considered, to a reasonable extent, to be independent of the direction orthogonal to the mesh.

The angular importance function has been used in neutron calculations by MCBEND to perform splitting and rouletting taking into account particles' directions. The use of such directional importance biasing could prove most beneficial in problems dominated by streaming paths. The method was tried initially in a problem consisting of a solid iron block: there was no improvement in acceleration using this method over a similar calculation using a scalar importance function. With a void in the problem there was some improvement in the variance on the result but not to the extent anticipated. The reason for this disappointing performance was found to be that the treatment of voided regions in the FENDER code lacked information on the angular dependence of the current emerging into the void. A verdict on the full potential of the directional importance biasing method must await the development of a technique that more accurately predicts the flux gradients around voids.

The approximation to the adjoint angular flux developed for the directional importance biasing method has also been used to test the method of collision angle biasing. To avoid extensive reprogramming of the routines in MCBEND that deal with the angular distributions in the nuclear data, a problem was contrived in which the material could either absorb neutrons in a collision or scatter them mono-energetically and isotropically. This allowed easy calculation of the weights to be given to biased neutrons. With a 50% probability of absorption no particles were scored in the calculation using collision angle biasing. In a second run with a zero probability of absorption a coefficient of variation of 23.9% was recorded on the flux

scored compared with one of 9.2% when using a scalar importance function for the same problem. A large variance on the weights of scoring particles indicated that the use of splitting and rouletting in combination with the method may improve its efficacy. It is suggested that this is done before a full assessment of the potential of the method is given.

An angular importance function can also be applied to the variance reduction technique of path-length stretching (see Sub-section 3.3.2) where the degree to which the distance between collisions is increased is dependent upon the importance of the direction of the particle trajectory. It is suggested that the possibility of using the angular importance function provided in MCBEND for path-length stretching should be investigated.

The angular importance function could also be used to bias the source. The general version of MCBEND allows the direction of source particles to be selected from a biased distribution in much the same way as in the old angular biasing technique, namely, by the user defining a weighting function over a series of angular bins (see Sub-section 6.2.1). It is possible for this method of biasing to adversely affect the efficiency of the variance reduction technique used in the main body of the problem: using an angular biasing scheme that is derived from the importances used in the main problem reduces this possibility and should be studied.

The derivation of the angular importance function can be performed for any problem in which the scalar importances of FENDER are valid. The fact that FENDER is (at present) two-dimensional is not too restrictive since the importance function in a great number of problems can be considered, to

a large extent at least, to be two-dimensional and, in any case, most problems can be broken-down into a series of two-dimensional problems. The extension of the theory to the derivation of an angular importance from an adjoint scalar flux defined on a three-dimensional finite-element mesh is straightforward.

Although the discussion has been confined to neutron transport, the methods described are equally applicable to gamma-ray problems since FENDER is capable of providing importances for such problems. At present MCBEND is restricted to using multigroup data for neutron-gamma calculations; it would be a great improvement for fusion reactor shielding calculations if this option was available when using DICE data since gamma irradiation of the toroidal field coils is an important effect.

The provision of an angular importance function for Monte Carlo calculations has opened up the possibility of using, to an accuracy not hitherto available, variance-reduction techniques suitable for radiation streaming problems. Enhanced by the potential improvements outlined in this Chapter, these new techniques could be applied to the problem of radiation shielding down ducts which is probably the most difficult problem encountered in the design of radiation shielding for Tokamak reactors.

8. ACKNOWLEDGEMENTS

The work described in this thesis was performed in the Radiation Physics and Shielding Group at the Winfrith establishment of the United Kingdom Atomic Energy Authority. I would like to thank everyone who made my stay there as pleasurable as it was profitable.

I am particularly grateful to my Supervisor Professor Tony Goddard and also to Mr Alan Avery and Dr Peter Miller, who made many valuable suggestions during the course of the work.

I am also indebted to Dr John Butler of the Radiation Physics and Shielding Group at Winfrith and Dr Roger Hancox of the Applied Physics and Technology Division at Culham Laboratories for arranging the UKAEA bursary and for the interest that they have shown in my work.

Finally, I am especially thankful to Mrs Julie Ackland and Miss Alison Heath for the typing, and for helping greatly in preparing the final layout. Any residual errors are entirely my own.

9. REFERENCES

(1) "The JET Project", EUR-JET-R7 (February 1978)

(2) "An Introduction to Controlled Thermonuclear Fusion", M O Hagler and M Kristiansen (Lexington Press, 1977)

(3) "International Fusion Research", R S Pease, Atom, 315 (January 1983)

(4) "International Tokamak Reactor, Phase IIa, Part I", IAEA, Vienna, STI/PUB/638 (1983)

(5) "Shielding Studies for the Culham Conceptual Tokamak Reactor", C A Morrison, Symposium on Fusion Technology, Oxford (September 1980)

(6) "US INTOR Radiation Shield Design", Y Gohar and M A Abdou, Proc of the 6th International Conference on Radiation Shielding, Tokyo, Japan (May 1983)

(7) "The Shielding of Superconducting Magnets in a Fusion Reactor", G M McCracken and S Blow, HMSO, CLM-R 120 (1972)

(8) "Nuclear Analysis of a Tokamak Experimental Power Reactor Conceptual Design", M A Abdou and J Jung, Nuc Tech, 35 (Mid-August 1977)

(9) Unpublished. W S Cooper, LBL (1983)

(10) "Neutronic Calculations for the Tokamak Fusion Test Reactor Diagnostic Penetrations", L Ku and J G Kolibal, Nuc Tech/Fusion, 2 (April 1982)

(11) "Nuclear Reactor Theory", G I Bell and S Glasstone, Van Nostrand Reinhold, New York (1970)

(12) "Reactor Shielding for Nuclear Engineers", Schaeffer, ed, TID-25951, USAEC Technical Information Centre, Oak Ridge, Tennesse, USA (1973)

(13) "Computing Methods in Reactor Physics", H Greenspan, C K Kelber and D Okrent, eds, Gordon and Breach (1968)

(14) "Some Benchmark Shielding Problems Solved by the Finite-Element Method", R T Ackroyd et al, Proc of the 6th International Conference on Radiation Shielding, Tokyo, Japan (May 1983)

(15) "FENDER - A Finite-Element Code for the Solution of the Diffusion Equation in Shielding Design Applications", E Shuttleworth, International Seminar on the Role of Finite-Element Methods in Radiation Physics, Imperial College, London (April 1981)

(16) "Radiation Considerations for Superconducting Fusion Magnets", M A Abdou, Journal of Nuclear Materials, 72 (1978)

(17) "Solution of the Transport Equation by Sn Approximations", B G Carlson, LA-1599, Los Alamos (1953)

(18) "A User's Manual for ANISN", W W Engle, Jr, USAEC Report K-1693, US Atomic Energy Commission (1967)

(19) "The DOT-IV Two-Dimensional Discrete-Ordinates Transport Code with Space-Dependent Mesh and Quadrature", ORNL-TM-6529, Oak Ridge National Laboratory, USA (1979)

(20) "Random Sampling (Monte Carlo) Techniques in Neutron Attenuation Problems - I and II", H Kahn, Nucleonics (May and June 1950)

(21) "MCBEND Program Users' Guide", D E Bendall and R J Brissenden, (Unpublished)

(22) "Introduction to the Theory of Statistics", A M Mood, F A Graybill and D C Boes, McGraw-Hill (1974)

(23) "Importance: The Adjoint Function", J Lewins, Pergamon (1965)

(24) "Adjoint and Importance in Monte Carlo Applications", R R Coveyou, V R Cain and K J Yost, Nuc Sci and Eng, 27 (1967)

(25) "The Shielding of 15 MeV Neutrons by Iron - A Benchmark Experiment", D G Jones, J C H Miles and A G Sherwin, NRPB-M57, National Radiological Protection Board (1981)

(26) "The Development and Application of the Discrete Ordinates-Transfer Matrix Hybrid Method for Deterministic Streaming Calculations", B A Clark, LA-9357-T, Los Alamos National Laboratory (May 1982)

(27) "The Combinatorial Geometry Technique for the Description and Computer Processing of Complex Three-Dimensional Objects", W Guber, MAGI Project, 6951 MR-700 4/2

(28) Quoted in Reference (26)

(29) "Evaluation of the Streaming Matrix Method for Discrete-Ordinates Duct Streaming Calculations", B A Clark, W T Urban and D J Dudziak, Proc of the 6th International Conference on Radiation Shielding, Tokyo, Japan (May 1983)

(30) "Neutron and Gamma-Ray Streaming Calculations for the Engineering Test Facility Neutral Beam Injectors", R A Lillie, R T Santoro, R G Alsmiller, Jr, and J M Barnes, Nuc Tech/Fusion, 2 (April 1982)

(31) "Engineering Test Facility Vacuum Pumping Duct Shield Analysis", W T Urban, T J Seed and D J Dudziak, Nuc Tech/Fusion, 2 (April 1982)

(32) "Radiation Streaming Calculations for INTOR-J", Y Seki, H Iida et al, Nuc Tech/Fusion, 2 (April 1982)

(33) "Nuclear Analysis of Blanket and Shield Design for Tokamak Fusion Experimental Reactor", S Mori et al, Proc of the 6th International Conference on Radiation Shielding, Tokyo (May 1983)

(34) "Shielding of the Neutral Injector Beam Line in the Culham Conceptual Reactor Mk II", A F Avery, C A Morrison and C Parry, Proc of the 6th International Conference on Radiation Shielding, Tokyo, Japan (May 1983)

(35) "MCCAM: Monte Carlo calculations in the Adjoint Mode", C A Morrison, RPD/CAM/802, AEE Winfrith (December 1981)

(36) J T D Mitcheu, ANS 3rd Topical Meeting on Technology of Controlled Nuclear Fusion, Santa Fe, New Mexico (May 1978)

(37) "A Recursive Monte Carlo Method for Estimating Importance Function Distributions in Deep-Penetration Problems", M Goldstein and E Greenspan, Nuc Sci and Eng, 76 (1980)

(38) "Neutronics Analysis of Major Penetrations in Tokamaks using the Recursive Monte Carlo Method", M Goldstein, Proc of the 6th International Conference on Radiation Shielding, Tokyo, Japan (May 1983)

(39) "Neutron Streaming Analysis for Shield Design of the Fusion Materials Irradiation Test Facility", L L Carter, Nuc Tech/Fusion, 2 (April 1982)

(40) "Angular Biasing of the Collision Process in Multigroup Monte Carlo Calculations", J S Tang, T J Hoffman and P N Stevens, Nuc Sci and Eng, 64 (1977)

(41) "International Tokamak Reactor, Phase One", IAEA, Vienna, STI/PUB/619

(42) "Data Formats and Procedures for the Evaluated Nuclear Data File, ENDF", D Garber, C Dunford and S Pearlstein, BNL-NCS-50496 (ENDF 102), Brookhaven National Laboratory (1975)

(43) "The Aldermaston Nuclear Data Library as at May 1963", K Parker, AWRE-O-70/63, UK AWRE (1963)

(44) "Card Image Format of the Karlsruhe Evaluated Nuclear Data File KEDAK", D Woll, KFK-880 (EANDC(E)-112 "U", EUR 4160e), Kernforschungszentrum Karlsruhe (1968)

(45) "Nuclear Reactor Analysis", J J Duderstadt and L J Hamilton, John Wiley, New York (1976)

(46) "AMPX: A Modular Code System for Generating Coupled Multigroup Neutron-Gamma Libraries From ENDF/B", N M Greene et al, ORNL-TM-3706, Oak Ridge National Laboratory (1973)

(47) "A Guide to GALAXY 6 Part 1", J A Price, AWRE-013/75 (1975)

(48) "Generation and Testing of the Shielding Library EURLIB for Fission and Fusion Technology", E Caglioti et al, Proc. of the 5th International Conference on Reactor Shielding, Knoxville, USA (1977).

(49) "The MORSE Code - A Multigroup Neutron and Gamma-Ray Monte Carlo Transport Code", E A Straker et al, ORNL-4585 (September 1970)

(50) "DICE Mk V - The Preparation of Nuclear Data into a Form Suitable for Monte Carlo Calculations using an Electronic Computer", J B Parker ed, AWRE O-27/66 (1966)

(51) "Accurate Evaluation of Multigroup Transfer Cross-sections and their Legendre Coefficients", K-J Hong and J K Shultis, Nuc Sci and Eng, 80 (1982)

(52) "Neutron Displacement Damage Cross-Section for Structural Materials", D G Doran and N J Graves, HEDL-SA-1058

(53) "A Monte Carlo Technique for Selecting Neutron Scattering Angles from Anistropic Distributions", R R Coveyou, Nuc Sci and Eng, 21 (1965)

(54) "The Shielding of 14 MeV Neutron Generators", T O Marshall and A Knight, RPS/I/49, Radiological Protection Service

(55) "Neutron Streaming Through a Slit and Duct in Concrete Shields and Comparison with a Monte Carlo Analysis", H Hashikura et al, Nuc Sci and Eng, 84 (1983)

(56) "Integral Tests of Coupled Multigroup Neutron and Gamma Cross-Sections with Fission and Fusion Sources", J Schriewer et al, IAEA-OECD(NEA) Technical Committee Meeting of Differential and Integral Nuclear Data Requirements for Shielding Calculations, Vienna (October 1976)

(57) "Calculation of Neutron and Gamma-Ray Energy Spectra for Fusion Reactor Shield Design: Comparison with Experiment", R T Santoro et al, Nuc Sci and Eng, 78 (1981)

(58) "Comparison of Measured and Calculated Neutron and Gamma-Ray Energy Spectra Behind an In-Line Shielded Duct", R T Santoro et al, Journal of Fusion Energy, 2, 6 (1982)

(59) "The International Reactor Dosimetry File", D E Cullen, N Kochrov and P M McLaughlin, (IRDF-82), IAEA-NDS-41/R

(60) "Monte Carlo Perturbation Theory in Neutron Transport Calculations", M C G Hall, PhD Thesis, Imperial College, University of London (1980)

(61) "Compilation of Multigroup Cross-Section Covariance Matrices for Several Important Reactor Materials", J D Drischler and C R Weisbin, ORNL-5318, Oak Ridge National Laboratory, USA (1977)

(62) "Appications of Monte Carlo", H Kahn, AECU-3259, USAEC, Oak Ridge, Tennesse, USA (April 1954)

(63) "Treatment of Anisotropic Scattering in Numerical Neutron Transport Theory", H Brockmann, Nuc Sci and Eng, 77 (1981)

(64) "Low Cost Shield for Tokamak Fusion Reactors", Y Gohar, Nuc Tech/Fusion, 4 (September 1983)

(65) "Neutron-Induced Photon Production in MCNP", R C Little and R E Seamon, Proc of the 6th International Conference on Radiation Shielding, Tokyo, Japan (May 1983)

(66) "The Exploitation of a Simplified Albedo Theory for Neutron and Gamma-Ray Streaming in Practical Design Situations", P C Miller and A Packwood, Proc of the 4th International Conference on Reactor Shielding, Paris (October 1972)

(67) Closing Address, J Butler, Proc of the 6th International Conference on Radiation Shielding, Tokyo, Japan (May 1983)

(68) "Flux-Limited Diffusion and Fokker-Planck Equations", G C Pomraning, Nuc Sci and Eng, 85 (1983)

(69) "Linked Monte Carlo and Finite-Element Diffusion Methods for Reactor Shield Design", E Shuttleworth and S J Chucas, Proc of the 6th International Conference on Radiation Shielding, Tokyo, Japan (May 1983)

(70) "A Practical Introduction to Finite-Element Analysis", Y K Cheung and M F Yeo, Pitman Publishing Limited (1979)

(71) "NADCON - WRS System Module Number 23015 for Mixing ADC Method A Data for Neutrons", M J Grimstone, AEEW-R1159

(72) Unpublished. S J Chucas, AEE Winfrith

(73) "Importance Function Biasing of the Deep-Penetration Monte Carlo Calculation", P N Stevens, Nuc Tech/Fusion, 5 (January 1984)

(74) "A Weight Window/Importance Generator for Monte Carlo Streaming Problems", T E Booth, Proc of the 6th International Conference on Radiation Shielding, Tokyo, Japan (May 1983)

TABLE 1

Materials Used in No-Duct Model of Tokamak

Component	Density ($g.cm^{-3}$)	Materials
First Blanket	3.035	Li_7Pb_2, Stainless Steel, C, He, Void
Second Blanket	1.864	Li_4SiO_4, C, He, Void, Stainless Steel
Hot-Shield	6.024	Stainless Steel, B_4C, Void
Duct Space	0.7800	Stainless Steel, Void
Cold-Shield	4.425	Stainless Steel, Borated Water
Gamma-Ray Shield	11.34	Lead
Magnet	8.341	Iron, Copper, Niobium

TABLE 2

Lower Energy Boundaries in MeV of EURLIB Multigroup (First 80 Groups)

1.3499E+01	1.2214E+01	1.1052E+01	1.0000E+01
9.0484E+00	8.1873E+00	7.4082E+00	7.0469E+00
6.7032E+00	6.3763E+00	6.0653E+00	5.4881E+00
4.9659E+00	4.7240E+00	4.4933E+00	4.0657E+00
3.6788E+00	3.3287E+00	3.0112E+00	2.7253E+00
2.4660E+00	2.3460E+00	2.2313E+00	2.0190E+00
1.8268E+00	1.6530E+00	1.4957E+00	1.3534E+00
1.2246E+00	1.1080E+00	1.0026E+00	9.0718E-01
8.2085E-01	7.4274E-01	6.7206E-01	6.0810E-01
5.5023E-01	4.9787E-01	4.5049E-01	4.0762E-01
3.6883E-01	3.3373E-01	3.0197E-01	2.7324E-01
2.4724E-01	2.2371E-01	2.0242E-01	1.8316E-01
1.6573E-01	1.4996E-01	1.3569E-01	1.2277E-01
1.1109E-01	8.6517E-02	6.7379E-02	5.2475E-02
4.0868E-02	3.1828E-02	2.6050E-02	2.4788E-02
2.3570E-02	2.1870E-02	1.9305E-02	1.5034E-02
1.1709E-02	9.1188E-03	7.1017E-03	5.5308E-03
4.3074E-03	3.3546E-03	2.6126E-03	2.0347E-03
1.5846E-03	1.2341E-03	9.6112E-04	7.4852E-04
5.8295E-04	4.5400E-04	3.5357E-04	2.7536E-04

TABLE 3

Flux-Weighting-Spectrum used in EURLIB Multigroup Data (see Figure 11 for Graph)

Energy Range	Weighting Spectrum
Thermal → 5 kT (1)	Thermal Maxwellian
5 kT → 0.82 MeV	1/E (2)
0.82 MeV → 14.92 MeV	Fission Spectrum

1. kT = 0.02533 eV at 300K
2. $1/\Sigma_t E$ for Fe, U235, U238 and Pu239

TABLE 4

Integrated Copper Damage Responses Computed for TFCs in 'No-Duct' Model of Tokamak

Nuclear Data Used	Copper Damage Rate (Displacements Per Atom Per Year)
UKNDL Point - DICE VI	1.20×10^{-6}
UKNDL Multigroup - P_5	0.97×10^{-6}
EURLIB Multigroup - P_3	0.82×10^{-6}

TABLE 5

Densities used in FENDER and MCBEND Calculations for 15 MeV Neutron Attenuation in Iron Benchmark

	FENDER	MCBEND
	(Atoms/Barn.cm)	
Mild Steel		
Fe	7.32×10^{-2}	8.65×10^{-2}
Mn	5.61×10^{-4}	6.62×10^{-4}
C	7.91×10^{-4}	9.34×10^{-4}
H	2.05×10^{-5}	2.42×10^{-5}
Concrete		
H	1.06×10^{-1}	8.76×10^{-1}
O	5.20×10^{-1}	4.30×10^{-2}
Al	2.88×10^{-2}	2.38×10^{-3}
Si	2.12×10^{-1}	1.74×10^{-2}
Ca	3.48×10^{-2}	2.88×10^{-3}
Fe	3.96×10^{-3}	3.27×10^{-4}
Aluminium for Void	1.0×10^{-6}	-

TABLE 6

Saturated Activities* Calculated using EURLIB Multigroup Data by MCBEND and Measured by Experiment in the NRPB Iron Benchmark

Foil Position	Calculated (Coefficient of Variation)	Measured
	Bq.nucleus^{-1}.neutron^{-1}	
1	1.25×10^{-29} (13.3%)	7.73×10^{-30}
2	4.94×10^{-31} (11.4%)	4.54×10^{-31}
3	3.01×10^{-32} (9.7%)	3.52×10^{-32}
4	2.29×10^{-33} (9.7%)	2.99×10^{-33}

* normalised to one source neutron.

TABLE 7

Saturated Activities* Calculated by MCBEND using 'Point' Nuclear Data for the NRPB Iron Benchmark

Foil Position	Calculated Saturated Activity ($Bq.nucleus^{-1}.neutron^{-1}$)		
	Activity	Coefficient of Variation	
		Monte Carlo	Total+
1	1.36×10^{-29}	15.1%	30.4%
2	6.81×10^{-31}	15.1%	41.0%
3	4.74×10^{-32}	12.9%	54.4%
4	3.41×10^{-33}	11.7%	71.1%

* Normalised to one source neutron.
\+ Due to Monte Carlo and Nuclear Data Variances.

TABLE 8

Energy Groups used for Correlation Matrices of ENDF/B Data by Drischler and Weisbin (61)

Group	Energy Range (MeV)
1	14.92 → 4.400
2	4.400 → 2.600
3	2.600 → 1.350
4	1.350 → 0.708
5	0.708 → 0.580
6	0.580 → 0.410
7	0.410 → 0.310
8	0.310 → 0.262
9	0.262 → 6.2×10^{-2}
10	6.2×10^{-2} → 3.0×10^{-2}
11	3.0×10^{-2} → 1.5×10^{-2}
12	1.5×10^{-2} → 1.585×10^{-3}
13	1.585×10^{-3} → 2.145×10^{-4}
14	2.145×10^{-4} → 1.068×10^{-5}
15	1.068×10^{-5} → 5.043×10^{-6}

TABLE 9

Ratios of Angular Importances to Scalar Importances

The following Ratios are obtained from the expression for $I(\underline{r},\underline{\omega})$ in Sub-section 6.2.2

$\frac{D\nabla\phi^*}{\phi^*}$	Cosine of Angle Between Particle Trajectory and $\nabla\phi^*$						
	-1.0	-0.85	-0.5	0.0	0.5	0.85	1.0
0.01	0.971	0.975	0.985	1.0	1.015	1.025	1.030
0.10	0.769	0.804	0.885	1.0	1.136	1.232	1.273
0.50	0.400	0.490	0.700	1.0	1.500	1.850	2.000
1.00	0.250	0.363	0.625	1.0	1.750	2.275	2.500
5.00	0.062	0.203	0.531	1.0	2.250	3.125	3.500
10.00	0.032	0.177	0.516	1.0	2.364	3.318	3.727
100.00	0.003	0.153	0.502	1.0	2.485	3.525	3.970

TABLE 10

Shape Functions for a Triangular Element

Node i	Shape Function Si
1	$2L_1^2 - L_1$
2	$4L_1L_2$
3	$2L_2^2 - L_2$
4	$4L_2L_3$
5	$2L_3^2 - L_3$
6	$4L_3L_1$

The nodes are as defined in Figure 18. The L_k are as defined in Sub-section 6.2.3.

TABLE 11

Shape Functions for A Rectangular Element

Node i	Shape Function Si
1	$\frac{1}{4}(1-U)(1-V)(1-U-V)$
2	$\frac{1}{2}(1-U^2)(1-V)$
3	$\frac{1}{4}(1+U)(1-V)(-1+U+V)$
4	$\frac{1}{2}(1-V^2)(1+U)$
5	$\frac{1}{4}(1+U)(1+V)(-1+U+V)$
6	$\frac{1}{2}(1-U^2)(1+V)$
7	$\frac{1}{4}(1-U)(1+V)(-1+U+V)$
8	$\frac{1}{2}(1-V^2)(1-U)$

The nodes are as defined in Figure 19. U and V are as defined in Sub-section 6.2.3.

TABLE 12

Gradients of the Shape Functions with Respect to the Natural Coordinates for a Triangular Element

Node i	$\frac{\partial Si}{\partial L_1}$	$\frac{\partial Si}{\partial L_2}$	$\frac{\partial Si}{\partial L_3}$
1	$4L_1 - 1$	0	0
2	$4L_2$	$4L_1$	0
3	0	$4L_2 - 1$	0
4	0	$4L_3$	$4L_2$
5	0	0	$4L_3 - 1$
6	$4L_3$	0	$4L_1$

TABLE 13

Gradients of the Shape Functions with Respect to the Natural Coordinates for a Rectangular Element

Node i	$\frac{\partial Si}{\partial U}$	$\frac{\partial Si}{\partial V}$
1	$\frac{1}{4}(V-1)(2-2U-V)$	$\frac{1}{4}(U-1)(2-2V-U)$
2	$U(V-1)$	$\frac{1}{2}(U^2-1)$
3	$\frac{1}{4}(1-V)(2U+V)$	$\frac{1}{4}(1+U)(2-2V-U)$
4	$\frac{1}{2}(1-V^2)$	$-V(1+U)$
5	$\frac{1}{4}(1+V)(2U+V)$	$\frac{1}{4}(1+U)(2V+U)$
6	$-U(1+V)$	$\frac{1}{2}(1-U^2)$
7	$\frac{1}{4}(1+V)(2-2U-V)$	$\frac{1}{4}(1-U)(2V+U)$
8	$\frac{1}{2}(V^2-1)$	$V(U-1)$

TABLE 14

Gradients of the Shape Functions with Respect to the Natural Coordinates Averaged over a Triangular Element

Node i	$\left\langle \frac{\partial Si}{\partial L_1} \right\rangle$	$\left\langle \frac{\partial Si}{\partial L_2} \right\rangle$	$\left\langle \frac{\partial Si}{\partial L_3} \right\rangle$
1	1/3	0	0
2	4/3	4/3	0
3	0	1/3	0
4	0	4/3	4/3
5	0	0	1/3
6	4/3	0	4/3

TABLE 15

Gradients of the Shape Functions with Respect to the Natural Coordinates Averaged over a Rectangular Element

Node i	$\left\langle \frac{\partial Si}{\partial U} \right\rangle$	$\left\langle \frac{\partial Si}{\partial V} \right\rangle$
1	-1/12	-1/12
2	0	-1/3
3	1/12	-1/12
4	1/3	0
5	1/12	1/12
6	0	1/3
7	-1/12	1/12
8	-1/3	0

TABLE 16

Groups for Which Iron Block Problem was Solved by MCBEND

Group Number	Energy Range (MeV)
1	13.5 - 14.2
2	12.5 - 13.5
3	11.25 - 12.5
4	10.0 - 11.25
5	8.5 - 10.0
6	7.0 - 8.5
7	6.07 - 7.0
8	4.72 - 6.07

TABLE 17

Results of MCBEND Calculation with Scalar Importances on an Iron Block (Without Void)

Group	Group Flux	Coefficient of Variation on Flux (%)	Coefficient of Variation on Weight (%)	Number of Particles Scored
1	7.182×10^{-12}	9.1	39.7	26765
2	2.938×10^{-12}	8.0	32.7	13545
3	1.284×10^{-12}	7.2	26.4	7431
4	5.506×10^{-13}	8.0	25.9	3205
5	4.898×10^{-13}	9.0	22.7	3158
6	5.050×10^{-13}	8.0	22.0	3676
7	5.085×10^{-13}	8.2	22.5	4073
8	1.595×10^{-12}	7.4	20.8	12872

TABLE 18

Results of MCBEND Calculation with Directional Importances on an Iron Block (Without Void)

Group	Group Flux	Coefficient of Variation on Flux (%)	Coefficient of Variation on Weight (%)	Number of Particles Scored
1	7.669×10^{-12}	9.2	68.6	25012
2	2.723×10^{-12}	8.1	86.0	13152
3	1.598×10^{-12}	7.7	93.1	10361
4	5.666×10^{-13}	8.2	86.6	4050
5	4.882×10^{-13}	9.1	70.8	3046
6	4.967×10^{-13}	9.2	77.1	2892
7	4.901×10^{-13}	8.5	69.2	3126
8	1.561×10^{-12}	7.7	83.5	9847

TABLE 19

Results of MCBEND Calculation with Scalar Importances on an Iron Block (With a Void)

Group	Group Flux	Coefficient of Variation on Flux (%)	Coefficient of Variation on Weight (%)	Number of Particles Scored
1	1.967×10^{-11}	8.3	43.6	20345
2	6.217×10^{-12}	7.1	39.4	9332
3	3.161×10^{-12}	8.2	35.2	5420
4	1.166×10^{-12}	8.8	35.3	2112
5	1.013×10^{-12}	8.4	31.1	2134
6	1.238×10^{-12}	7.9	32.0	2742
7	9.313×10^{-13}	8.1	24.0	2489
8	3.398×10^{-12}	7.2	26.7	8901

TABLE 20

Results of MCBEND Calculation with Directional Importances on an Iron Block (With a Void)

Group	Group Flux	Coefficient of Variation on Flux (%)	Coefficient of Variation on Weight (%)	Number of Particles Scored
1	2.003×10^{-11}	8.3	64.3	19844
2	5.882×10^{-12}	7.4	81.0	8799
3	3.211×10^{-12}	8.1	42.4	5551
4	9.875×10^{-13}	9.1	71.1	2337
5	1.014×10^{-12}	8.5	36.9	1804
6	1.113×10^{-12}	7.8	40.4	3034
7	1.037×10^{-12}	7.8	69.2	4413
8	3.122×10^{-12}	6.9	70.4	9688

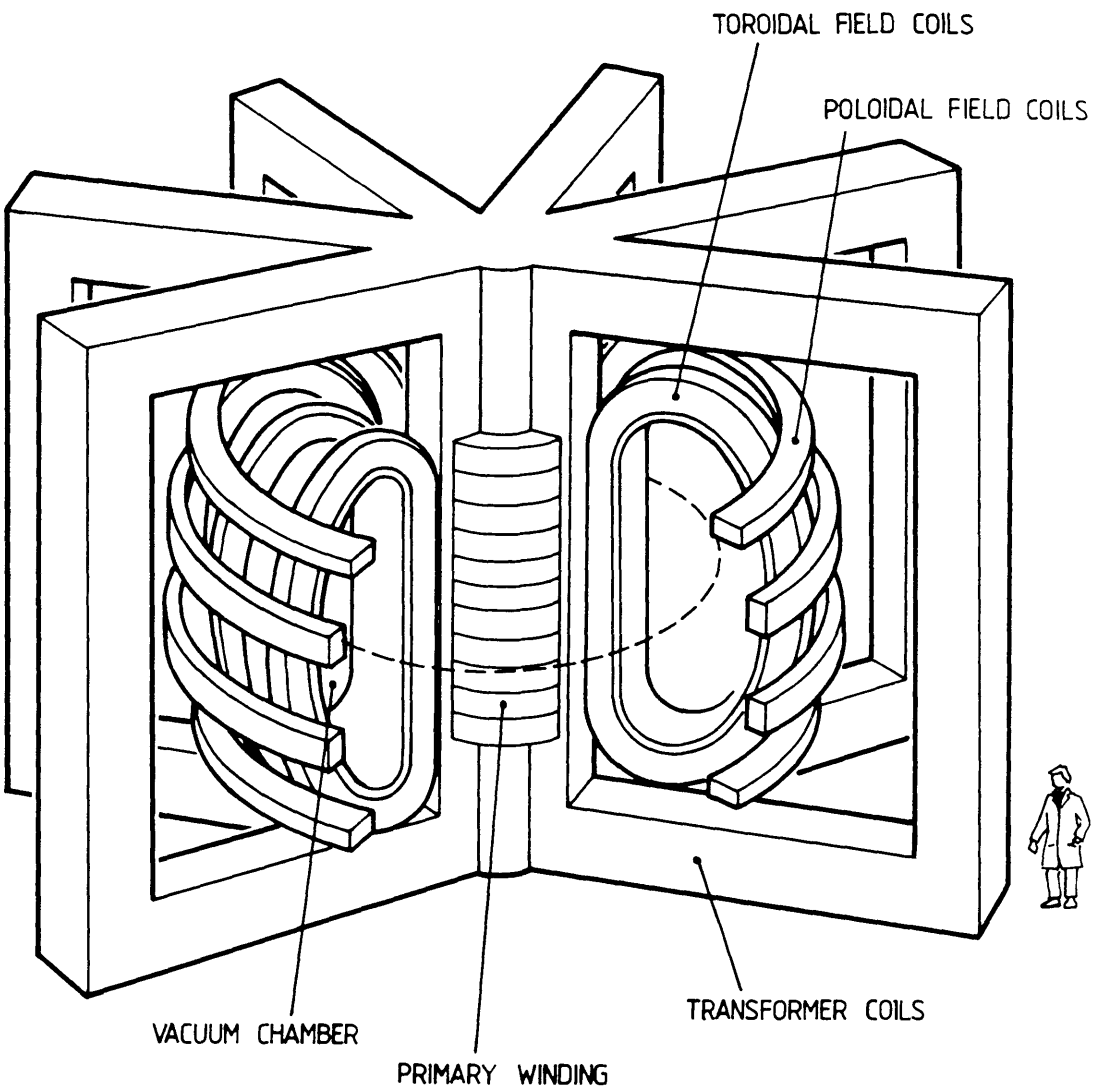

FIG. 1 PRINCIPAL FEATURES OF A TOKAMAK REACTOR

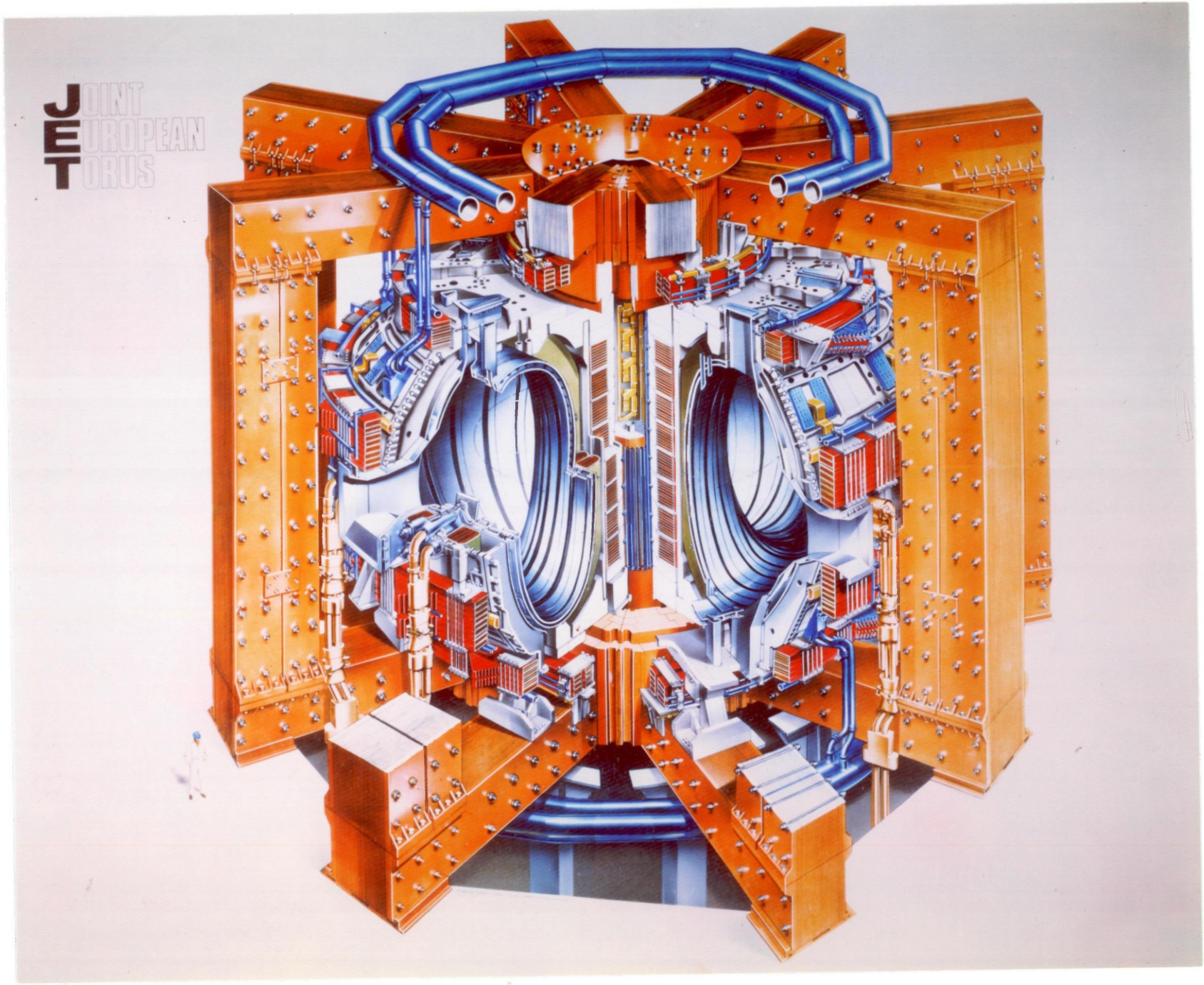

FIGURE 2: THE JOINT EUROPEAN TORUS

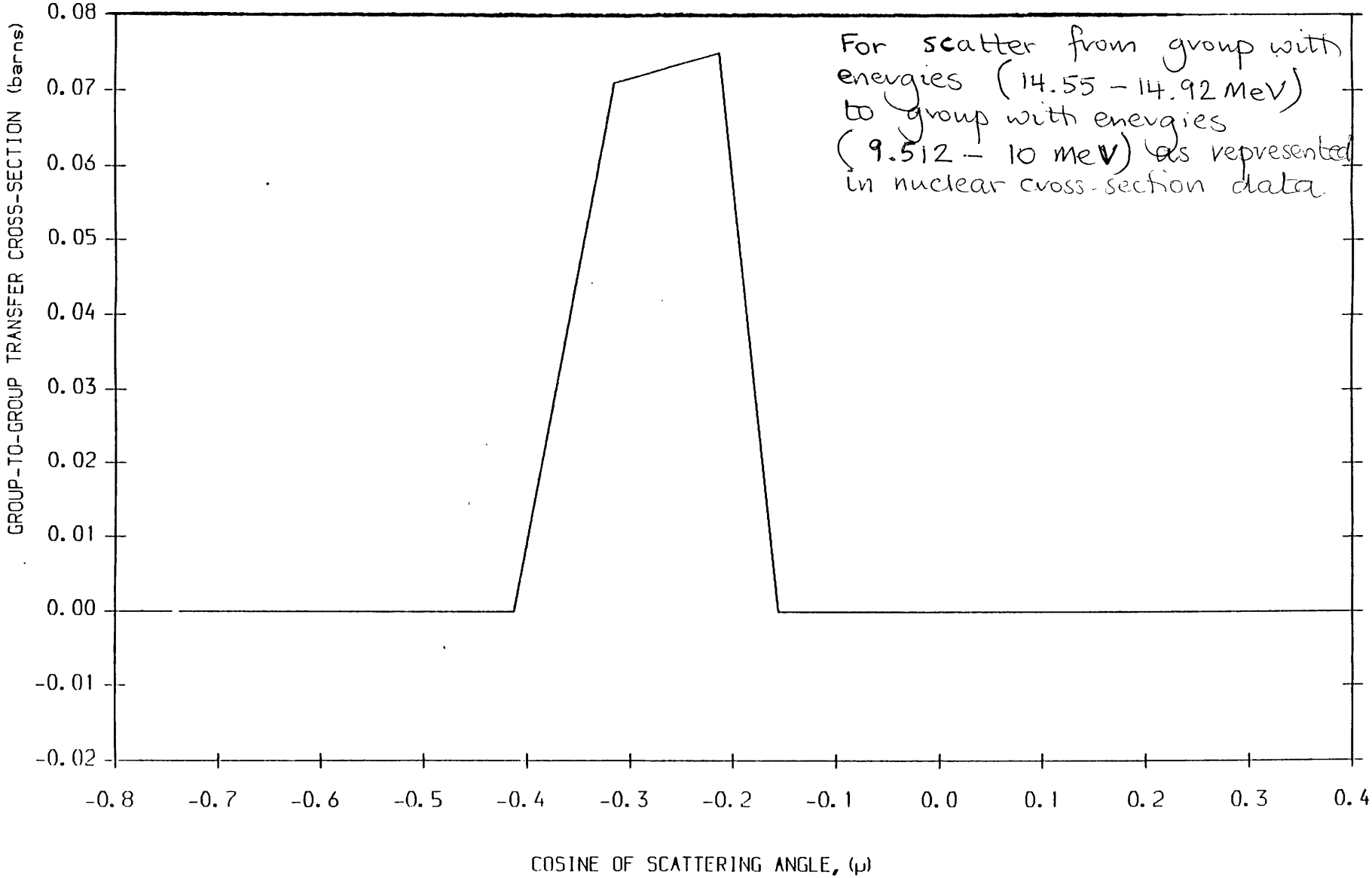

Figure 4. Li^7 cross-section.

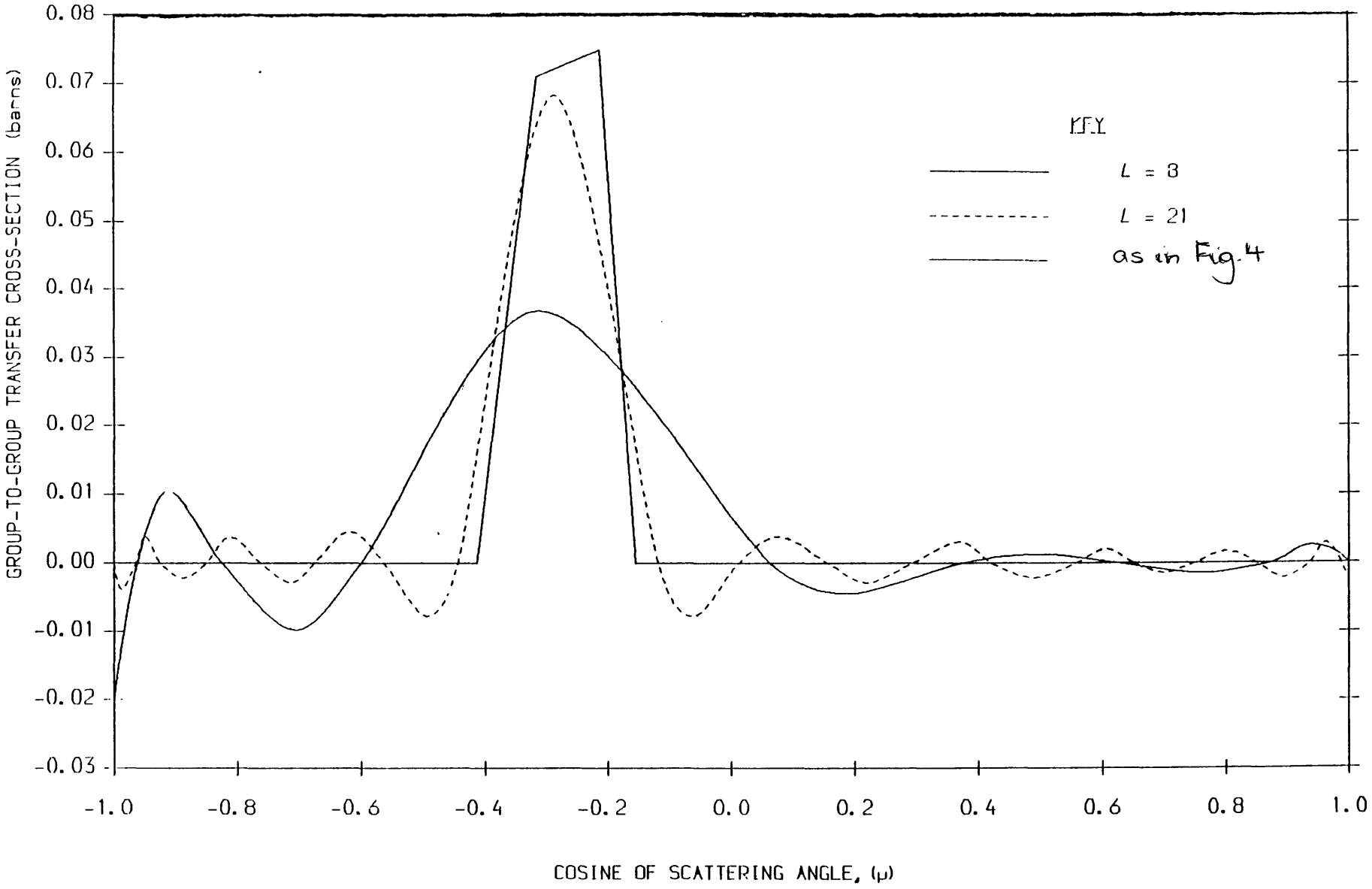

Figure 5. Legendre expansions of Li^7 cross-section.

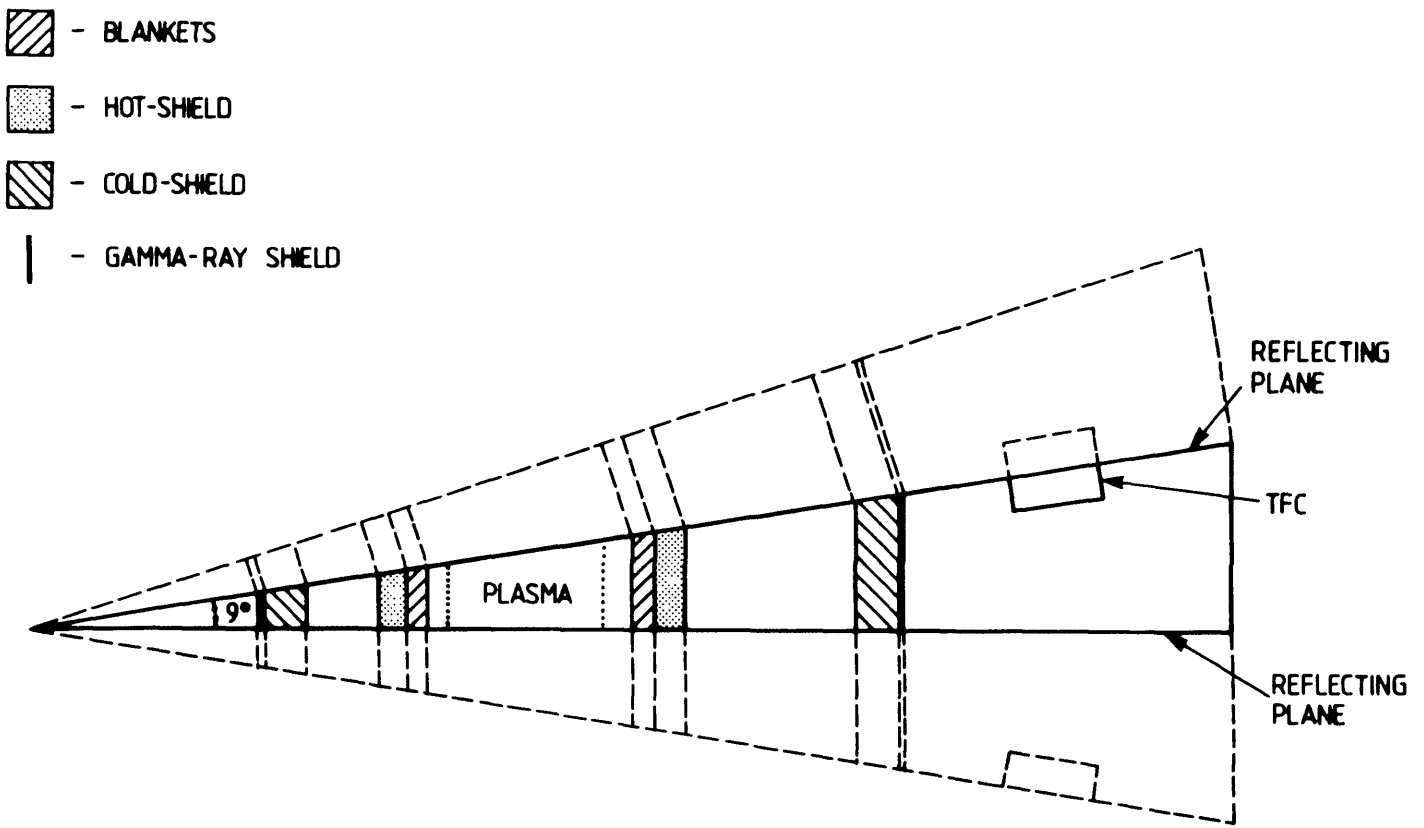

FIG. 6 SECTOR OF THE McBEND MODEL OF A TOKAMAK REACTOR DEFINING A 9° SEGMENT OF THE TORUS

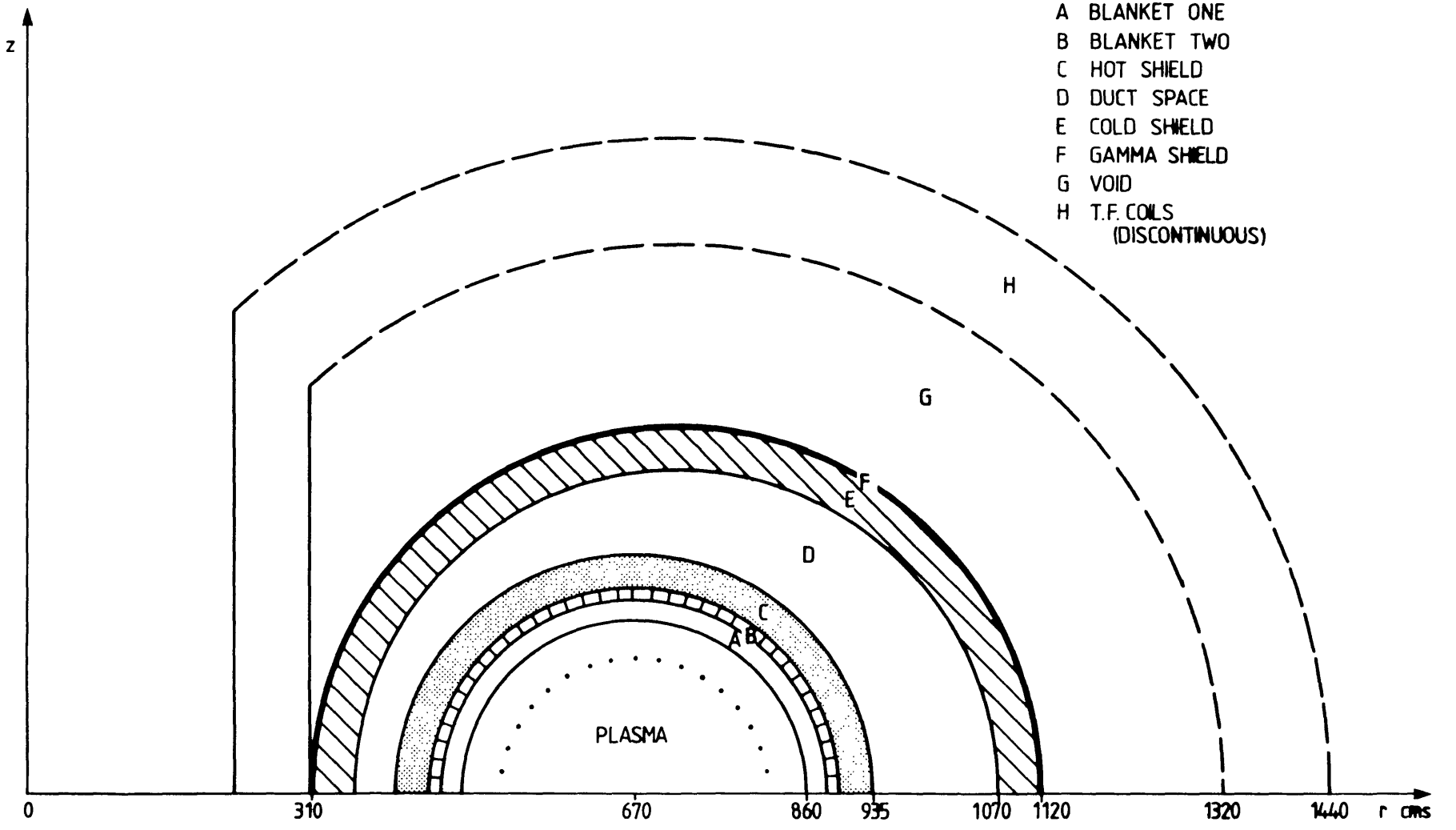

FIG. 7 VERTICAL CROSS-SECTION THROUGH THE McBEND MODEL OF A TOKAMAK REACTOR WITHOUT PENETRATIONS

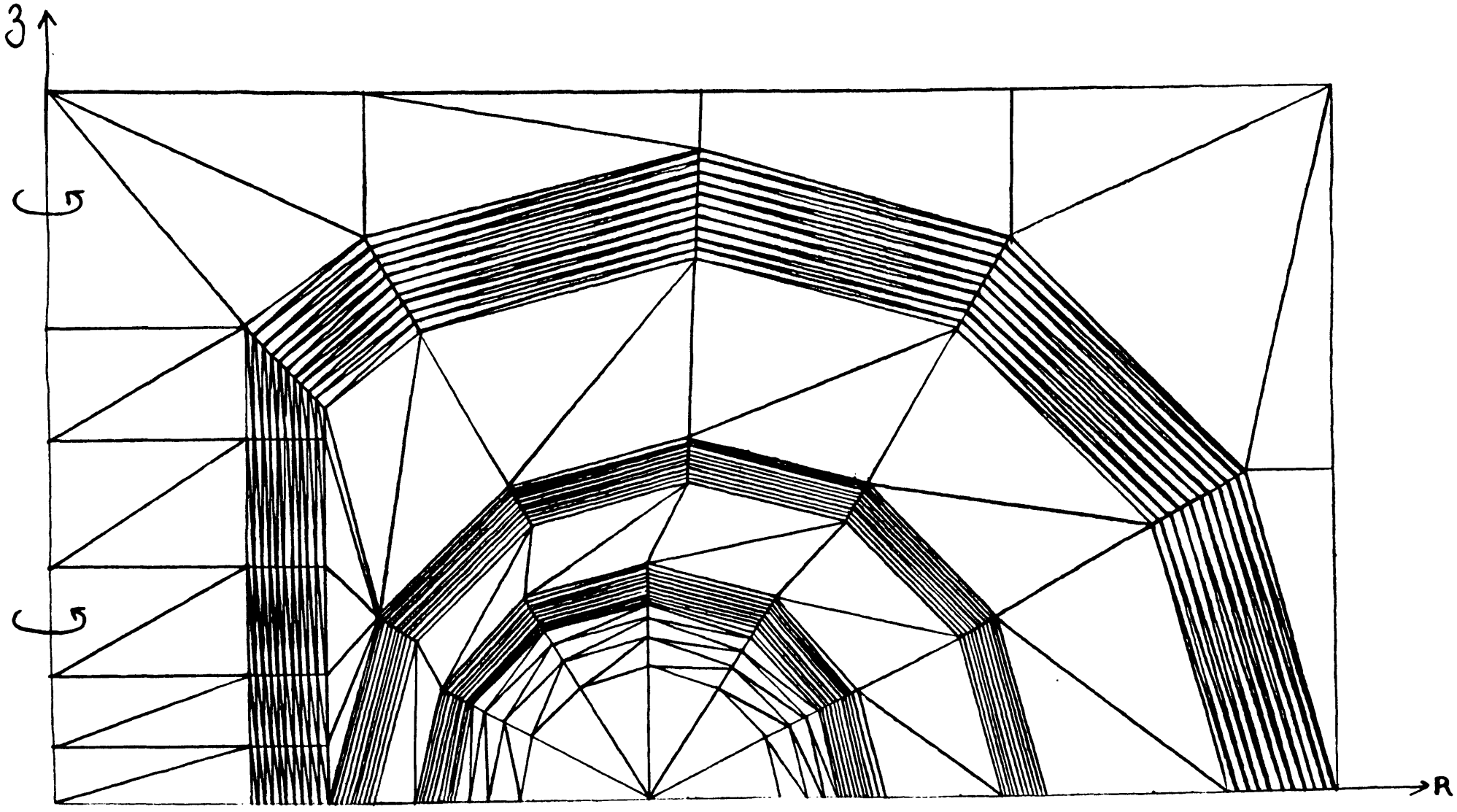

Figure 8. Finite-element mesh of Tokamak reactor without penetrations

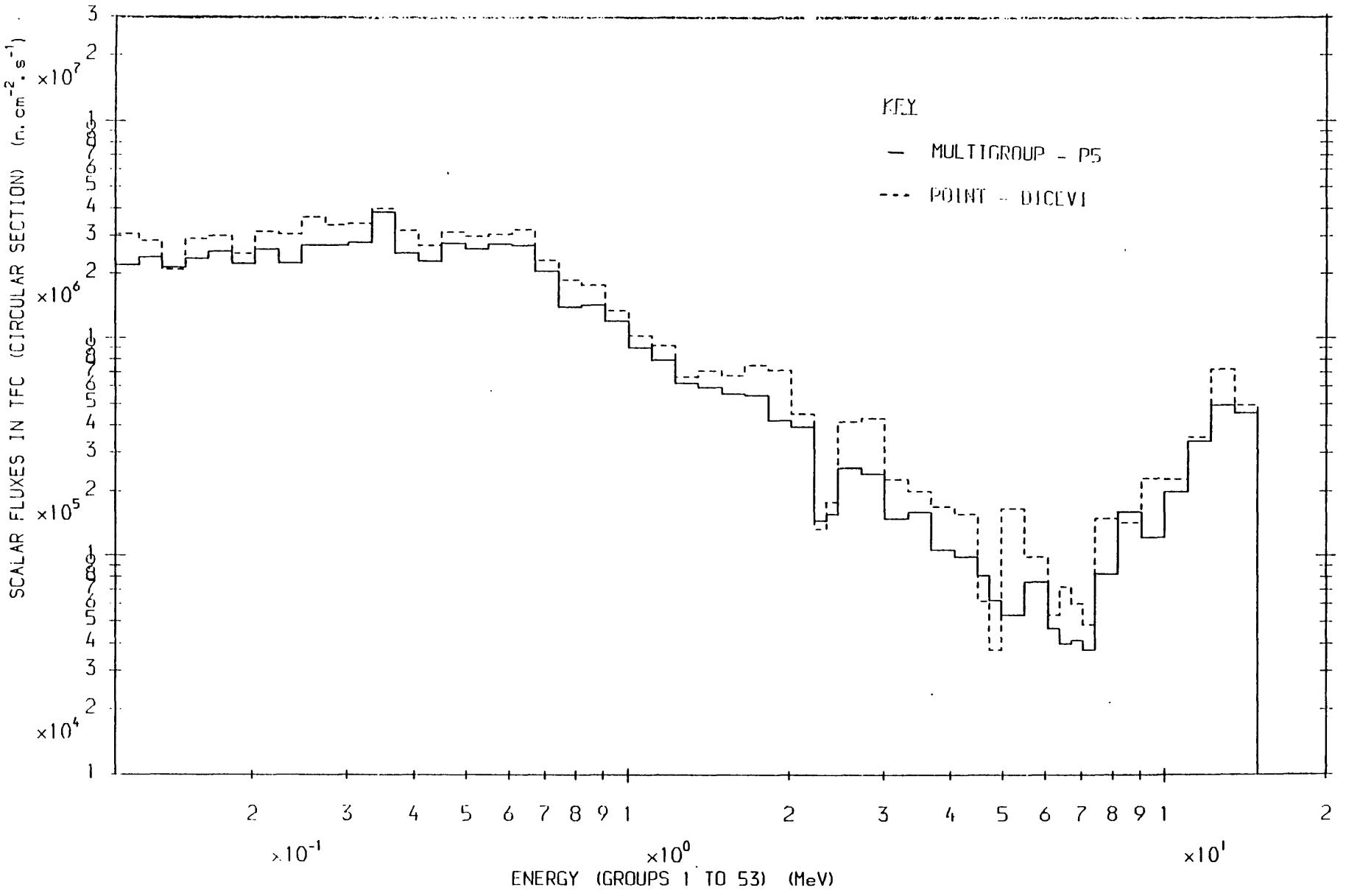

Figure 9. Comparison of point and multigroup fluxes in TFC.

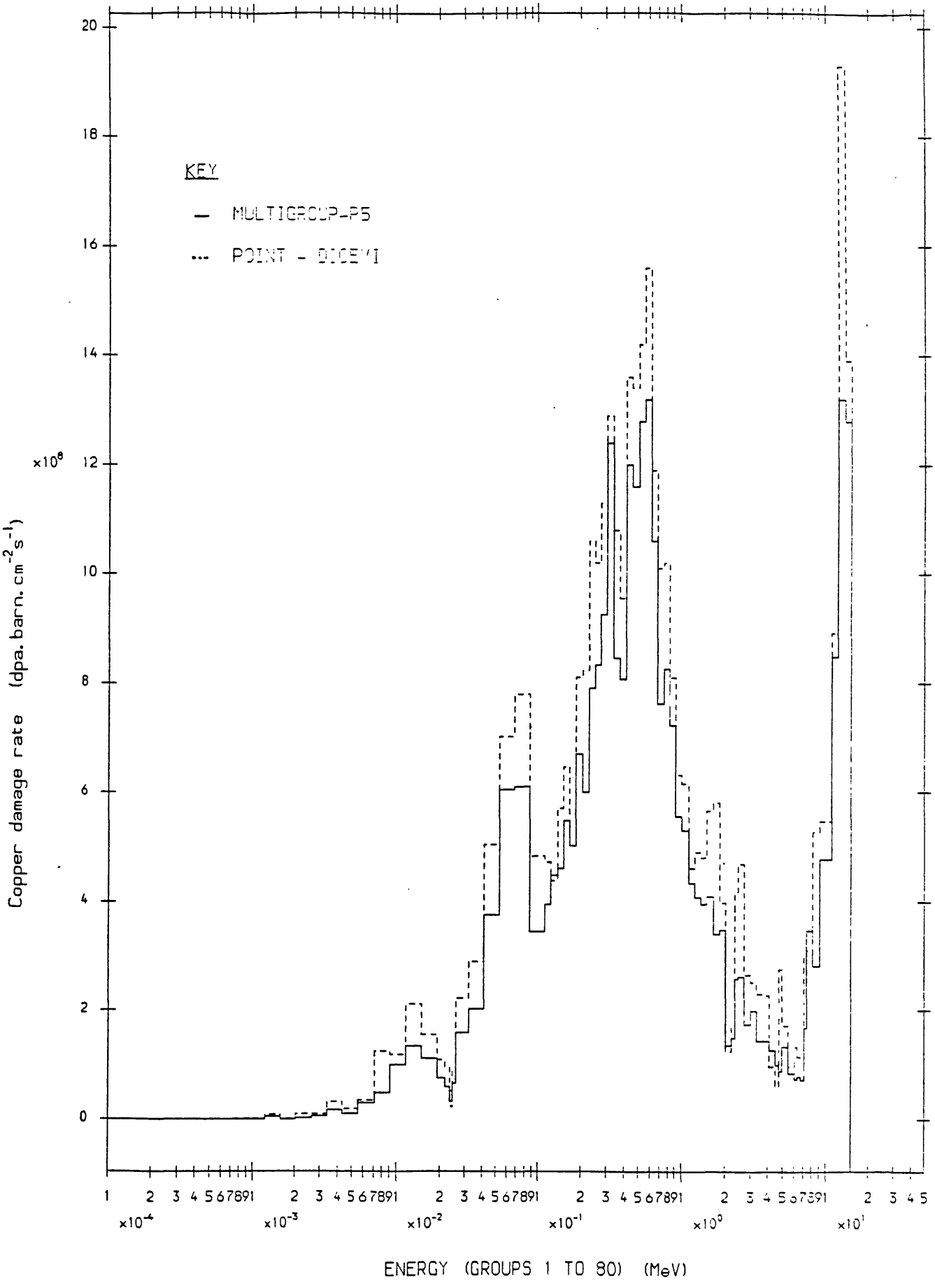

Figure 10. Comparison of copper damage rates in TFC.

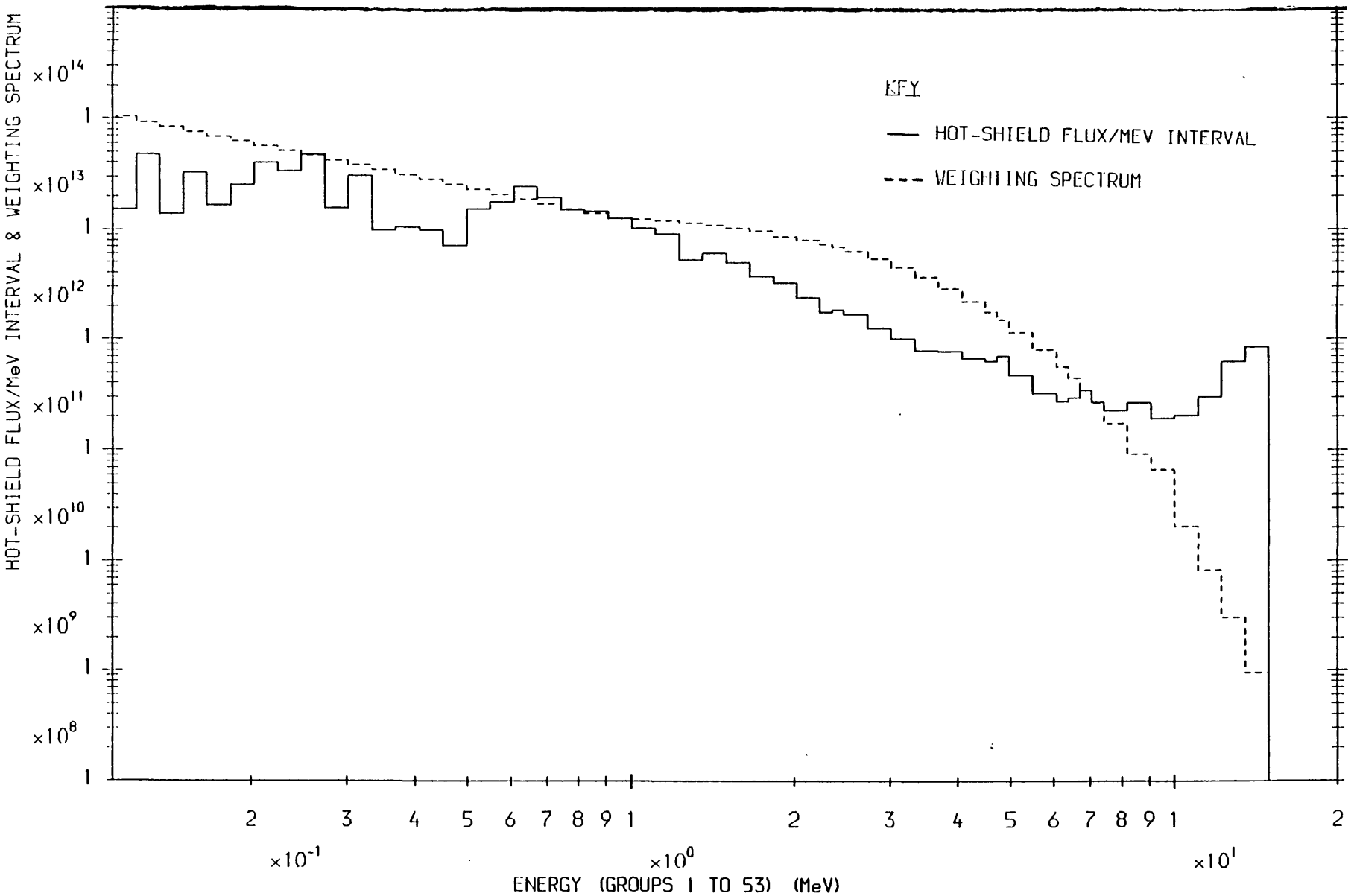

Figure 11 . Comparison of hot-shield flux with weighting-spectrum.

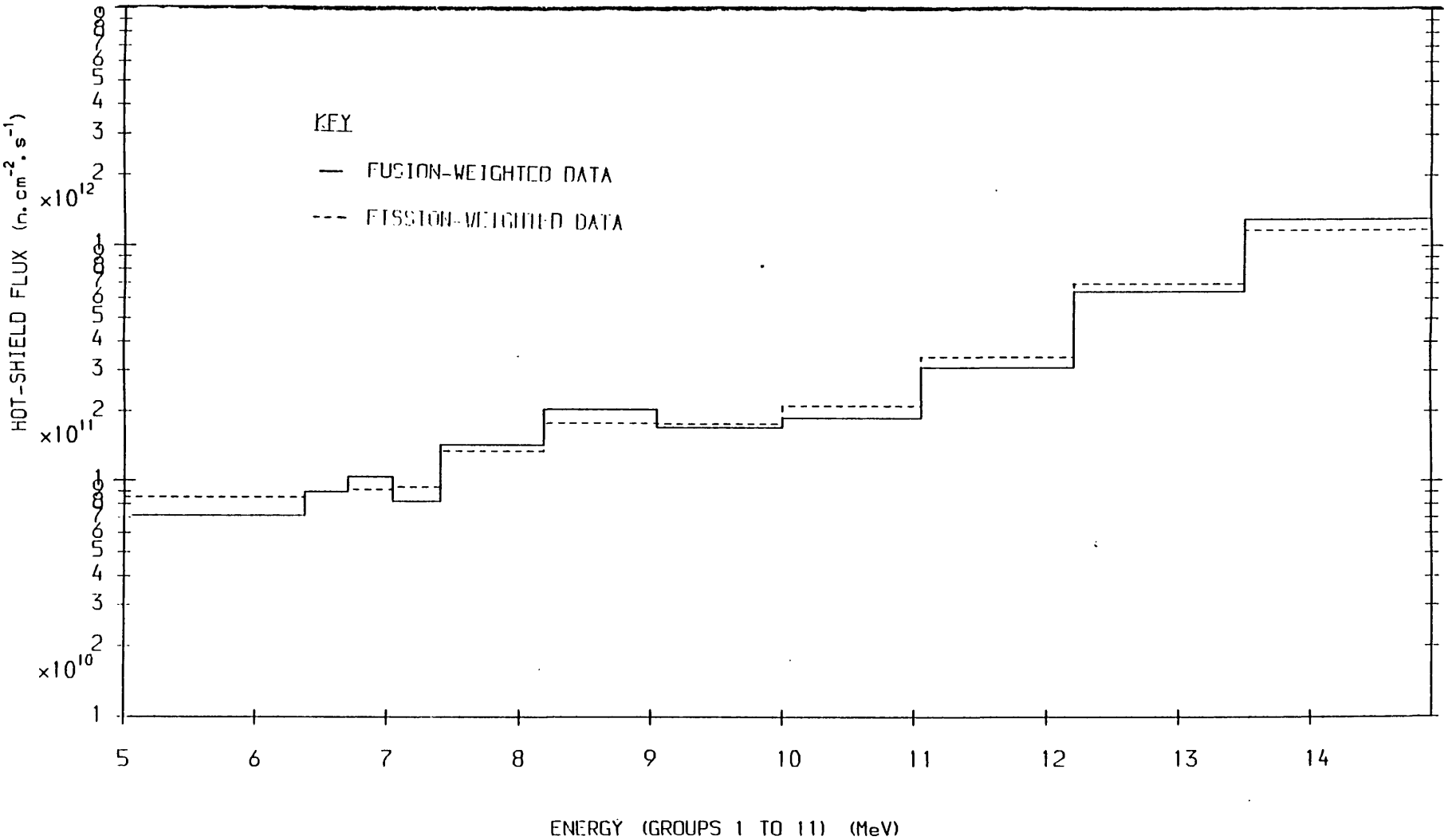

Fig. 12 . Comparison of fusion- & fission-weighted hot-shield fluxes.

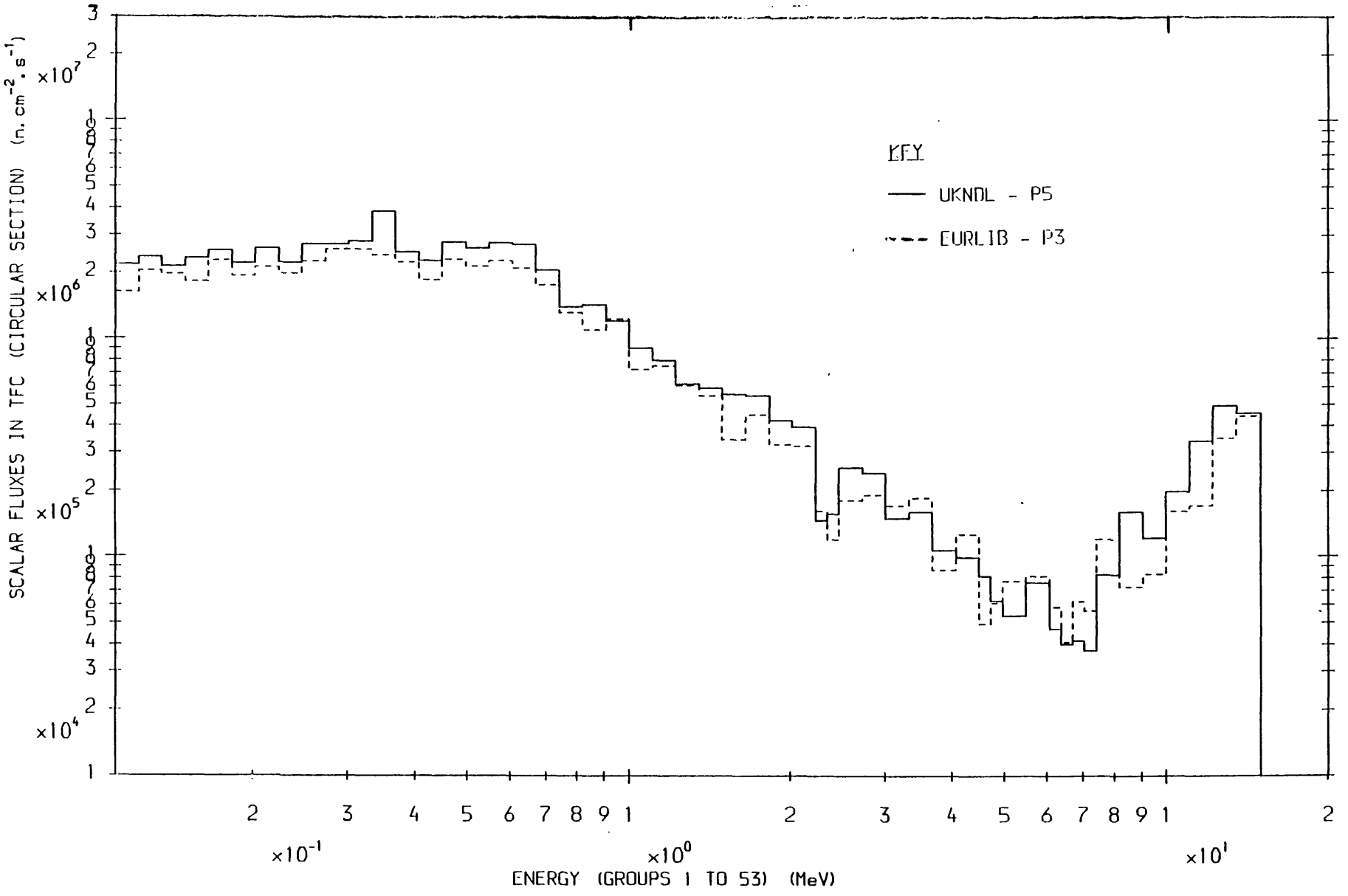

Figure 13. EURLIB AND UKNDL multigroup fluxes in TFC.

(a) CROSS-SECTION THROUGH X-Y

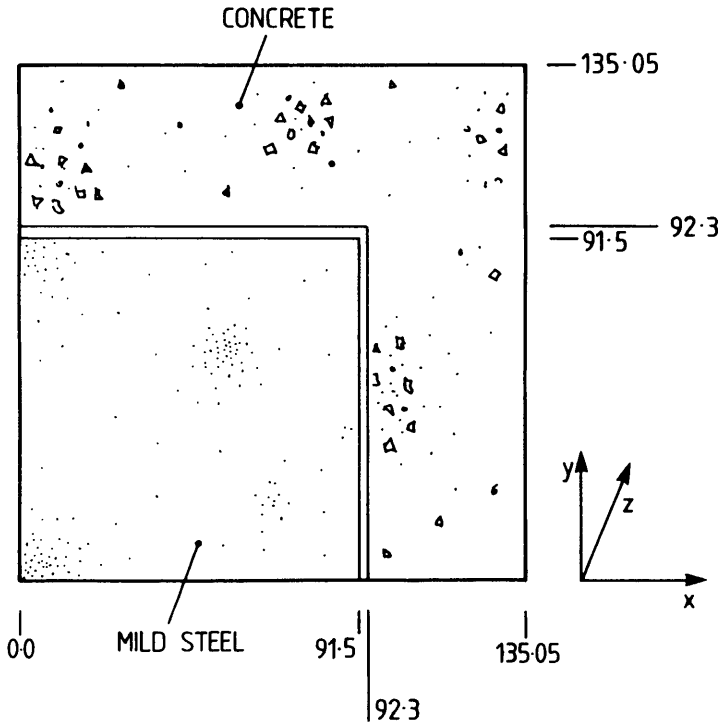

(b) CROSS-SECTION THROUGH Y-Z

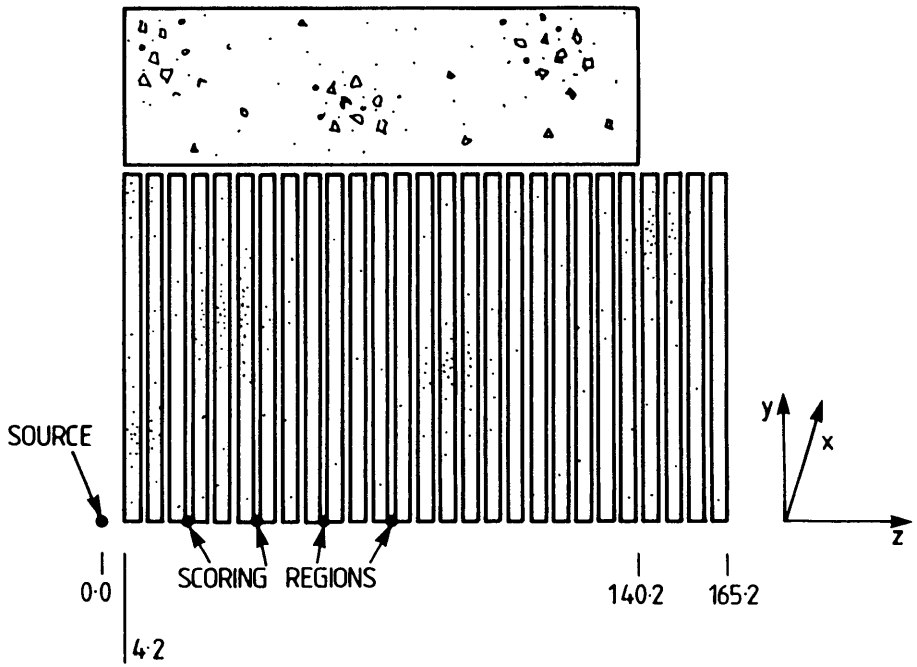

FIG. 14 McBEND MODEL OF THE NRPB IRON BENCHMARK EXPERIMENT

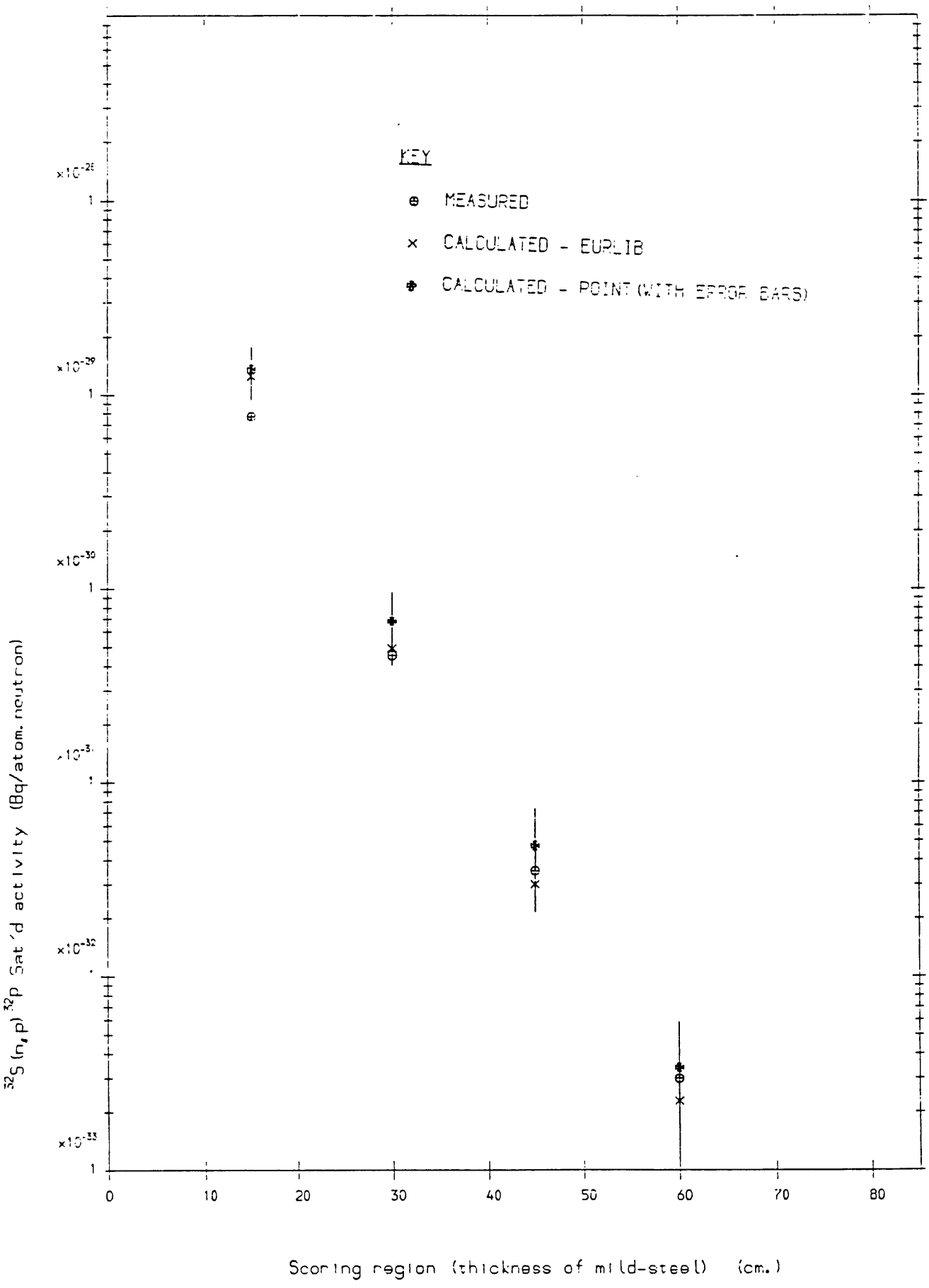

FIGURE 15. Measured and calculated activities in NRPB benchmark

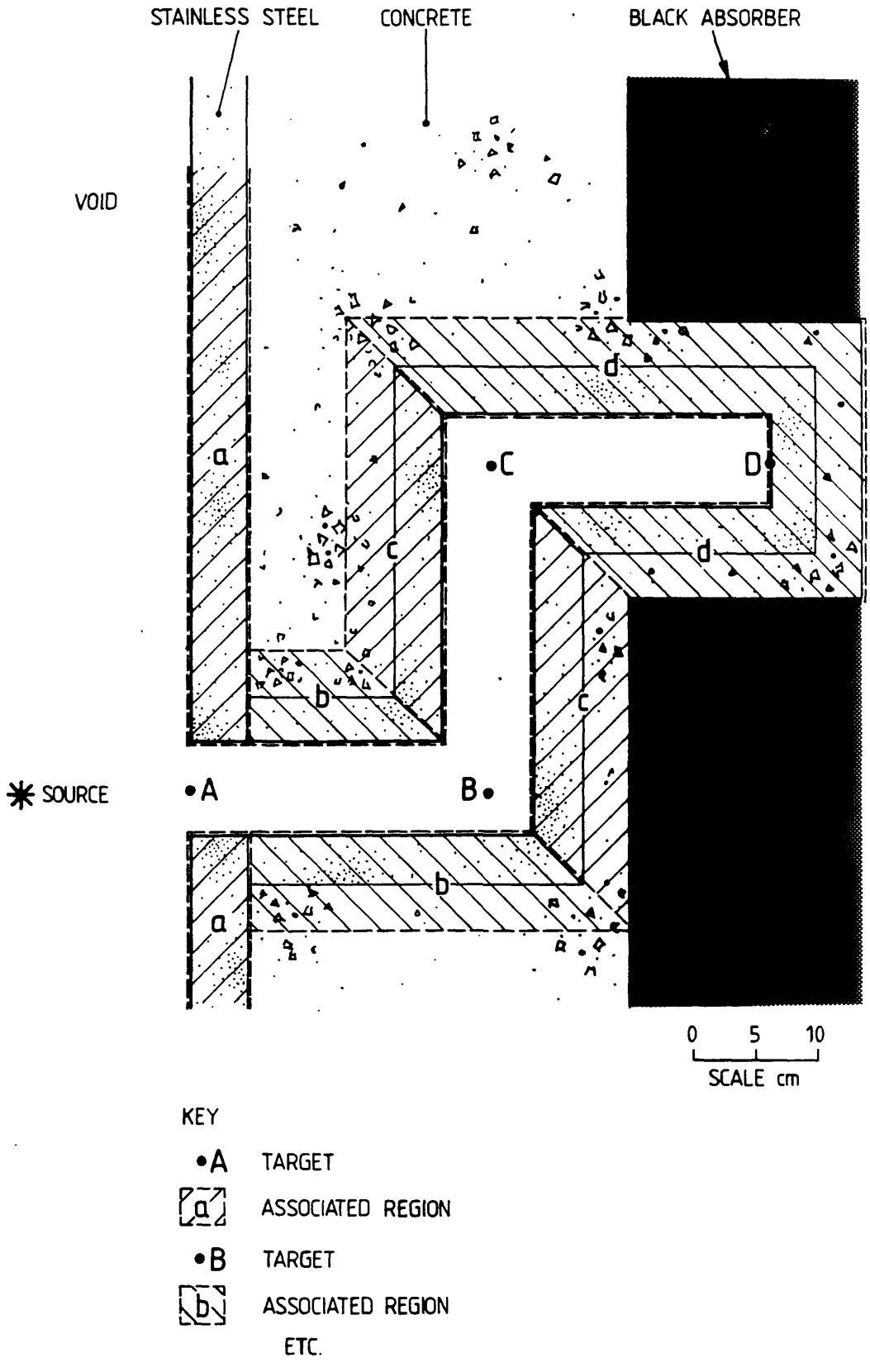

FIG. 16 DUCT PROBLEM TO TEST THE OLD ANGULAR BIASING METHOD OF McBEND

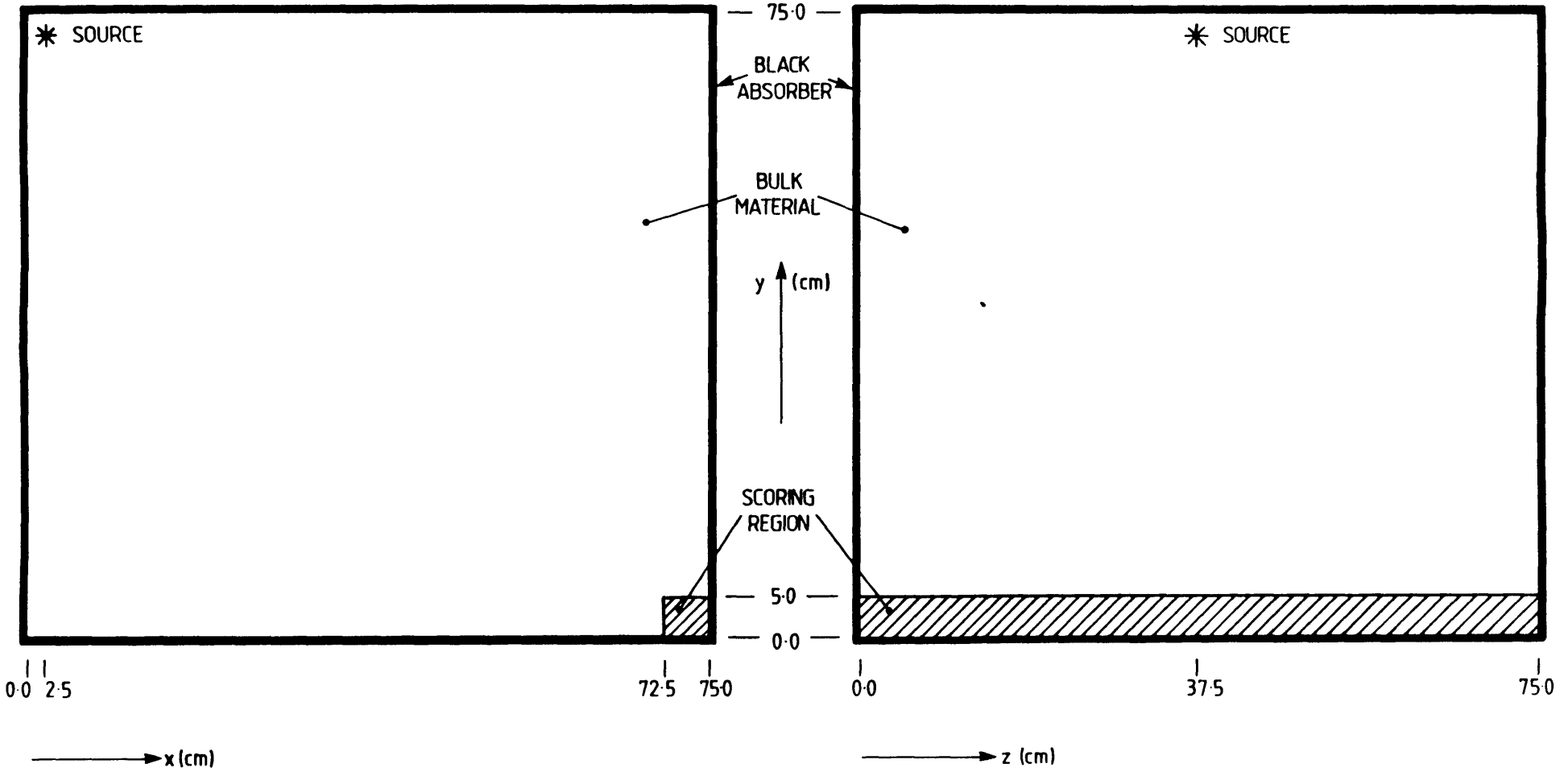

FIG. 20 PROBLEM TO TEST NEW ANGULAR BIASING METHOD IN McBEND

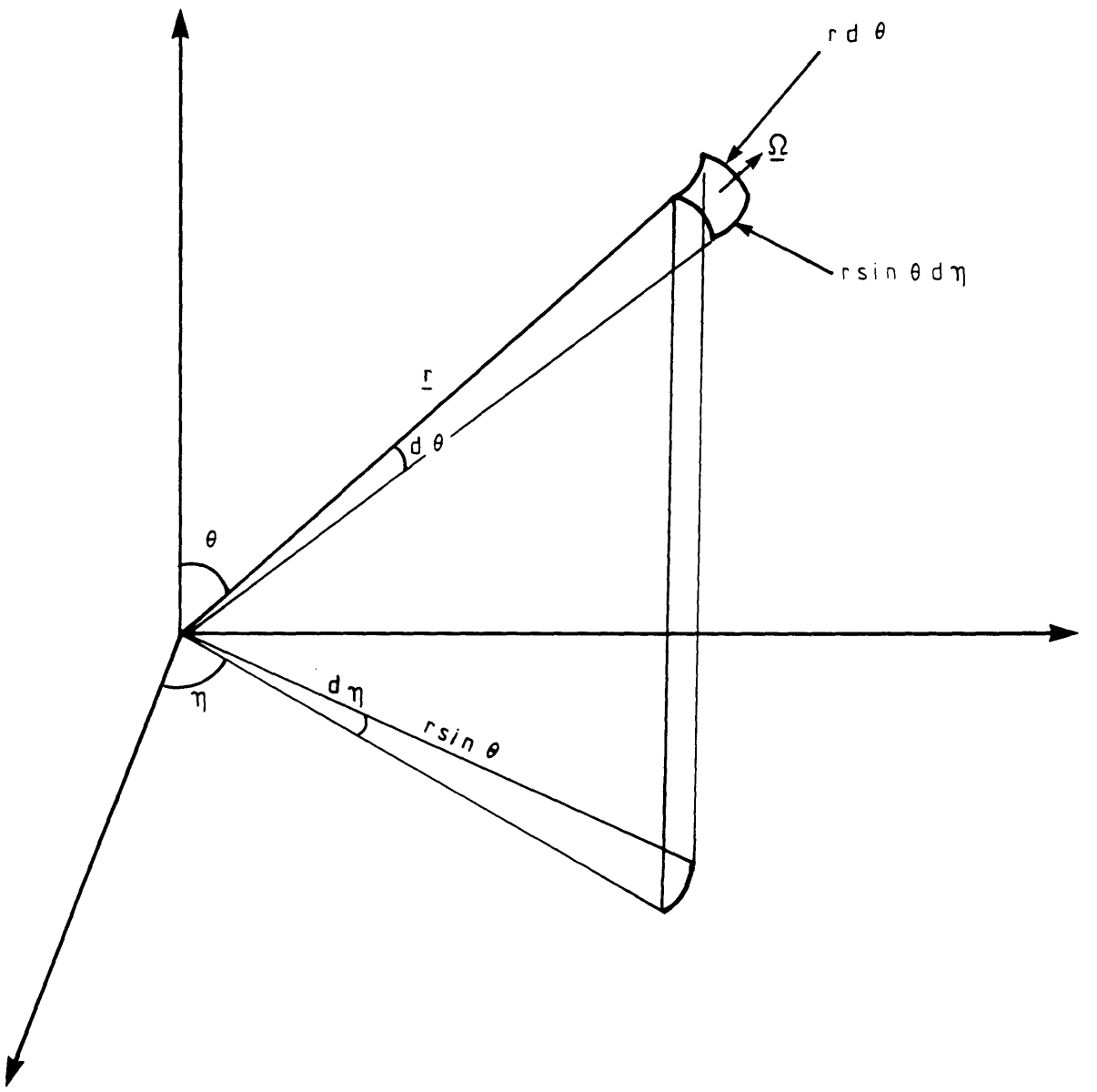

FIG. 21. RELATIONSHIP BETWEEN $P(r,\Omega)\,d\Omega$, $P(r,\theta)\,d\theta$ AND $P(r,\eta)\,d\eta$

A P P E N D I X A

PUTTING THE NEUTRON TRANSPORT EQUATION INTO MULTIGROUP FORM

The time independent neutron transport equation can be written as follows:

$$\underline{\Omega}.\underline{\nabla}\ \psi\ (\underline{r},\underline{\Omega},E) + \sigma_t(\underline{r},E)\ \psi(\underline{r},\underline{\Omega},E)$$

$$= \int_{E'} \int_{\Omega'} \sigma_s(\underline{r},E')\ p(\underline{r};E'\rightarrow E,\underline{\Omega}'\rightarrow\underline{\Omega})\psi(\underline{r},\underline{\Omega}',E')d\underline{\Omega}'dE'$$

$$+ S(\underline{r},\underline{\Omega},E)$$

This equation may be interpreted as a conservation equation accounting for additions to and losses from a 'packet' of neutrons contained within a unit element of the particle phase-space.

$\psi(\underline{r},\underline{\Omega},E)dEd\underline{\Omega}$ is the angular-flux-density of neutrons at $\underline{r}$ travelling in the solid angle $d\underline{\Omega}$ about $\underline{\Omega}$ with energies within dE of E;

$\sigma_t(\underline{r},E)$ is the total macroscopic neutron cross-section at $\underline{r}$ for neutrons of energy E;

$\sigma_s(\underline{r},E')$ is the total macroscopic scattering cross-section at $\underline{r}$ for neutrons of energy E';

$p(\underline{r};E'\to E,\underline{\Omega}'\to\underline{\Omega})$ is the probability of a neutron of energy E' and direction $\underline{\Omega}'$ being scattered at $\underline{r}$ into a direction $\underline{\Omega}$ with energy E;

$S(\underline{r},\underline{\Omega},E)dVd\underline{\Omega}dE$ is the total number of neutrons created at $\underline{r}$ per second, per unit volume, per unit solid angle, per unit energy.

At first sight it might appear that this equation could be cast into a multigroup form by integrating over the energy range of each group, say $E_1 < E < E_2$. However, supposing that the flux-density in this group could be defined as

$$\phi_g(\underline{r},\underline{\Omega}) = \int_{E_1}^{E_2} \phi(r\_,\Omega\_,E)\, dE,$$

then the $\sigma_t\phi$ term on the left of the neutron transport equation would become $\sigma_{t,g}(\underline{r},\underline{\Omega})\ \phi(\underline{r},\underline{\Omega})$ where

$$\sigma_{t,g}(\underline{r},\underline{\Omega}) = \frac{\int_{E_1}^{E_2} \sigma_t(\underline{r},E)\ \phi(\underline{r},\underline{\Omega},E)\ dE}{\phi_g(\underline{r},\underline{\Omega})}$$

Thus, the cross-section σ_t would acquire a dependence on $\underline{\Omega}$. This complication can be avoided by assuming a form for the angular dependence before integrating. This is usually achieved by an expansion in spherical harmonics which reduces to an expansion in Legendre polynomials if an axis of symmetry exists.

It is most often the case that the scattering probability, given by p in the neutron transport equation, is a function of $\underline{\Omega}.\underline{\Omega}'$ only; that is, there is azimuthal symmetry. Thus, the scattering term can be written as

$$\sigma_s(\underline{r},E')p(\underline{r};E'\rightarrow E,\underline{\Omega}',\underline{\Omega}) = \sigma_s(\underline{r},E')p(r;E'\rightarrow E;\mu_o)$$

where $\mu_o = \underline{\Omega}.\underline{\Omega}'$.

This is then expanded in a set of Legendre polynomials of μ_o to give:

$$\sigma_s(\underline{r},E')p(\underline{r};E'\rightarrow E,\underline{\Omega}'\rightarrow\underline{\Omega}) = \sum_{\ell=0}^{\infty} \frac{2\ell+1}{4\pi} \sigma_{s\ell}(\underline{r};E'\rightarrow E)P_\ell(\mu_o)$$

with $$\sigma_{s\ell}(\underline{r};E'\rightarrow E) = 2\pi \int_{-1}^{1} \sigma_s(\underline{r},E')p(\underline{r};E'\rightarrow E,\mu_o)P_\ell(\mu_o)d\mu_o$$

and the P_ℓ being the well-known Legendre polynomials, defined as:

$$P_o(x) = 1$$

$$P_n(x) = \frac{1}{2^n n!} \frac{d^n}{dx^n}(x^2 - 1)^n \quad \text{for } n = 1, 2, 3 \ldots$$

The angular distributions of the neutron flux-density $\phi(\underline{r},\underline{\Omega},E)$ and the source $S(\underline{r},\underline{\Omega},E)$ are treated in a similar

way (again assuming independence in azimuthal angle) to give

$$\psi(\underline{r},\mu,E) = \sum_{m=0}^{\infty} \frac{2m+1}{4\pi} \Phi_m(\underline{r},E)\, P_m(\mu)$$

and

$$S(\underline{r},\mu,E) = \sum_{m=0}^{\infty} \frac{2m+1}{4\pi} S_m(\underline{r},E)\, P_m(\mu)$$

where

$$\Phi_m(\underline{r},E) = 2\pi \int_{-1}^{1} \Phi(\underline{r},\mu,E)\, P_m(\mu)\, d\mu$$

and

$$S_m(\underline{r},E) = 2\pi \int_{-1}^{1} S(\underline{r},\mu,E)\, P_m(\mu)\, d\mu$$

The expression for the scattering term is substituted into the neutron transport equation and, after the use of the 'addition theorem' for Legendre polynomials, the equation is integrated over the azimuthal angles of scatter. The expansions for the flux-density and source terms are then introduced into the resulting equation and the result multiplied by $P_n(\mu)$. Integrating over $-1 \leq \mu \leq 1$ and using the orthogonality of the Legendre polynomials an infinite set of coupled differential equations is obtained.

Hence, the directional dependence has been treated by means of an expression in terms of a complete set of orthogonal functions - the Legendre polynomials. The resulting set of equations is exact: it involves no approximations other than those inherent in the transport equation itself. These equations are now put into multigroup form to allow treatment of the energy variable.

Firstly, the energy range of interest is divided into a series of contiguous energy intervals (typically 20 to 100) chosen so that, wherever possible, the variation of important cross-sections within each group is relatively small. The groups are numbered sequentially such that the energy decreases as the group number increases. The differential equations are then integrated over all the energy groups resulting in a further (still infinite) set of equations in which 'group flux expansion coefficients' correspond to the flux-density and 'group constants' to the cross-sections of the original neutron transport equation.

More specifically, the group flux expansion coefficients $\Phi_{n,g}$ can be defined by

$$\Phi_{n,g}(\underline{r}) = \int_{E_g}^{E_{g-1}} \Phi_n(\underline{r},E')dE' \equiv \int_g \Phi_n(\underline{r},E')dE'$$

and the group constants by

$$\sigma_{t_{n,g}}(\underline{r}) \equiv \frac{\int_g \sigma_t(\underline{r},E)\ \Phi_n(\underline{r},E)dE}{\Phi_{n,g}(\underline{r})}$$

and

$$\sigma_{s_{n,g'\to g}}(\underline{r}) \equiv \frac{\int_{g} \Phi_n(\underline{r},E') \int_{g} \sigma_{s_n}(\underline{r};E'\to E)\,dE\,dE'}{\Phi_{n,g'}(\underline{r})}$$

(The latter are also known as transfer cross-sections.)

It should be noted that this new set of equations is still mathematically equivalent to the neutron transport equation. However, two difficulties remain to make the system intractable as it stands: there are an infinite number of equations and the group constant definitions involve the functions $\Phi_n(\underline{r},E)$ for which the equations are being solved and are, therefore, unknown.

The first problem is overcome by truncating the series of equations after N+1 terms, this is then called a P_N approximation.

The second problem is dealt with by giving the $\Phi_n(\underline{r},E)$ values corresponding to an estimate of the flux spectrum anticipated for the problem. The function $\Phi_n(E)$ used in preparing multigroup data for a particular material in the problem is known as a 'flux-weighting-spectrum'.

The multigroup method of treating the energy variable is not restricted to solving the neutron transport equation: it has been applied, for example, to solving diffusion theory approximations to radiation transport.

A P P E N D I X B

CALCULATION OF THE VARIANCE ON RESULTS OF A MONTE CARLO CALCULATION

It is required to calculate the relative variance-covariance matrix $\tilde{V}_c$ of ℓ calcuations $\underline{c}$ which are functions of elastic, $\underline{n}$, and non-elastic, $\underline{x}$, cross-sections.

The definition of a relataive variance-covariance matrix for a random variable $\underline{c}$ is

$$\tilde{V}_c = \left\langle \left(\frac{\delta \underline{c}}{\underline{c}}\right)\left(\frac{\delta \underline{c}}{\underline{c}}\right)^T \right\rangle$$

where $\langle \underline{a} \rangle$ denotes the expectation of matrix $\underline{a}$. The elements of $\tilde{V}_c$ are

$$\tilde{v}_{c_{ij}} = \frac{\sigma^2(c_i c_j)}{c_i c_j}$$

and

$$\tilde{v}_{c_{ii}} = \frac{\sigma^2(c_i)}{c_i^2} \quad \text{for the diagonals.}$$

For analysis in K energy groups δc_i can be written:

$$\delta c_i = \frac{\partial c_i}{\partial x_1}.\delta x_1 + \ldots + \frac{\partial c_i}{\partial x_K}.\delta x_K + \frac{\partial c_i}{\partial n_1}.\delta n_1 + \ldots$$

$$+ \frac{\partial c_i}{\partial n_K}.\delta n_K + c_i \frac{\delta S}{S} + \delta \alpha_i$$

where the $\delta \alpha_i$ are derived from the Monte Carlo statistics and δS is the error in the source S. The remainder of the terms are attributable to the uncertainties in the group non-elastic cross-sections and the group elastic cross-sections.

Considering ℓ measurements, dividing each of the ℓ equations by its corresponding c_i and defining the sensitivities as

$$U_{x_{ij}} = \frac{x_j}{c_i} \frac{\partial c_i}{\partial x_j} \quad \text{and} \quad U_{n_{ij}} = \frac{n_j}{c_i} \frac{\partial c_i}{\partial n_j}$$

for the non-elastic and elastic cross-sections respectively, gives in matrix form:

$$\begin{pmatrix} \frac{\delta c_1}{c_1} \\ \vdots \\ \frac{\partial c_\ell}{c_\ell} \end{pmatrix} = \begin{pmatrix} \frac{x_1}{c_1}\frac{\partial c_1}{\partial x_1} & \cdots & \frac{x_K}{c_1}\frac{\partial c_1}{\partial x_K} & \frac{n_1}{c_1}\frac{\partial c_1}{\partial n_1} & \cdots & \frac{n_K}{c_1}\frac{\partial c_1}{\partial n_K} & 1 & 1 & 0\ldots0 \\ \vdots & & & & & & & & \\ \frac{x_1}{c_\ell}\frac{\partial c_\ell}{\partial x_1} & & \cdot & & \cdot & \frac{n_K}{c_\ell}\frac{\partial c_\ell}{\partial n_K} & 1 & 0\ldots0 & 1 \end{pmatrix} \begin{pmatrix} \frac{\partial x_1}{x_1} \\ \vdots \\ \frac{\partial n_K}{n_K} \\ \vdots \\ \frac{\delta S}{S} \\ \frac{\partial \alpha}{c_1} \\ \vdots \\ \frac{\partial \alpha_\ell}{c_\ell} \end{pmatrix}$$

Or,

$$\left(\frac{\delta c}{c}\right) = W \left(\frac{\delta p}{p}\right)$$

where W is the sensitivity matrix; ie, the matrix with $U_{x_{ij}}$ and $U_{n_{ij}}$ for elements.

Therefore,

$$\tilde{V}_c = \left\langle W \left(\frac{\delta p}{p}\right) \left(\frac{\delta p}{p}\right)^T W^T \right\rangle \equiv W \tilde{V}_p W^T$$

where $\tilde{V}_p$ is the relative variance-covariance matrix of the parameter vector $\left(\frac{\delta p}{p}\right)$.

$$
\tilde{V}_p = \begin{array}{cccccccccc}
\tilde{\sigma}^2(x_1) & \tilde{\sigma}^2(x_1x_2) & \cdots & \tilde{\sigma}^2(x_1x_K) & \tilde{\sigma}^2(x_1n_1) & \cdots & \tilde{\sigma}^2(x_1n_K) & 0 & \cdots & 0 \\
\tilde{\sigma}^2(x_2x_1) & \tilde{\sigma}^2(x_2) & \cdots & \tilde{\sigma}^2(x_2x_K) & \tilde{\sigma}^2(x_2n_1) & \cdots & \tilde{\sigma}^2(x_2n_K) & 0 & \cdots & 0 \\
\vdots & & & & & \vdots & & \vdots & & \\
\tilde{\sigma}^2(x_Kx_1) & \tilde{\sigma}^2(x_Kx_2) & \cdots & \tilde{\sigma}^2(x_K) & \tilde{\sigma}^2(x_Kn_1) & \cdots & \tilde{\sigma}^2(x_Kn_K) & 0 & \cdots & 0 \\
\tilde{\sigma}^2(n_1x_1) & \tilde{\sigma}^2(n_1x_2) & \cdots & \tilde{\sigma}^2(n_1x_K) & \tilde{\sigma}^2(n_1) & \cdots & \tilde{\sigma}^2(n_1n_K) & 0 & \cdots & 0 \\
\vdots & & & & & & & \vdots & & \\
\tilde{\sigma}^2(n_Kx_1) & \tilde{\sigma}^2(n_Kx_2) & \cdots & \tilde{\sigma}^2(n_Kx_K) & \tilde{\sigma}^2(n_Kn_1) & \cdots & \tilde{\sigma}^2(n_K) & 0 & \cdots & 0 \\
0 & 0 & \cdots & 0 & 0 & \cdots & 0 & \tilde{\sigma}^2(s) & \cdots & 0 \\
\vdots & & & & & & & \vdots & \dfrac{\tilde{\sigma}^2(\alpha_1)}{C_1^2} & 0 \\
0 & 0 & \cdots & 0 & 0 & \cdots & 0 & 0 & \cdots & \dfrac{\tilde{\sigma}^2(\alpha l)}{Cl^2}
\end{array}
$$

Therefore, knowing the values of the variances and covariances in the matrix $\tilde{V}_p$ and the sensitivities in the matrix W, the variance-covariance matrix $\tilde{V}_c$ can be found.

The sensitivities can be estimated in MCBEND by using the DUCKPOND facility. This facility is available only in MCBEND calculations using DICE-VI point energy nuclear data. The nuclear cross-sections used by DICE-VI are derived from the UKNDL (43). Unfortunately, no information is available on the variances and covariances on the UKNDL data. However, such information is available for a similar set of nuclear cross-sections, the ENDF-B (42). Since the methods by which the cross-sections are measured and accumulated for the ENDF-B and the UKNDL are very similar, it is reasonable to assume that the variances on the cross-sections are approximately the same.

The variance-covariance information on the ENDF-B cross-sections have been published by ORNL (61). The information is in the form of correlation matrices and fractional standard deviations for the total, total elastic and total non-elastic cross-sections of a range of materials in the ENDF-B.

The fractional standard deviation, f_{x_i}, on a cross-section, x_i, is given by $f_{x_i} = \frac{\sigma(x_i)}{x_i}$. The correlation, $r(x_i x_j)$, between two cross-sections, x_i and x_j, is defined by

$$r(x_i x_j) = \frac{\sigma^2(x_i x_j)}{\sigma(x_i)\sigma(x_j)}.$$

The required relative variances and covariances can be found from these definitions as follows:

$$\frac{\sigma^2(x_i x_j)}{x_i x_j} = r(x_i x_j)\, f_{x_i}\, f_{x_j}$$

and

$$\frac{\sigma^2(x_i n_j)}{x_i n_j} = r(x_i, n_j)\, f_{x_i}\, f_{x_j}$$

The fifteen group scheme over which these values are given (see Table 8) differs from that in which DUCKPOND calculated the sensitivities. The sensitivities were calculated in the first 32 groups of the EURLIB group scheme (see Table 2), of which only the sensitivities in the first 26 groups were considered significant. These 26 groups are covered by the first three groups of the ORNL scheme.

The 26 group scheme was temporarily increase to 29 groups by putting in three extra group boundaries corresponding to the lower energy boundaries of the first three ORNL groups. This was done in order to calculate the variances and covariances for the 26 group scheme which was achieved as follows.

For groups k in the 29 group scheme within the group p of the ORNL scheme and groups m contained within group q, it was assumed that

$$\frac{\sigma^2(x'_k\ x'_m)}{x'_k\ x'_m} = \frac{\sigma^2(X_p\ X_q)}{X_p\ X_q}$$

where the x' values are the cross-sections in the expanded EURLIB scheme and the X values are the cross-sections in the ORNL scheme. The 29 group structure can be collapsed to the 26 groups of the EURLIB group scheme by assuming that

$$\frac{\sigma^2(x_i\ x_j)}{x_i\ x_j} = \frac{\sum \sigma^2(x'_k\ x'_m)\ \delta U_k\ \delta U_m}{\sum x'_k\ x'_m\ \delta U_k\ \delta U_m}$$

where the left hand side values are the 26 group variances and covariances and the δU are the lethargy intervals of the 29 group scheme.

A P P E N D I X C

Derivation of an An Approximation to the Adjoint Angular Flux from the Adjoint Scalar Flux

The angular flux in one-dimension (in the x-direction, say) can be expanded in a series of Legendre polynomials as follows:

$$\phi(x,\mu,E) = \sum_{m=0}^{\infty} \frac{2m+1}{4\pi} \Phi_m(x,E)\, P_m(\mu)$$

where $\phi(x,\mu,E)\, dx d\mu dE$ is the angular flux at x of particles with energy E and direction defined by the cosine μ with x;

$P_m(\mu)$ is the Legendre polynomial of μ of order m; and

$$\Phi_m(x,E) = 2\pi \int_{-1}^{1} \Phi(x,\mu,E)\, P_m(\mu) d\mu.$$

(See Appendix A for the definition of the Legendre polynomials.)

From the definition of $\Phi_m(x,E)$ it can be seen that:

(a) $$\Phi_0(x,E) = 2\pi \int_{-1}^{1} \Phi(x,\mu,E)\, d\mu,$$

since $P_0 = 1$, which is simply the scalar flux $\phi(x,E)$, and

(b) $$\Phi_1(x,E) = 2\pi \int_{-1}^{1} \mu\, \Phi(x,\mu,E)\, d\mu,$$

since $P_1 = \mu$, which is simply the current $J(x)$ at x in the direction $\underline{x}$.

If one makes the assumption that ψ can be adequately described by an expansion including up to P_1 terms only then:

$$\psi(x,\mu,E) \approx \frac{1}{4\pi} [\phi(x,E) + 3\, J(x).\mu].$$

This 'P_1 approximation' to the angular flux is consistent with the diffusion theory approximation. This can be demonstrated by using a similar approximation to the equations resulting from treating the neutron transport equation by expansion in Legendre polynomials (see Appendix A). This results in an expression, for a one-group infinite-medium problem with an isotropic, plane source,

$$\frac{d\,\Phi_0(x)}{dx} + 3\,\Phi_1(x) = 0$$

which can be written:

$$\Phi_1(x) = -\frac{1}{3}.\frac{d\Phi_0(x)}{dx}$$

or

$$J(x) = -D.\frac{d\phi(x)}{dx}$$

The last expression, where lengths are expressed in terms of the mean-free-path and D is the diffusion coefficient, is just a form of Fick's Law (11).

The expansion of the angular flux in one dimension can be generalised to two and three dimensions to give:

$$\psi(\underline{r},\hat{\underline{\Omega}},E) = \frac{1}{4\pi}\left[\phi(\underline{r},E) + 3\ \underline{J}(\underline{r},E).\hat{\underline{\Omega}}\right]$$

This expression is also valid for expanding the adjoint angular flux, ψ^*, in terms of the adjoint scalar flux, ϕ^*. So,

$$\psi^*(\underline{r},\hat{\underline{\Omega}},E) = \frac{1}{4\pi}\left[\phi^*(\underline{r},E) + 3\ \underline{J}(\underline{r},E).\hat{\underline{\Omega}}\right]$$

which can be cast into group form to give, for each energy group g:

$$\psi^*_g(\underline{r},\hat{\underline{\Omega}}) = \frac{1}{4\pi}\left[\phi^*_g(\underline{r}) + 3\, \underline{J}^*_g(\underline{r}).\hat{\underline{\Omega}}\right]$$

where $\underline{J}^*_g(\underline{r})$ is the adjoint current of particles in group g at $\underline{r}$ in the direction $\underline{r}$.

In the adjoint case Fick's Law takes the form (23), for a group g,

$$\underline{J}^*_g(\underline{r}) = + D_g \underline{\nabla}\, \phi^*_g(\underline{r})$$

Substituting this expression into the previous one results in:

$$\psi^*_g(\underline{r},\underline{\Omega}) = \frac{1}{4\pi}\left[\phi^*_g(\underline{r}) + 3\, D_g \left|\underline{\nabla}\phi^*_g(\underline{r})\right| . \mu\right]$$

where $\mu = \dfrac{\underline{\nabla}\phi^*_g(\underline{r}).\hat{\underline{\Omega}}}{\left|\underline{\nabla}\phi^*_g(\underline{r})\right|}$

Appendix D

APPENDIX D

THE ADJOINT FUNCTION AND IMPORTANCE

If u and v are functions of the same variables, $\underline{\theta}$, and satisfy certain boundary and continuity conditions then a 'self-adjoint' operator, M say, is one for which

$$\int u\, M\, v \;\; d\underline{\theta} = \int v\, M\, u \;\; d\underline{\theta}$$

where integration is over all $\underline{\theta}$ accessible by u and v.

If an operator, M, is not self-adjoint it is possible to define an operator, M^*, that is adjoint to M by the requirement that

$$\int u\, M^*\, v^* \;\; d\underline{\theta} = \int v^*\, M\, u \;\; d\underline{\theta}$$

where u^* and v^* are the adjoint functions and which, although functions of the same variables $\underline{\theta}$, may satisfy different boundary conditions to the functions u and v.

Using operator notation the time-independent neutron transport equation of Appendix A can be written

$$L\Psi(\underline{r},\underline{\Omega}, E) + S(\underline{r},\underline{\Omega}, E) = 0$$

where

$$L\Psi(\underline{r},\underline{\Omega}, E) = -\underline{\Omega}.\underline{\nabla}\,(\underline{r},\underline{\Omega}, E) - \sigma_t(\underline{r}, E)\Psi(\underline{r},\underline{\Omega}, E) + \int_{E'}\int_{\underline{\Omega}'} \sigma_s(\underline{r}, E')\; p(r;\, E' \rightarrow E, \underline{\Omega}' \rightarrow \underline{\Omega})\, \Psi(\underline{r},\underline{\Omega}', E')\; d\underline{\Omega}' dE$$

and all other functions are as defined in Appendix A.

The operator L is not self-adjoint; however, it is possible is define an operator that is adjoint to L. In fact, in the notation adopted, the following operator L^* is adjoint to L :

$$L^*\Psi^*(\underline{r},\underline{\Omega}, E) = \underline{\Omega}\,.\underline{\nabla}\Psi^*(\underline{r},\underline{\Omega}, E) - \sigma_t(\underline{r}, E)\Psi^*(\underline{r},\underline{\Omega}, E) + \int_{E'}\int_{\underline{\Omega}'} \sigma_s(r, E)\; p(r;\, E \rightarrow E', \underline{\Omega} \rightarrow \underline{\Omega}')\, \Psi^*(\underline{r},\underline{\Omega}', E')\; d\underline{\Omega}' dE$$

when Ψ^* satisfies the boundary condition that $\Psi^*(\underline{r},\underline{\Omega},E) = 0$ for all r on the boundary surface $\hat{\underline{n}}$ when $\hat{\underline{n}}.\underline{\Omega} > 0$.

It can be seen that the above expressions for L and L^* differ only in that

- the gradient (or streaming) terms have opposite signs
- the incident and emergent parts of the scattering probability have been interchanged

That L^* is indeed adjoint to L requires that

$$\iiint \Psi^* L \Psi \, dV \, d\underline{\Omega} dE = \iiint \Psi L^* \Psi^* \, dV \, d\underline{\Omega} dE$$

be true for any functions Ψ and Ψ^* satisfying the boundary conditions at the surface of the volume V. It is evident that this is equivalent to showing that

$$\iiint (\Psi^*(\underline{\Omega}.\underline{\nabla}\Psi) - \Psi(\underline{\Omega}.\underline{\nabla}\Psi^*)) \, dV \, dE \, d\underline{\Omega} = 0$$

which, using the identities

$$\underline{\Omega}.\underline{\nabla}\Psi = \underline{\nabla}.\underline{\Omega}\Psi \quad \text{and} \quad \underline{\Omega}.\underline{\nabla}\Psi^* = \underline{\nabla}.\underline{\Omega}\Psi^*,$$

is identical to

$$\iiint \underline{\nabla}.\underline{\Omega}(\Psi^*\Psi) \, dV \, d\underline{\Omega} dE = 0$$

The Divergence Theorem can be used to convert this to a surface integral which allows the requirement to be stated as

$$\hat{\underline{n}}.\underline{\Omega}(\Psi^*\Psi) \, dA \, d\underline{\Omega} dE = 0$$

where the surface integration is over the surface A_B, upon which the boundary conditions are imposed. However, on A_B $\Psi^* = 0$ for $\hat{\underline{n}}.\underline{\Omega} > 0$ and $\Psi = 0$ for $\hat{\underline{n}}.\underline{\Omega} < 0$. Therefore, the L^* defined above is a valid adjoint operator to the time-independent neutron transport operator.

If the time-independent neutron transport equation is multiplied by the adjoint function, Ψ^*; the time-independent adjoint neutron transport equation is multiplied by the angular flux, Ψ; and the difference of the two resulting equations is integrated over all variables - then, from the definition of the adjoint operator, it can be shown that

$$\int \psi^*(\underline{r},\underline{\Omega}, E) \, S(\underline{r},\underline{\Omega}, E) \, dV \, d\underline{\Omega} dE = \int S^*(\underline{r},\underline{\Omega}, E)\Psi^*(\underline{r},\underline{\Omega}, E) \, dV \, d\underline{\Omega} dE$$

Appendix D

where $S^*(\underline{r},\underline{\Omega},E)$ is defined as the contribution of a neutron at $\underline{r}$ of energy E and travelling in a direction $\underline{\Omega}$, to the response to the source $S(\underline{r},\underline{\Omega},E)$ as detected at $\underline{r}$.

The source $S(r,\underline{\Omega},E)$ in this expression is arbitrary. If it is considered to be a unit source for some particular values of r, $\underline{\Omega}$ and E ($\underline{r}_0$, $\underline{\Omega}_0$, E_0, say) then

$$\Psi^*(\underline{r}_0,\underline{\Omega}_0,E_0) = \int S^*(\underline{r},\underline{\Omega},E)\Psi(\underline{r},\underline{\Omega},E)\,dV\,d\underline{\Omega}\,dE$$

which shows that the adjoint function, Ψ^*, at a particular point in the particle phase-space is proportional to the detected response of a unit source of neutrons at that point.

Hence, the adjoint function is a measure of the 'importance' of a neutron to the detector response.

The adjoint function can be found for most neutron transport problems in much the same way as can the angular flux. For example, the finite-element diffusion code FENDER <15> and the Monte-Carlo code McBEND <21> both provide the option of calculating the adjoint function.

One change from the 'forward' calculation that requires some consideration is the definition of the source. In the multigroup treatment (described in Appendix A) the forward group source is an integral quantity:

$$S_g(\underline{r},\underline{\Omega}) = \int_{\Delta E_g} S(\underline{r},\underline{\Omega},E)\,dE$$

where S is a source per unit energy; whereas, the adjoint group source is an energy-averaged cross-section

$$S_g(r) = \frac{\int_{\Delta E_g}\Sigma(\underline{r},E)\,dE}{\int_{\Delta E_g} dE}$$

where $\Sigma(\underline{r},e)$ is a response cross-section for a flux at $\underline{r}$.

The other essential difference between forward and adjoint neutron transport calculations is the transposition of the scattering probability variables as indicated in the expressions for L^* and L above. This difference manifests itself in FENDER by having to:

1. invert the group scheme for which the adjoint is to be solved such that group one becomes the lowest energy group

2. transpose the scattering-matrix so that the elements

$\Sigma_s^{g' \to g}(\underline{r}, \underline{\Omega}' \to \underline{\Omega})$ become $\Sigma_s^{g \to g'}(\underline{r}, \underline{\Omega} \to \underline{\Omega}')$.

The scattering treatment in adjoint Monte-Carlo also requires inversion of the forward group cross-section scheme. The treatment itself is achieved by transposing the cross-section matrix employed when sampling the scattering-kernel during collisions. An additional complication is the fact that the flux-spectrum-weighting (see Appendix A) for the cross-section data used in the adjoint calculation should be the group adjoint flux per unit energy interval. However, it is is more convenient to use forward flux-spectrum weighted group cross-sections as these are more readily available.

Appendix D